

Cite this: *Nanoscale Adv.*, 2024, 6, 1331

# Nanocrystals as performance-boosting materials for solar cells

Boping Yang,<sup>a</sup> Junjie Cang,<sup>b</sup> Zhiling Li<sup>a</sup> and Jian Chen<sup>\*c</sup>

Nanocrystals (NCs) have been widely studied owing to their distinctive properties and promising application in new-generation photoelectric devices. In photovoltaic devices, semiconductor NCs can act as efficient light harvesters for high-performance solar cells. Besides light absorption, NCs have shown great significance as functional layers for charge (hole and electron) transport and interface modification to improve the power conversion efficiency and stability of solar cells. NC-based functional layers can boost hole/electron transport ability, adjust energy level alignment between a light absorbing layer and charge transport layer, broaden the absorption range of an active layer, enhance intrinsic stability, and reduce fabrication cost. In this review, recent advances in NCs as a hole transport layer, electron transport layer, and interfacial layer are discussed. Additionally, NC additives to improve the performance of solar cells are demonstrated. Finally, a summary and future prospects of NC-based functional materials in solar cells are presented, addressing their limitations and suggesting potential solutions.

Received 29th November 2023  
Accepted 31st January 2024

DOI: 10.1039/d3na01063e

rsc.li/nanoscale-advances

## 1. Introduction

Nanocrystals (NCs), sometimes termed as quantum dots (QDs) or nanoparticles (NPs), with a size less than 100 nm, are popular worldwide and have been paid extensive attention owing to their outstanding photoelectric properties. In the energy field, photovoltaic devices based on semiconductor NCs are among the most potential systems with high power conversion efficiency (PCE), good stability, low cost, facile fabrication, and other advantages.<sup>1–16</sup> In recent years, NCs have been widely used as light harvesting layers in high-performance solar cells. Semiconducting NCs such as PbX (X = S, Se, and Te), CdSe, and CuInS<sub>2</sub> have been suggested as excellent light harvesters in third-generation solar cells.<sup>11,14,15,17–22</sup> Additionally, perovskite NCs are also good alternatives for light harvesting in solar cells.<sup>12–14,16,23–28</sup> Besides active layers (light harvesting layers), functional layers based on NCs, mainly including hole transport layers (HTLs),<sup>29–99</sup> electron transport layers (ETLs)<sup>100–173</sup> and interfacial functional layers (IFLs),<sup>174–221</sup> are of great importance in solar cells. Notably, NC additives also boost the performance of solar cells through defect passivation, plasmonic effect, solar concentration, light up-conversion and down-conversion/shifting, light scattering and reflection, and heat sinks.<sup>222–258</sup>

To efficiently transport charge in solar cells, HTLs and ETLs must have suitable energy levels matching the active layers such

as dyes, Si, Pb-based light harvesting layers, and perovskite films. For example, to fabricate high-performance perovskite solar cells (PSCs), the work function of HTLs and ETLs should have hole and electron transport layers aligned with the valence band edge and conduction band edge of a perovskite. As is well known, the energy levels of NCs can be easily controlled and adjusted by changing their sizes, ligands, and dopants during their synthesis process, which is favourable to satisfy the energy alignment. Meanwhile, the easily-accomplished modifications in NCs mentioned above also favour high mobility to allow carrier transport and form a more effective current circulation path. Furthermore, the transmittance of HTL or ETL based on NCs can be improved during synthesis processes, which leads to less light loss and thus, higher performance of solar cells. Consequently, NCs are a good choice as HTLs and ETLs for efficient solar cells and have gained much attention.

Some researchers found that inserting different IFLs in solar cells could promote the power conversion efficiency (PCE) and stability of the devices. Good IFL can modulate the formation of adjacent layers (especially the perovskite layer in PSCs), optimize energy alignment, and impede charge recombination. As multi-functional IFL, NCs have been extensively investigated due to their compatible properties, such as appropriate morphology for compact, smooth films, gradual energy level to transfer carriers, and self-stability to protect the devices.

Besides acting as a separate functional layer in efficient solar cells, NCs have also been used as additives to improve active layer quality, accelerate carrier transfer, convert infrared or ultraviolet light to visible light, scatter and reflect light, sink heat, and other functions.<sup>222–258</sup> The addition of NCs could enlarge the grain size of perovskite film, reduce the

<sup>a</sup>College of Science, Guizhou Institute of Technology, Guiyang, 550003, China. E-mail: bpyang023@163.com

<sup>b</sup>School of Electrical Engineering, Yancheng Institute of Technology, Yancheng, 224051, China

<sup>c</sup>College of Artificial Intelligence and Electrical Engineering, Guizhou Institute of Technology, Guiyang, 550003, China. E-mail: cjycit@163.com



recombination, enhance charge extraction, improve the charge mobility, broaden the spectral response range, and so on.

In this review, functional materials based on NCs for high-performance solar cells are summarized. NCs as HTL, ETL, IFL, and additives for NC-light-harvestor solar cells (NC-LHSCs), PSCs, organic solar cells (OSCs), Si solar cells, and dye-sensitized solar cells (DSSCs) are successively analyzed. In Section 2, NCs as charge transport layers are analyzed in detail. This can provide a deep understanding of the extensive application of NCs in solar cells. As an important functional layer, IFL based on NCs is summarized in the next section. Section 4 describes NCs as efficient additives in different functional layers due to their small sizes and excellent photoelectric properties. Finally, we discuss the existing challenges of NCs for boosting the performance of solar cells and provide some feasible suggestions on these issues, expecting to improve the performance of solar cells based on NCs.

## 2. Nanocrystals as charge transport layers

In this section, we focus on NCs-based charge transport layers for solar cells, mainly including top/bottom HTL and ETL in n-i-p and p-i-n solar cells.

### 2.1 Nanocrystals as HTL

As known to us, solar cells work as follows: absorption of sun light, generation and separation of hole–electron pairs, transport of holes through HTL and electrons through ETL, and current produced by the flow of electrons through external circuits. Solar cells using NCs as HTL are not exceptional, and the typical structures of solar cells based on NC HTL are shown in Fig. 1. According to the position of HTL, we call HTL between the ITO/FTO and active layer as bottom HTL while the HTL between metal electrode and active layer as top HTL.

**2.1.1 Recent NC HTL.** Semiconductor NCs have shown great potential in photoelectronic devices due to their excellent properties. The advances of NC HTLs for solar cells are listed in Table 1, including the size of NCs, device structure, PCE, and stability of solar cells.

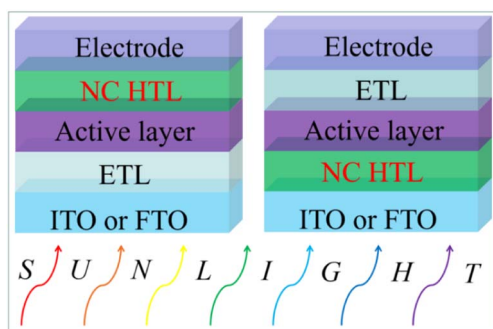


Fig. 1 Typical structure of solar cells based on top (left) and bottom (right) NC HTLs.

Lead chalcogenide NCs, especially PbS, have been massively used as efficient top HTL in NC-LHSCs.<sup>29–56</sup> Additionally, other metal chalcogenide NCs are also excellent choices as top HTL for high-performance perovskite solar cells (PSCs), mainly containing CuInS<sub>2</sub>/ZnS (core/shell),<sup>57</sup> CdZnSe@ZnSe,<sup>58</sup> Cu<sub>2</sub>ZnSnS<sub>4</sub>/Se<sub>4</sub>,<sup>59</sup> SnS,<sup>60</sup> CuInSe<sub>2</sub>,<sup>61</sup> Ag–In–Ga–S,<sup>62</sup> Cu<sub>12</sub>Sb<sub>4</sub>S<sub>13</sub>,<sup>63</sup> Cu<sub>2</sub>SnS<sub>3</sub>,<sup>64</sup> CuGaS,<sup>65</sup> and CuInS<sub>2</sub>.<sup>66</sup> Metal oxide NCs of NiO have shown potential for hole transport on top of the light harvesting layer in PSCs and Si solar cells.<sup>67–69</sup> Besides NiO, some other metal oxide NCs such as MoO<sub>2</sub>,<sup>70</sup> Co<sub>3</sub>O<sub>4</sub>,<sup>71</sup> Cu<sub>2</sub>O,<sup>72</sup> CuCrO<sub>2</sub>,<sup>73</sup> CuGaO<sub>2</sub>,<sup>74</sup> and CsPbI<sub>3</sub> (ref. 75) have been used as efficient top HTL for PSCs due to their excellent properties. It can be noticed that when PbS NCs are used as top HTL in solar cells, the light harvesting layers are mostly based on the PbS/Se family. There are not many perovskite used as light harvest materials when PbS/Se is used as top HTL. Only MAPbI<sub>3</sub> was applied in 2015, and 7.88% PCE was gained.<sup>29</sup> We suppose this is because the PbS NCs with long carbon chains or 1,2-ethanedithiol are not good at charge transport. If high-temperature annealing is adopted to enhance the conductivity of PbS, the perovskite underneath will be destroyed. This encourages us to regulate the synthesis or modification of NCs with less or even no charge transfer inhibition capture and improve their electronic properties.

Similar to top HTL, NCs can also be applied as bottom HTL for high-performance solar cells. NCs of PbS,<sup>76</sup> Cu<sub>2</sub>ZnSnS<sub>4</sub>,<sup>77,78</sup> NiO<sub>x</sub> and its doped derivatives,<sup>79–91</sup> CuO,<sup>92</sup> and ternary oxides of CuCrO<sub>2</sub>,<sup>93,94</sup> CuGaO<sub>2</sub>,<sup>95</sup> NiCo<sub>2</sub>O<sub>4</sub>,<sup>96,97</sup> ZnCoO<sub>4</sub>,<sup>98</sup> and doped ternary oxide In:CuCrO<sub>2</sub> (ref. 99) have offered excellent hole transport ability in PSCs and PTB7-Th-based organic solar cells (OSCs).

Ever since demonstrated as efficient HTL by Luther *et al.* in 2008,<sup>248</sup> PbS NCs with a 1,2-ethanedithiol (EDT) ligand (named as PbS-EDT or EDT-PbS) have been massively applied for hole transport in solar cells. From the established NC HTLs listed in Table 1, we can find some regular patterns: (i) as top HTL, EDT-linked sulphides were mainly used in NC-LHSCs but were not popular in PSCs. This is because EDT will strongly attack the perovskite materials in the n-i-p device and decrease the device performance.<sup>61</sup> (ii) As bottom HTL, oxides are widely used and sulphides are rare. We speculate that it is (iii) NiO<sub>x</sub> with high hole transport quality mostly used to transport holes in PSCs.

The previous light harvesting NC layers are mainly based on the Pb-based chalcogenide family or their mixture. NC-LHSCs using NCs as HTL have gained high PCE above 13%,<sup>45,50</sup> but this is significantly lower than that of the theoretical value.<sup>11</sup> Some strategies were also adopted to modify the light-harvesting NCs, which is not the keynote in this review. The current relatively low PCE of NC-LHSCs may be on account of non-radiative recombination resulting from the high density of surface traps due to some intrinsic properties of NCs, such as high surface-to-volume ratios. Using NC top HTL, the PCE value can be improved. Some oxides, for instance, NiO, Ti-doped MoO<sub>2</sub>, Co<sub>3</sub>O<sub>4</sub>, Cu<sub>2</sub>O, CuCrO<sub>2</sub>, and CuGaO<sub>2</sub>, have acted as excellent top HTL in high-performance PSCs. As shown in Fig. 2a, SnS NCs prepared by the one-pot hot-injection method were utilized as top HTL in efficient and stable



Table 1 Recent advances in selected NC HTLs for solar cells (EDT = 1,2-ethanedithiol, relative humidity = RH)

|         | NC   | Active layer  | PCE (%)                               | Long-term stability   | Ref.  |  |    |
|---------|--|---|---------------------------------------|---|---|--|----|
| Top HTL | PbS-EDT  | CH <sub>3</sub> NH <sub>3</sub> PbI <sub>3</sub><br>PbS   | 7.88                                  | 8% decay after 2 days   | 29  |  |    |
|         |  |   | 11.6                                  | Null  | 30  |  |    |
|         |  |   | 10.4                                  | 100%, after 103 days in the dark under ambient conditions   | 32  |  |    |
|         |  |   |                                       | 9.44  | ~100%, after 4 months in ambient air  | 33   |    |
|         |  |   |                                       | 13.2  | Null  | 37   |    |
|         |  |   |                                       | 10.4  | ①96%, after baking on a hotplate in air for 120 min; ②97%, after 60 min oxygen plasma treatment                             | 38   |    |
|         |  |   |                                       | 13.3  | Null  | 39   |    |
|         |  |   |                                       | 10.5  | Null  | 40   |    |
|         |  |   |                                       | 13.0  | Null  | 41   |    |
|         |  |   | PbS-PbI <sub>2</sub>                  | 11.2 ± 0.22   | Nearly no drop of PCE after 180 h under continuous heating at 85 °C in ambient air >90, after 600 h under ambient condition | 44   |    |
|         |  |   |                                       | 11.29   |   | 45   |    |
|         |  |   | PbS:F                                 | 12.7  | Null  | 46   |    |
|         |  |   | PbX <sub>2</sub> -PbS                 | 8.16  | Null  | 47   |    |
|         |  |   |                                       | 10.35   | Null  | 48   |    |
|         |  |   |                                       | 10.6  | Null  | 49   |    |
|         |  |   | PbS-PbX <sub>2</sub> -KI <sub>3</sub> | 12.1  | 94%, after 20 h continuous operation in air   | 50   |    |
|         |  |   | PbSe-PbS                              | 1.24 (infrared PCE)   | ~95%, after 25 days in air  | 51   |    |
|         |  |   | PbSe-PbI <sub>2</sub>                 | 10.4  | 90%, after 30 days in ambient condition   | 51   |    |
|         |  |   | CsMAFA-PbS                            | 11.3  | 96%, after 1200 h shelf storage   | 53   |    |
|         |  |   | MAPbI <sub>3</sub> -PbS               | 9.5   | 95%, after 2 months in ambient environment  | 54   |    |
|         |  |   | Sb <sub>2</sub> Se <sub>3</sub>       | 6.5 (certified)   | Null  | 55   |    |
|         |  |   | KPbS                                  | 12.6  | 83%, after 300 h under continuous operation at MPP in ambient air   | 56   |    |
|         |  |   | CuInS <sub>2</sub> /ZnS core/shell    | MAPbI <sub>3</sub>  | 8.38  | Null   | 57 |
|         |  |   | CdZnSe@ZnSe                           | CdZnSe@ZnSe   | 8.65  | Null   | 58 |
|         |  |   | Cu <sub>2</sub> ZnSnSe <sub>4</sub>   | MAPbI <sub>3</sub>  | 9.72  | Null   | 59 |
|         |  |   | Cu <sub>2</sub> ZnSnS <sub>4</sub>    |   | 10.72   |  |    |
|         |  |   | SnS                                   | (CsPbI <sub>3</sub> ) <sub>0.05</sub> (FAPbI <sub>3</sub> ) <sub>0.79</sub><br>(MAPbI <sub>3</sub> ) <sub>0.16</sub><br>(PbI <sub>3</sub> ) <sub>0.03</sub> | 13.7  | ①99%, after 1000 h storage in air; ②75%, after 500 h under continuous 1 sun illumination in a N <sub>2</sub> atmosphere at 25 °C | 60 |
|         | CuInSe <sub>2</sub>                              | MAFAPbClBrI   | 12.8                                  | 78%, after 96 h in air  | 61  |  |    |
|         | Ag-In-Ga-S                                       | CsPbBr <sub>3</sub>   | 8.46                                  | 96.1%, after 240 h in air   | 62  |  |    |
|         | Cu <sub>12</sub> Sb <sub>4</sub> S <sub>13</sub> | CsPbI <sub>3</sub>  | 10.02                                 | 94%, after storage in ambient air for 360 h   | 63  |  |    |
|         | Cu <sub>2</sub> SnS <sub>3</sub>                 | Cs <sub>0.05</sub> (MA <sub>0.17</sub> -FA <sub>0.83</sub> ) <sub>0.95</sub> Pb(I <sub>0.83</sub> Br <sub>0.17</sub> ) <sub>3</sub>   | 13.01                                 | 90%, after 1200 h in an ambient atmosphere  | 64  |  |    |
|         | CuGaS  | (FAPbI <sub>3</sub> ) <sub>1-x</sub> (MAPbBr <sub>3</sub> ) <sub>x</sub>  | 17.56                                 | 81%, aging for 30 days  | 65  |  |    |
|         | CuInS <sub>2</sub>                               | (FAPbI <sub>3</sub> ) <sub>1-x</sub> (MAPbBr <sub>3</sub> ) <sub>x</sub>  | 18.81                                 | 91%, aging for 30 days  | 66  |  |    |
|         | NiO  | MAPbI <sub>3</sub>  | 6.2                                   | Null  | 67  |  |    |
|         |  | MAPbI <sub>3</sub> NCs  | 10.89                                 | Null  | 68  |  |    |
|         | Ti-doped MoO <sub>2</sub>                        | MAPbI <sub>3</sub>  | 15.8                                  | ~95%, after 15 days with 50–70% RH  | 70  |  |    |
|         | Co <sub>3</sub> O <sub>4</sub>                   | MAPbI <sub>3</sub>  | 13.27                                 | Up to 2500 hours under ambient conditions   | 71  |  |    |
|         | Cu <sub>2</sub> O                                | Cs <sub>0.05</sub> FA <sub>0.81</sub> MA <sub>0.14</sub> PbI <sub>2.55</sub> Br <sub>0.45</sub>                                       | 18.9                                  | 80%, after 30 days in air with ~30% RH  | 72  |  |    |
|         | CuCrO <sub>2</sub>                               | Cs <sub>0.05</sub> (MA <sub>0.15</sub> FA <sub>0.85</sub> ) <sub>0.95</sub><br>Pb(I <sub>0.85</sub> Br <sub>0.15</sub> ) <sub>3</sub> | 16.68                                 | 88%, after 500 h at the MPP under one sun and a N <sub>2</sub> atmosphere   | 73  |  |    |
|         | CuGaO <sub>2</sub>                               | MAPbI <sub>3</sub>  | 18.51                                 | >85%, after 30 days at 25 °C with 30–55% humidity without encapsulation   | 74  |  |    |
|         | CsPbI <sub>3</sub>                               | MAPbI <sub>3</sub>  | 17.0                                  | Null  | 75  |  |    |



Table 1 (Contd.)

|        | NC                                 | Active layer  | PCE (%)                         | Long-term stability   | Ref. |
|--------|------------------------------------|---|---------------------------------|---|------|
| Bottom | PbS                                | MAPbI <sub>3</sub>  | 7.5                             | Null  | 76   |
| HTL    | Cu <sub>2</sub> ZnSnS <sub>4</sub> | MAPbI <sub>3</sub>  | 15.4                            | Null  | 77   |
|        |                                    |   | 6.02                            | 87%, after 43 days in N <sub>2</sub> atmosphere   | 78   |
|        | Ni–NiO core–shell                  | P3HT  | 0.86                            | Null  | 79   |
|        | NiO <sub>x</sub>                   | Cs <sub>0.08</sub> (MA <sub>0.17</sub> FA <sub>0.83</sub> ) <sub>0.92</sub> | 12.8                            | Null  | 81   |
|        |                                    | Pb(I <sub>0.83</sub> Br <sub>0.17</sub> ) <sub>3</sub>                      |                                 |   |      |
|        |                                    | MAPbI <sub>3</sub>  | 16.1                            | 90%, after 60 days in air at RT   | 84   |
|        |                                    | Cs <sub>0.05</sub> (MA <sub>0.17</sub> FA <sub>0.83</sub> ) <sub>0.95</sub> | 18.6                            | >80%, after 1000 h  | 85   |
|        |                                    | Pb(I <sub>0.9</sub> Br <sub>0.1</sub> ) <sub>3</sub>                        |                                 |   |      |
|        |                                    | MAPbI <sub>3</sub>  | 17.60                           | 93%, after 30 days  | 86   |
|        |                                    |   | 1.02 cm <sup>2</sup> :          | 90%, after 500 h in the thermal aging test  | 87   |
|        |                                    |   | 18.49 (rigid)                   | (85 °C, 85% RH)   |      |
|        |                                    |   | and 15.89                       |   |      |
|        |                                    |   | (flexible)                      |   |      |
|        | Cu:NiO <sub>x</sub>                |   | 15.01                           | 86%, after 1 month in an ambient environment at 25 °C with about 40% humidity   | 88   |
|        |                                    |   | (flexible, >1 cm <sup>2</sup> ) |   |      |
|        |                                    |   | 18.3                            | Null  | 89   |
|        | (Li,Cu):NiO <sub>x</sub>           | MAPbI <sub>3-x</sub> Cl <sub>x</sub>  | 20.80                           | 95%, after 60 days of storage   | 90   |
|        | NiO <sub>x</sub>                   | CsPbI <sub>x</sub> Br <sub>3-x</sub>  | 16.1                            | 85%, after 350 h light soaking  | 91   |
|        | CuO                                | MAPbI <sub>3</sub>  | 15.3                            | Null  | 92   |
|        | CuCrO <sub>2</sub>                 |   | 19.0                            | ~90, after 30 days in an Ar-filled dry glove box and continuously irradiated by a UV optical fiber with 5 mW cm <sup>-2</sup> | 94   |
|        | CuGaO <sub>2</sub>                 |   | 15.6                            | Null  | 95   |
|        | NiCo <sub>2</sub> O <sub>4</sub>   | MAPbI <sub>3-x</sub> Cl <sub>x</sub>  | 18.23                           | ~90%, after 500 h illumination at AM 1.5G   | 96   |
|        | ZnCo <sub>2</sub> O <sub>4</sub>   | PTB7-Th:PC <sub>71</sub> BM   | 9.37                            | >60%, after 60 h in ambient environment with 50% RH without capsulation   | 98   |
|        |                                    | MAPbI <sub>3-x</sub> Cl <sub>x</sub>  | 18.14                           | >60%, after 110 h in ambient environment with capsulation and under continuous 1 sun illumination soaking                     |      |
|        | In:CuCrO <sub>2</sub>              | Cs <sub>0.05</sub> (MA <sub>0.15</sub> FA <sub>0.85</sub> ) <sub>0.95</sub> | 20.54                           | ~90%, after 800 h of continuous radiation in glovebox   | 99   |
|        |                                    | Pb(I <sub>0.85</sub> Br <sub>0.15</sub> ) <sub>3</sub>                      |                                 |   |      |

(CsPbI<sub>3</sub>)<sub>0.05</sub>(FAPbI<sub>3</sub>)<sub>0.79</sub>(MAPbI<sub>3</sub>)<sub>0.16</sub> PSCs. The high PCE mainly resulted from good surface coverage and an excellent hole extraction ability demonstrated by Nyquist plots. Additionally, SnS-based PSC presented better air stability than the 2,2',7,7'-tetrakis[*N,N*-di(4-methoxyphenyl)amino]-9,9'-spirobifluorene (spiro-OMeTAD)-based device. Surface-modified Cu<sub>2</sub>O NCs boosted the efficiency of PSC to 18.9% with distinctly better stability than the reference device based on spiro-OMeTAD.<sup>61</sup> One important reason is the difference in hydrophobicities illustrated by water contact angles in Fig. 2b. Ternary oxide CuGaO<sub>2</sub>NCs with promising photoelectronic properties boosted the n-i-p PSCs with higher PCE and stability than spiro-OMeTAD (Fig. 2c).<sup>75</sup>

In n-i-p type solar cells, NiO<sub>x</sub> and its doped family oxide NCs are the most popular NC HTLs because of their facile synthesis and outstanding photoelectronic properties.<sup>86,101</sup> Meanwhile, sulphides of PbS and Cu<sub>2</sub>ZnSnS<sub>4</sub> together with multi basic oxides of CuCrO<sub>2</sub>, CuGaO<sub>2</sub>, NiCo<sub>2</sub>O<sub>4</sub>, ZnCo<sub>2</sub>O<sub>4</sub>, and In:CuCrO<sub>2</sub> are valuable substitutes for NiO<sub>x</sub> family. Ligand-free NiO<sub>x</sub> NCs in ethanol (E-NiO<sub>x</sub>) are spin-coated onto a substrate to form a smooth and compact NiO<sub>x</sub> film that has good hole extraction capability. As seen in Fig. 3a, this E-NiO<sub>x</sub> bottom HTL can be

used both in rigid and flexible PSC, producing high PCE and stability. Similar to top HTL, ternary oxide NCs like CuCrO<sub>2</sub> were also utilized as bottom HTL for high-performance solar cells. The low-temperature solution-processed CuCrO<sub>2</sub> NCs provide suitable electronic structure, charge carrier transport properties, and greater UV light-harvesting, demonstrating its potential as an efficient HTL for highly efficient and photostable n-i-p PSCs (Fig. 3b).

**2.1.2 Advantages of NC HTL.** One important inherent advantage of semiconductor NCs is their bandgap variation along with modification. The conduction band, valence band, and Fermi level of PbS NCs can be modified by changing surface ligands (Fig. 4), thus enhancing the performance of solar cells.<sup>252</sup> Fig. 4 shows that the energy level of PbS NCs is easily changed in a large range by different ligands, facilitating energy matching with the light-harvesting layer and other functional layers. Compared with mostly used organic HTLs of spiro-OMeTAD, poly(3,4-ethylenedioxythiophene):poly(styrene-sulfonate) (PEDOT:PSS) and poly[bis(4-phenyl)(2,4,6-trimethylphenyl)amine] (PTAA), inorganic NCs show higher stability with good hole transport ability, suggesting great potential for boosting solar cell performance. Equally



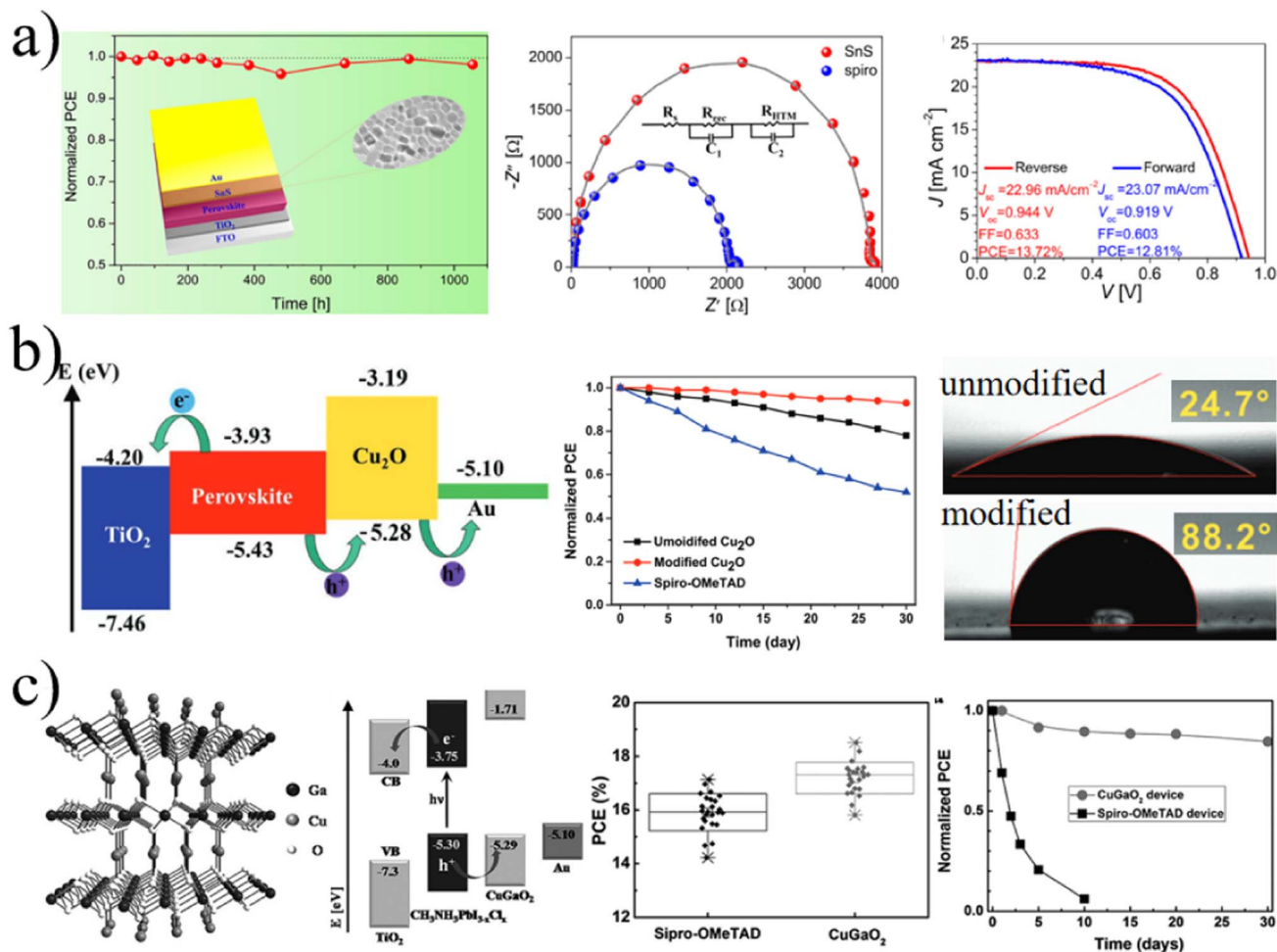


Fig. 2 (a) Evolution of PCE over time of the unencapsulated SnS-based PSCs in the ambient air of ~30–50% humidity, Nyquist plots at 0.9 V forward bias measured in the dark, forward, and reverse  $J-V$  curves of champion PSCs based on SnS. (b) Schematic view of PSC configuration, device performance durability of PSCs based on different HTLs in ambient air for 30 days, and water contact angles of unmodified and modified Cu<sub>2</sub>O. (c) Schematic illustration of the crystal structure of CuGaO<sub>2</sub>, device architecture of a regular PSC based on CuGaO<sub>2</sub>, standard deviations of PCEs to evaluate reproducibility by statistics of 50 devices based on CuGaO<sub>2</sub> and Spiro-OMeTAD.<sup>61</sup> Copyright 2019, American Chemical Society. (b) Adapted with permission.<sup>75</sup> Copyright 2019, Wiley-VCH. (c) Adapted with permission.<sup>75</sup> Copyright 2017, Wiley-VCH.

important, facile synthesis and low cost would be helpful for the commercialization of new-generation solar cells.

**2.1.3 Potential NC HTL.** To further develop more strategies for fabricating high-performance solar cells and boost the device PCE and stability, we should find more potential NCs for efficient hole transport in solar cells. According to the previous reports and our understanding, excellent NC HTLs should satisfy the following requirements: (i) matched energy level alignments with other functional layers; (ii) high hole mobility and conductivity; (iii) enhancing the quality of adjacent layers; (iv) intrinsic resistance to heat, light and water; (v) convenient fabrication with low cost; and (vi) high transmittance for bottom HTL and reflectivity for top HTL. NCs have many good properties such as easily-controlled energy level, excellent spreading and filling ability due to their small sizes, stable intrinsic structure, skilled synthesis process, and variant surface ligand. Considering the above rules and the advantages

of NCs, besides the existing NC HTLs, some other p-type sulphide and oxide NCs have huge potential for efficient and stable solar cells. Additionally, semiconductor NCs with enhanced hole-transporting ability by p-type doping are also good alternatives.

## 2.2 Nanocrystals as ETL

**2.2.1 Recent advances of NC ETL.** As important as HTL, ETL is also of great significance for high-performance solar cells to transport electrons and block holes, and it acts as well as a trap passivating layer and water/oxygen preventing layer. The typical structure of solar cells based on NC ETL is shown in Fig. 5.

ZnO is good at electron transport in photoelectrical devices due to excellent properties such as bandgap (3.3 eV), low cost, high electron mobility ( $\sim 10^{-5}$ – $10^2 \text{ cm}^2 \text{ V}^{-1} \text{ s}^{-1}$ ), and matching energy levels.<sup>100,101</sup> ZnO NCs with different sizes have been used



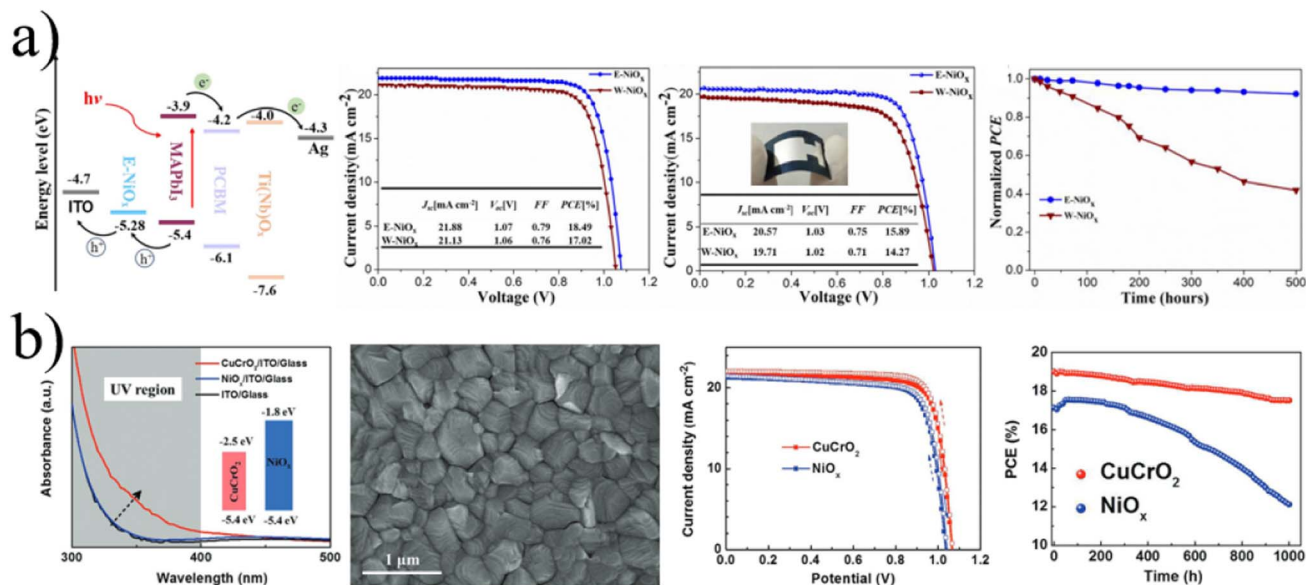


Fig. 3 (a) Energy level diagram of the materials used in the device,  $J$ - $V$  curves of rigid and flexible PSCs, normalized PCE. (b) UV-vis spectra of the CuCrO<sub>2</sub> and NiO<sub>x</sub> layer with optimum thickness with energy level in the inset. Adapted with permission.<sup>87,94</sup> Copyright 2018, Wiley-VCH.

as efficient top ETL in NC-LHSCs, OSCs, and PSCs.<sup>43,84,85,91,101-108</sup> TiO<sub>2</sub> and SnO<sub>2</sub>NCs are as popular as ZnO for electron transport due to their outstanding photoelectronic properties of high mobility and conductivity.<sup>250</sup> Certainly, these oxide NCs can be modified by doping, ligand changing, and other strategies. Tetrabutylammonium hydroxide (TBAOH)-capped metal oxide NCs for SnO<sub>2</sub> also extend to TiO<sub>2</sub>, ITO and CeO<sub>2</sub>NCs as top ETL for PSCs.<sup>108</sup> TiO<sub>2</sub>NCs have always been as the top ETL for PSCs.<sup>109-111</sup> CeO<sub>x</sub>,<sup>112</sup> In<sub>2</sub>O<sub>3</sub> and its Sn doped derivative formed bilayer ETL,<sup>113</sup> and CdSe<sup>114</sup> were also used for high-performance n-i-p PSCs. As efficient bottom ETL, modified TiO<sub>2</sub> by Sn, Al, Co, Cu, and N doping and N, F and S co-doped graphene NCs were widely used in dye-sensitized solar cells (DSSCs) based on N719 and N3 (*cis*-Ru(H<sub>2</sub>dcbpy)<sub>2</sub>(NCS)<sub>2</sub>, H<sub>2</sub>dcbpy = 4,4'-dicarboxy-2,2'-bipyridyl).<sup>115-120</sup> Additionally, TiO<sub>2</sub>, CdS NCs-modified TiO<sub>2</sub>, and Nb-doped TiO<sub>2</sub>NCs were applied for electron transport in PSCs with high PCE and stability.<sup>121-123</sup> Meanwhile,

TiO<sub>2</sub>NCs have been widely applied in n-i-p solar cells using chalcogenide NC as light harvesters, such as CdSe, CdS, and PbS.<sup>124-130</sup> Similarly, ZnO NCs were used as ETL for n-i-p PbS-

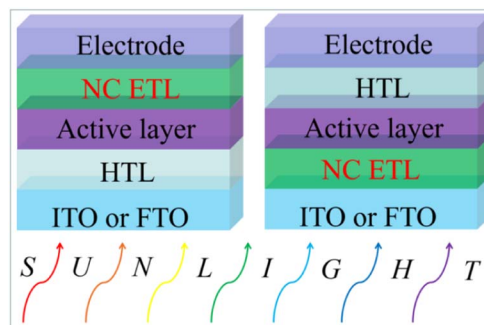


Fig. 5 Structure of solar cells based on top (left) and bottom (right) NC ETLs.

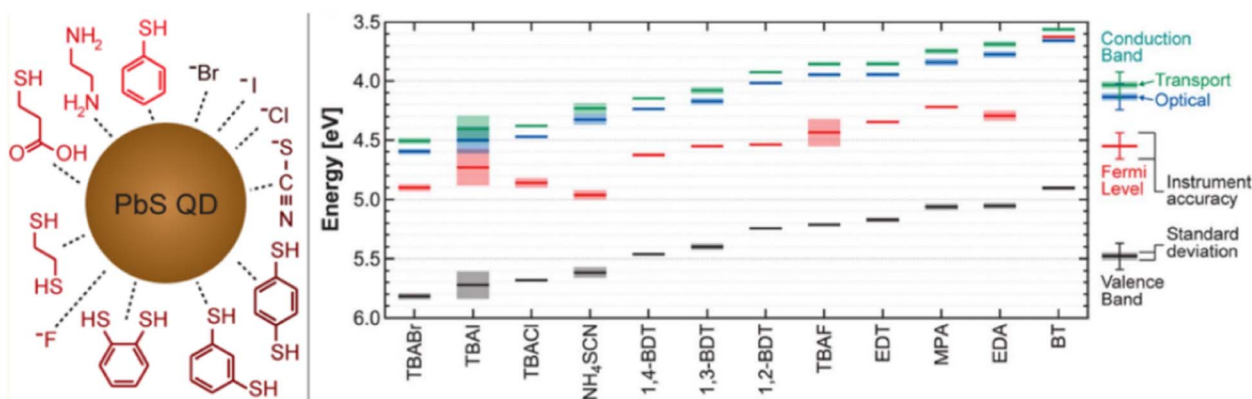


Fig. 4 Energy band position of PbS NC films for different surface ligands. Adapted with permission.<sup>249</sup> Copyright 2014, American Chemical Society.



Table 2 Recent advances in NC ETLs (bathocuproine = BCP)

|  | NC  | Active layer   | PCE (%)  | Long-term stability  | Ref.   |     |
|--|---|--|--|--|--|-----|
| Top ETL  | ZnO   | PbS–PbX <sub>2</sub>   | 10.35  | Null   | 43   |     |
|  |   | PCDTBT:PC <sub>61</sub> BM   | 2.66   | Null   | 100  |     |
|  |   | CsPbI <sub>3</sub> NCS   | 13.1   | 80%, after 40 h under 25 °C with 30–40% RH   | 103  |     |
|  |   | MAPbI <sub>3</sub>   | 17.2   | 66%, after 120 days stored in air  | 105  |     |
|  |   | MAPbI <sub>3</sub>   | 16.1   | 90% after 60 days in air at RT   | 84   |     |
|  |   | Cs <sub>0.05</sub> (MA <sub>0.17</sub> FA <sub>0.83</sub> ) <sub>0.95</sub> Pb(I <sub>0.9</sub> Br <sub>0.1</sub> ) <sub>3</sub>   | 18.6   | >80% after 1000 h  | 85   |     |
|  |   | CsPbI <sub>x</sub> Br <sub>3-x</sub>   | 16.1   | 85%, after 350 h light soaking   | 91   |     |
|  |   | Ag modified BCP:ZnO  | MAPbI <sub>3</sub>   | 15.5   | Null   | 106 |
|  |   | In:ZnO   | MAPbI <sub>3</sub>   | 16.2   | 85% after 460 h of light soaking   | 107 |
|  |   | TBAOH-SnO <sub>2</sub>   | MAPbI <sub>3</sub>   | 18.77  | 90% after aging at 45 °C for 240 h, followed by 65 °C for 240 h and 85 °C for 240 h                                    | 108 |
|  |   | TiO <sub>2</sub>   | Cs <sub>0.05</sub> (MA <sub>0.15</sub> FA <sub>0.85</sub> ) <sub>0.95</sub> Pb(I <sub>0.85</sub> Br <sub>0.15</sub> ) <sub>3</sub> | 20.5   | ~90% after 350 h MPP tracking test   | 109 |
|  |   | Carbide-TiO <sub>2</sub>   | CsPbI <sub>2</sub> Br  | 14.8   | ①>94%, after 1000 h at 85 °C in dark under N <sub>2</sub> ; ②>90%, after 1000 h at 60 °C under continuous illumination | 110 |
|  |   | CeO <sub>x</sub>   | MAPbI <sub>3</sub>   | 16.7   | 100%, after 200 h in air with 30% RH   | 112 |
|  | Sn:In <sub>2</sub> O <sub>3</sub> /In <sub>2</sub> O <sub>3</sub> (bilayer) | Cs <sub>0.05</sub> (MA <sub>0.15</sub> FA <sub>0.85</sub> ) <sub>0.95</sub> Pb(I <sub>0.85</sub> Br <sub>0.15</sub> ) <sub>3</sub> | 20.65  | ①91.9% after 69 days under 85 °C; ②91.8% after 2000 h, 12 h continuous 1 sun illumination and then 12 h interval in the dark | 113  |     |
|  | Bottom ETL  | CdSe   | MAPbI <sub>3</sub>   | 15.1   | Null   | 114 |
|  |   | Sn:TiO <sub>2</sub>  | N719   | 6.24   | Null   | 115 |
|  |   | Al:TiO <sub>2</sub>  |  | 4.27   | Null   | 116 |
|  |   | Co:TiO <sub>2</sub>  |  | 4.85   | Null   | 117 |
|  |   | Ti <sub>0.94</sub> Cu <sub>0.06</sub> O <sub>2</sub>   | N3/electrolyte   | 6.51   | Null   | 118 |
| TiO <sub>2</sub> modified by N, F and S, co-doped graphene NCS |   | N719   | 11.7   | ~85.5, after one month   | 120  |     |
| TiO <sub>2</sub>   |   | Cs–FA–MA mixed cation perovskite   | 19.03  | 84%, after 30 days   | 121  |     |
| CdS NCS-modified TiO <sub>2</sub>                              |   | MAPbI <sub>3</sub>   | 8.16   | Null   | 122  |     |
| Nb-doped TiO <sub>2</sub>                                      |   | Cs <sub>0.05</sub> (MA <sub>0.15</sub> FA <sub>0.85</sub> ) <sub>0.95</sub> Pb(I <sub>0.85</sub> Br <sub>0.15</sub> ) <sub>3</sub> | 18.97  | Null   | 123  |     |
| TiO <sub>2</sub>   |   | CdS  | 4.59   | Null   | 125  |     |
| Cu <sub>2</sub> O doped TiO <sub>2</sub>                       |   | CdSe/CdS/ZnS/electrolyte   | 3.01   | Null   | 126  |     |
| TiO <sub>2</sub>   |   | Mn–CdSe  | 3.55   | Null   | 128  |     |
| TiO <sub>2</sub>   |   | CdSe/ZnS/SiO <sub>2</sub> /Cu <sub>2</sub> S   | 4.00   | Null   | 129  |     |
| Cl@ZnO   |   | PbS  | 11.6   | Null   | 30   |     |
| ZnO  |   | PbX <sub>2</sub> –PbS  | 9.5  | 95%, after 2 months in ambient environment   | 33   |     |
| MgZnO  |   | PbS  | 10.4   | 100%, after 103 days in the dark under ambient conditions  | 32   |     |
| ZnO  |   | Lead halide-PbS  | 12.7   | Null   | 46   |     |
| ZnO  |   | PbS  | 13.1 ± 0.1   | Null   | 37   |     |
| ZnO  |   | PbS NC   | 12.44  | Null   | 140  |     |
| Cs-ZnO   |   | PbS  | 10.43  | 97%, after 3 months under 20 °C and 30% RH without any encapsulation   | 144  |     |
| ZnO  |   | CsPbBr <sub>3</sub> –CsPb <sub>2</sub> Br <sub>5</sub>   | 6.81   | No detectable decay after 100 days under 25 °C and 45% RH  | 146  |     |
| ZnO  | PTB7-Th:PC <sub>71</sub> BM   | 12.02  | Null   | 147  |  |     |
| Na–ZnO   | p-DTS(FBTTh <sub>2</sub> ) <sub>2</sub> :PC <sub>70</sub> BM                | 9.2  | 90%, after 28 h  | 149  |  |     |
| SnO <sub>2</sub>   | N719  | 3.2  | Null   | 151  |  |     |
| Ni:SnO <sub>2</sub>  |   | 3.6  |  |  |  |     |
| Zn:SnO <sub>2</sub>  |   | 4.2  |  |  |  |     |
| SnO <sub>2</sub>   | Eosin-Y   | 3.89   | Null   | 155  |  |     |
| Sn <sub>0.92</sub> O <sub>2</sub> :Sb <sub>0.08</sub>          |   | 4.15   | Null   | 156  |  |     |



Table 2 (Contd.)

| NC   | Active layer   | PCE (%)                            | Long-term stability  | Ref. |
|--|--|------------------------------------|--|------|
| SnO <sub>2</sub>                             | PBDR-T & ITIC-4  | 12.023                             | ①>90%, up to 75 h after exposure to an ambient atmosphere with continuous illumination; ②>95%, after storage in N <sub>2</sub> for 200 h with continuous illumination                                    | 157  |
|  | PM6:Y6   | 14.9                               | 81%, after 15 days stored in the air at RM without encapsulation   | 158  |
|  | PTB7-Th:PC <sub>71</sub> BM  | 10.30                              | Null   | 159  |
|  | PM7:ITC6-4F  | 13.93                              | Null   |      |
| Cl@SnO <sub>2</sub>                          | PM6:Y6   | 15.38                              | 94.3%, after 100 h light aging   |      |
|  | CsPbI <sub>3</sub> NCs   | 14.5                               | 80%, without encapsulation under 1-sun light soaking and 50% relative humidity for 8 h   | 27   |
| Ga:SnO <sub>2</sub><br>SnO <sub>2</sub>      | Cs <sub>0.05</sub> (MA <sub>0.17</sub> FA <sub>0.83</sub> ) <sub>0.95</sub> Pb(I <sub>0.83</sub> Br <sub>0.17</sub> ) <sub>3</sub> | 18.18                              | Null   | 161  |
|  | CsPbI <sub>3</sub> /FAPbI <sub>3</sub>   | 16.07                              | 96%, after 1000 h in ambient storage   | 162  |
|  | Cs <sub>x</sub> (MA <sub>0.17</sub> FA <sub>0.83</sub> ) <sub>(100-x)</sub> Pb(I <sub>0.83</sub> Br <sub>0.17</sub> ) <sub>3</sub> | 17.92                              | 89%, after 2500 h stored under 20 ± 5% RH  | 163  |
|  | MAPbI <sub>3</sub>   | 13.90<br>(flexible device)         | Null   | 164  |
|  | (CsPbI <sub>3</sub> ) <sub>0.04</sub> (FAPbI <sub>3</sub> ) <sub>0.82</sub> (MAPbBr <sub>3</sub> ) <sub>0.14</sub>                 | 20.34 ± 0.5                        | 90%, after 720 h storage   | 165  |
|  | Cs <sub>0.05</sub> (MA <sub>0.17</sub> FA <sub>0.83</sub> ) <sub>0.95</sub> Pb(I <sub>0.83</sub> Br <sub>0.17</sub> ) <sub>3</sub> | 20.79                              | Null   | 167  |
|  | FAPbI <sub>3</sub>   | 25.39<br>(0.0803 cm <sup>2</sup> ) | ①80% after 1000 h in ambient air at 25% RH and 25 °C without sealing; ②70.5% after 700 h light soaking; ③95% (encapsulated cell) after 100 h MPP tracking and 2 h dark recovery under ambient conditions | 168  |
|  |  | 23.3 (1 cm <sup>2</sup> )          | Null   |      |
|  |  | 21.7 (20 cm <sup>2</sup> )         | Null   |      |
|  |  | 20.6 (64 cm <sup>2</sup> )         | Null   |      |
| SnO <sub>2</sub> /TiO <sub>2</sub> (bilayer) | CsPbI <sub>2</sub> Br  | 15.86                              | ①~95%, after 1 month storage in N <sub>2</sub> glovebox without encapsulation; ②>80%, after 1 month stored under RT and 20–30% RH without encapsulation  | 169  |
| SnO <sub>2</sub> /InP–ZnS (bilayer)          | PM6:Y6   | 15.22                              | >80%, after 500 h in N <sub>2</sub> without encapsulation  | 170  |
| Ni:Co <sub>3</sub> S <sub>4</sub>            | N719   | 6.01                               | Null   | 171  |
|  |  | 6.82                               |  |      |
| NiCo <sub>2</sub> S <sub>4</sub>             |  | 7.43                               |  |      |
| Zn <sub>2</sub> SnO <sub>4</sub>             |  | 4.9 ± 0.2                          |  | 172  |
| Y:SrSnO <sub>3</sub>                         | FA <sub>0.85</sub> MA <sub>0.15</sub> Pb(I <sub>0.85</sub> Br <sub>0.15</sub> ) <sub>3</sub>                                       | 19.0                               | 91%, after 1000 h stored in N <sub>2</sub>   | 173  |

based NC-LHSCs,<sup>30,32,35,39,40,44,45,58,131–145</sup> PSCs,<sup>146</sup> and OSCs.<sup>147–149</sup> SnO NCs as ETL for DSSCs,<sup>150–156</sup> for OSCs,<sup>157–159</sup> and for PSCs,<sup>27,160–168</sup> have been demonstrated. Additionally, a bilayer of SnO<sub>2</sub>/TiO<sub>2</sub> (ref. 169) and SnO<sub>2</sub>/InP–ZnS<sup>170</sup> were used for PSCs and DSSCs. Ni-doped Co<sub>3</sub>S<sub>4</sub> and Co<sub>4</sub>S<sub>3</sub> and ternary sulphide NCs of NiCo<sub>2</sub>S<sub>4</sub> and Zn<sub>2</sub>SnO<sub>4</sub> have been used for DSSCs,<sup>171,172</sup> while

doped SrSnO<sub>3</sub> NCs for PSCs.<sup>173</sup> NCs have been used as IFL for NC-LHSCs,<sup>49,141,174–179</sup> OSCs,<sup>180–185</sup> DSSCs,<sup>186–195</sup> PSCs,<sup>196–212</sup> and Si solar cells.<sup>213–220</sup> FAPbBr<sub>3</sub> perovskite NCs have been used as a multifunctional luminescent-downshifting passivation layer for GaAs solar cells.<sup>221</sup>



Explored dopants (orange)  
Potential dopants (turquoise)

\* Lanthanide series  
\*\* Actinide series

Fig. 6 Summary of the explored and potential elements as dopants in  $\text{TiO}_2$ -based electron transporters for PSCs in the periodic table, as in 2017.<sup>253</sup> Copyright 2017, Wiley-VCH.

From the reported literature listed in Table 2, selenide NCs of CdSe, and doped sulfide NCs of  $\text{Ni}:\text{Co}_2\text{S}_4$ ,  $\text{Ni}:\text{Co}_4\text{S}_3$ , and  $\text{Ni}:\text{Co}_2\text{S}_4$  have shown their potential, suggesting more substitutes for traditional NC ETL. The advantages of NC ETL and some potential NCs suitable as ETLs are discussed in the following sections.

**2.2.2 Advantages of NC ETL.** Compared with common organic ETLs such as fullerenes ( $\text{C}_{60}/\text{C}_{70}$ ) and phenyl-C61-butyric acid methyl ester (PCBM), semiconductor NCs can easily overcome the shortcomings of poor stability, high cost, and unsuitable energy levels. In detail, PCBM film degrades at  $85^\circ\text{C}$ , indicating its thermal instability.<sup>110</sup> The cost of synthesis and purification for organic electron transport materials is higher than most semiconductor NCs.<sup>252</sup> Moreover, the semiconductor NCs can offer adjustable energy levels by easily

controlling the size. The above advantages strongly demonstrate that semiconductor NCs are a very good choice as efficient ETL in high-performance solar cells.

**2.2.3 Potential NC ETL.** Thanks to their unique application advantages in solar cells, NC ETLs have been widely used, boosting the devices to higher PCE and stability. More oxide and chalcogenide NCs as well as their doped congeners are anticipated alternatives. As we know,  $\text{TiO}_2$ NCs always act as splendid ETL in solar cells. The properties of  $\text{TiO}_2$ NCs can also be improved by doping, enhancing the device performance. As shown in Fig. 6, many elements were successfully doped in  $\text{TiO}_2$  as ETL for PSCs. Meanwhile, more elements are potential dopants for high-quality  $\text{TiO}_2$  and this suggests that there is much room for doped- $\text{TiO}_2$ NC ETL. Additionally, we reasonably

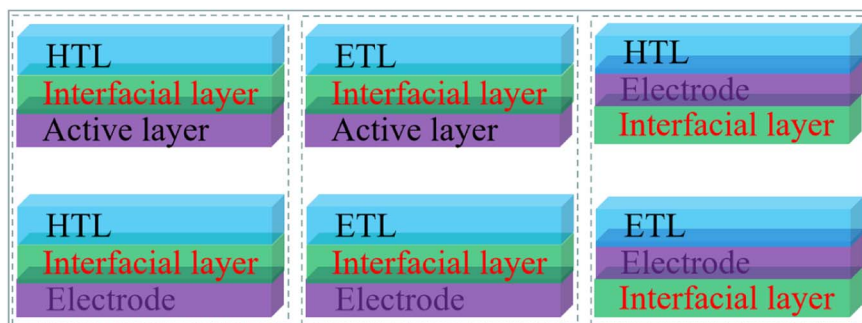


Fig. 7 Typical position sketch of interfacial layers in solar cells.

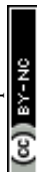


Table 3 Recent advances in selected NCIFLs

|   | IFL and its adjacent layers   | PCE (%) | Functions  | Ref. |
|---|---|---------|--|------|
| PbCdS   | TiO <sub>2</sub> /PbCdS/CdS   | 3.35    | Enhance light absorption; suppress interfacial recombination   | 174  |
| CdS + amine/ZnS   | TiO <sub>2</sub> :Al <sup>3+</sup> /CdS + amine/ZnS/<br>electrolyte/CuS   | 2.4     | Decrease electron–hole recombination   | 175  |
| Cu <sub>x</sub> S   | CIZS + mp-TiO <sub>2</sub> /electrolyte/Cu <sub>x</sub> S/<br>electrode   | 1.13    | Null   | 176  |
| CdSe  | ZnO/CdSe/PbS  | 7.9     | Suppress interface recombination; contribute additional photogenerated carriers                          | 141  |
| NiO   | PbS-EDT/NiO/Au  | 10.4    | Improve hole extraction efficiency; suppress the penetration of moisture and oxygen; good band alignment | 49   |
| PbS-EDT   | PbS-TBAI/PbS-EDT/P3HT   | 8.7     | Adjust the valence band; improve charge transfer   | 177  |
| CsPbBr <sub>3</sub>   | PbSe-MPA/CsPbBr <sub>3</sub> /Au  | 7.22    | Suppress carrier recombination   | 178  |
| ZnO   | Mg-doped ZnO/ZnO/PbS  | 7.06    | Decrease the interface recombination   | 179  |
| CdSe  | ZnO/CdSe/P3HT:PCBM  | 2.25    | Increase conductivity; electron transport and hole block   | 180  |
| CuInS <sub>2</sub> -ZnS   | TiO <sub>2</sub> /CuInS <sub>2</sub> -ZnS/PCDTBT:PC <sub>71</sub> BM  | 7.01    | Increase the electron extraction; reduce impedance   | 181  |
| CdSe  | P3HT:PCBM/CdSe/Al   | 3.08    | Down-conversion, reduce charge recombination   | 182  |
| ZnCdS   | TiO <sub>2</sub> /ZnCdS/PTB7:PC <sub>71</sub> BM  | 7.75    | Suppress the recombination; reduce the series resistance   | 183  |
| SnO <sub>2</sub>  | ITO/SnO <sub>2</sub> /ZnO   | 7.16    | Enhance optical transmission; reduce energy barrier; suppress carrier recombination                      | 184  |
| Ag <sub>2</sub> Se  | TiO <sub>2</sub> /Ag <sub>2</sub> Se/N719   | 5.89    | Null   | 186  |
| CdS   | TiO <sub>2</sub> /CdS/N719  | 7.54    | Suppress the charge recombination; increase the optical absorption                                       | 187  |
| CeO <sub>2</sub> :Eu <sup>3+</sup>  | N719/CeO <sub>2</sub> :Eu <sup>3+</sup> /electrolyte  | 8.36    | Down-convert UV light to visible light, light scattering   | 190  |
| NaGdF <sub>4</sub> :Eu <sup>3+</sup>  | FTO/TiO <sub>2</sub> /N719/electrolyte/Pt/FTO/<br>NaGdF <sub>4</sub> :Eu <sup>3+</sup>  | 9.34    | Act as luminescent down-conversion centers and light scatterers in the ultraviolet and visible domains   | 191  |
| CaCe <sub>2</sub> (MoO <sub>4</sub> ) <sub>4</sub> :Er <sup>3+</sup> /Yb <sup>3+</sup>                            | Electrolyte/CaCe <sub>2</sub> (MoO <sub>4</sub> ) <sub>4</sub> :Er <sup>3+</sup> /Yb <sup>3+</sup> /<br>Pt  | 7.78    | Convert the NIR and UV radiation to visible emissions  | 192  |
| NaYF <sub>4</sub> :20%Yb, 2%<br>Er@NaYF <sub>4</sub> :7%Eu  | N719/NaYF <sub>4</sub> :20%Yb,2%<br>Er@NaYF <sub>4</sub> :7%Eu/Pt   | 7.664   | Convert NIR and UV lights to visible lights  | 193  |
| SrF <sub>2</sub> :Pr <sup>3+</sup> -Yb <sup>3+</sup>  | FTO/SrF <sub>2</sub> :Pr <sup>3+</sup> -Yb <sup>3+</sup> /TiO <sub>2</sub> -N719  | 9.07    | Absorb blue light and emit green and red light   | 194  |
| BaWO <sub>4</sub> :Pr <sup>3+</sup>   | TiO <sub>2</sub> /BaWO <sub>4</sub> :Pr <sup>3+</sup> /N719   | 8.08    | Absorb UV light and emit blue, green, and red light  | 195  |
| MAPbBr <sub>0.9</sub> I <sub>2.1</sub>  | TiO <sub>2</sub> /MAPbI <sub>3</sub> /MAPbBr <sub>0.9</sub> I <sub>2.1</sub>  | 13.32   | Facilitate hole transfer from MAPbI <sub>3</sub> to HTL  | 196  |
| CuInS   | MAPbI <sub>3</sub> /CuInS/spiro-MeOTAD  | 13.8    | Enhance charge transfer; suppress charge recombination pathways  | 198  |
| MgO   | FTO/MgO/SnO <sub>2</sub>  | 18.23   | Smoother surface; less FTO surface defects; suppressed electron–hole recombination                       | 199  |
| CdS   | TiO <sub>2</sub> /CdS/MAPbI <sub>3</sub>  | 10.52   | Longer electron lifetime; lower charge carrier recombination rate  | 200  |
| SnO <sub>2</sub>  | PC <sub>61</sub> BM/SnO <sub>2</sub> /Al  | 19.7    | Block holes; enhance the conductivity; reduce the recombination  | 201  |
| Cl-SnO <sub>2</sub>   | FTO/Cl-SnO <sub>2</sub> /CsMAFAPbI <sub>3</sub> Br <sub>3-x</sub>   | 17.3    | Fill the pinholes; passivate the trapping defects  | 202  |
| FAPbX <sub>3</sub>  | MAPbI <sub>3</sub> /FAPbX <sub>3</sub> /C60   | 7.59    | Enhance absorption   | 203  |
| PbS   | MAPbI <sub>3</sub> /PbS/spiro-OMeTAD  | 19.24   | Enhance hole extraction; retard interfacial recombination; improve perovskite film morphology            | 204  |
| CuO <sub>x</sub>  | NiO <sub>x</sub> /CuO <sub>x</sub> /MAPbI <sub>3</sub>  | 19.91   | Lead higher transfer efficiency and lower carrier recombination  | 205  |
| MAPbBr <sub>0.9</sub> I <sub>2.1</sub>  | SnO <sub>2</sub> /MAPbBr <sub>3</sub> /MAPbBr <sub>0.9</sub> I <sub>2.1</sub>   | 20.21   | Optimize the energy level; improve hole extraction   | 206  |
| Co-CuGaO <sub>2</sub>   | Cs <sub>0.05</sub> (MA <sub>0.15</sub> FA <sub>0.85</sub> ) <sub>0.95</sub> Pb(I <sub>0.85</sub> Br <sub>0.15</sub> ) <sub>3</sub> /<br>Co-CuGaO <sub>2</sub> /spiro-OMeTAD | 20.39   | Reduce the energy gap; prevent direct contact between PVK and oxygen and moisture                        | 207  |
| MoS <sub>2</sub> :RGO   | MAPbI <sub>3</sub> /MoS <sub>2</sub> :RGO/spiro-OMeTAD  | 20.12   | Extract holes and block electrons  | 208  |
| CsCu <sub>5</sub> S <sub>3</sub>  | MAFAPbI <sub>3</sub> /CsCu <sub>5</sub> S <sub>3</sub> /spiro-OMeTAD  | 22.29   | Favor for energy levels; reduce carrier recombination  | 209  |
| Cu <sub>2-x</sub> S@SiO <sub>2</sub> @Er <sub>2</sub> O <sub>3</sub>  | TiO <sub>2</sub> /Cu <sub>2-x</sub> S@SiO <sub>2</sub> @Er <sub>2</sub> O <sub>3</sub> /MAPbI <sub>3</sub>  | 17.8    | Upconvert infrared light to visible light  | 210  |
| NaYF <sub>4</sub> :Yb <sup>3+</sup> ,Er <sup>3+</sup> /<br>@NaYF <sub>4</sub> :Yb <sup>3+</sup> ,Nd <sup>3+</sup> | IR-783 + NaYF <sub>4</sub> :Yb <sup>3+</sup> ,Er <sup>3+</sup> /<br>@NaYF <sub>4</sub> :Yb <sup>3+</sup> ,Nd <sup>3+</sup> + Au/<br>CsMAFAPbBrI                             | 20.5    | Convert IR to visible light, scatter light   | 212  |
| MoS <sub>2</sub>  | SiO <sub>x</sub> /MoS <sub>2</sub> /MoO <sub>x</sub>  | 22.8    | Provide electron-blocking and hole-extraction properties   | 213  |
| PbS   | PbS/c-Si solar cell   | 12.6    | Luminescent solar concentrator   | 214  |
| CdS   | Si solar cell/CdS   | 9.37    | Reduce the reflectance spectral ranging from 250 to 1100 nm, passivation, and down-conversion            | 216  |



Table 3 (Contd.)

|  | IFL and its adjacent layers                             | PCE (%)                               | Functions   | Ref. |
|--|---|---------------------------------------|---|------|
| $Zn_xCd_{1-x}S-ZnS:Mn$                 | Si solar cell/ $Zn_xCd_{1-x}S-ZnS:Mn$                   | $14.271 \pm 0.268$                    | Down-conversion   | 217  |
| $Cd_{0.5}Zn_{0.5}S-ZnS:Mn$             | Si solar cell/ $Cd_{0.5}Zn_{0.5}S-ZnS:Mn$               | 17.90                                 | Down-convert UV light of 250–450 nm to yellow-orange light at 583 nm  | 218  |
| $NaGdF_4:Ce@NaGdF_4:Nd/Yb@NaYF_4$      | c-Si solar cell/<br>$NaGdF_4:Ce@NaGdF_4:Nd/Yb@NaYF_4$   | 0.8 (under<br>254 nm<br>illumination) | Expand the spectrum of quantum cutting in the NIR   | 219  |
| $CsPbCl_{1.5}Br_{1.5}:Yb^{3+},Ce^{3+}$ | c-Si solar cell/ $CsPbCl_{1.5}Br_{1.5}:Yb^{3+},Ce^{3+}$ | 21.5                                  | Larger absorption cross-section, weaker electron-phonon coupling and higher inner luminescent quantum yield | 220  |

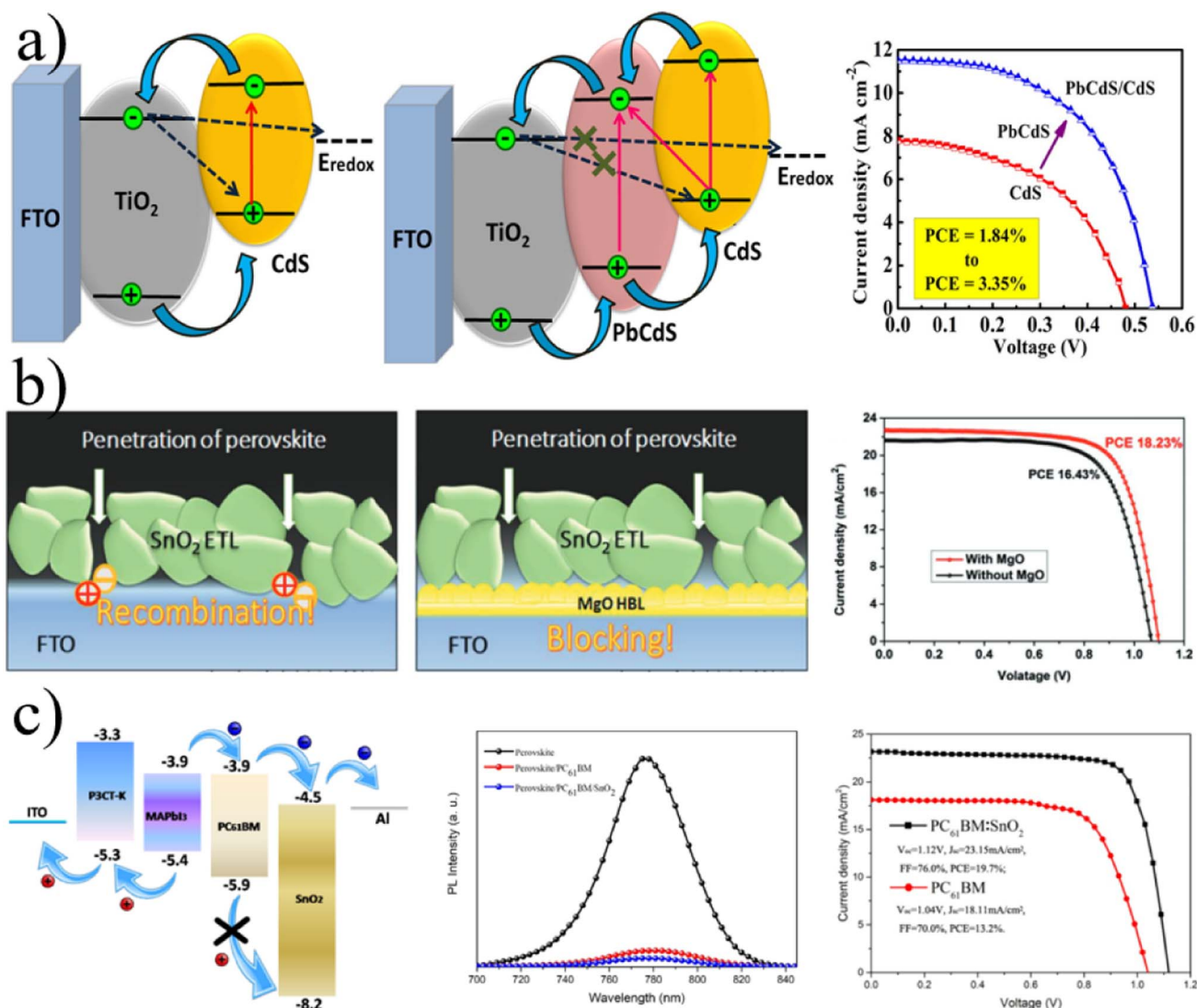


Fig. 8 (a) Schematic illustration of the possible electron transfer process in bare CdS and PbCdS/CdS based solar cells and  $J$ – $V$  curves of CdS and PbCdS/CdS based solar cells. (b) The perovskite can directly contact the FTO surface along a shunt pathway in the absence of SnO<sub>2</sub> ETLs; the MgO<sub>2</sub> layer can inhibit the penetration of perovskite reaching the FTO surface, and the best performance of the PSCs with and without MgO. (c) Corresponding energy level diagram of PSCs, steady-state PL spectra of the perovskite film deposited on the PC<sub>61</sub>BM layer and PC<sub>61</sub>BM:SnO<sub>2</sub> bilayer,  $J$ – $V$  characteristics in the illumination for the devices based on the PC<sub>61</sub>BM layer and PC<sub>61</sub>BM:SnO<sub>2</sub> bilayer. (a) Adapted with permission.<sup>174</sup> Copyright 2017, Elsevier. (b) Adapted with permission.<sup>199</sup> Copyright 2017, Wiley-VCH. (c) Adapted with permission.<sup>201</sup> Copyright 2018, American Chemical Society.



think this strategy is also applicable to other oxide NCs like  $\text{SnO}_2$  due to its comparable nature with  $\text{TiO}_2$ .

### 3. Nanocrystals as IFL

Besides HTL and ETL, another essential layer is the interfacial functional layer (IFL). Interfaces play a non-ignorable role in improving both PCE and stability through many paths. The position of a typical IFL is shown in Fig. 7. The IFL can be located at different positions in the solar cells to make different contributions. NCs IFL can enhance light absorption, decrease carrier recombination, improve charge transport ability, reduce impedance, convert ultraviolet (UV) or near-infrared (NIR) light to visible light, enhance optical transmission, decrease trap states of the active layer, and so on. Table 3 shows the recent advances of NC IFLs, and the detailed discussion is as follows.

#### 3.1 Suppressing recombination

As shown in Fig. 7, IFL is a separate layer between the charge transport layer/active layer or charge transport layer/electrode. So, it can convincingly act as a functional layer to prevent hole–electron recombination. Ternary semiconductor NCs of  $\text{PbCdS}$  were deposited on  $\text{TiO}_2$  as an IFL to impede the direct contact between ETL and the active layer of  $\text{CdS}$ , thus suppressing recombination efficiently and boosting the device PCE significantly (Fig. 8a). As the same, oxide NCs of  $\text{MgO}$  and  $\text{SnO}_2$

film inserted between ETLs and electrodes blocked holes and reduced recombination (Fig. 8b and c).<sup>199,201</sup>

#### 3.2 Charge transport improvement

As we know, charge transport ability inevitably affects the performance of solar cells. As shown in Fig. 9a,  $\text{MAPbBr}_{0.9}\text{I}_{2.1}$  NCs with good energy alignment enhance the hole transport ability and the PCE of the PSCs.  $\text{Co-CuGaO}_2$  NCs with  $\sim 20$  nm size were synthesized by hydrothermal method and used for surface passivation at the interface of perovskite and spiro-OMeTAD. Furthermore, the larger bandgap and lower valence band energy of  $\text{Co-CuGaO}_2$  reduced the energy gap between  $\text{Co-CuGaO}_2$  and perovskite. Considering that the reduced energy gap improved hole conduction and electron blocking, the PCE of PSCs was enhanced from 18.60% to 20.39%.<sup>207</sup>  $\text{MoS}_2$  NCs were also used to improve hole transport and the device PCE and stability (Fig. 9b).

#### 3.3 Light conversion and harvest enhancement

It is known that the active layer of recent solar cells cannot respond to the whole solar spectrum, resulting in energy loss and relatively low efficiency. Broadening the absorption of the active layer is an efficacious strategy to reduce energy loss and enhance the performance of solar cells.  $\text{CdS}$  NCs with general Stocks shifts were used in Si solar cells for spectral range

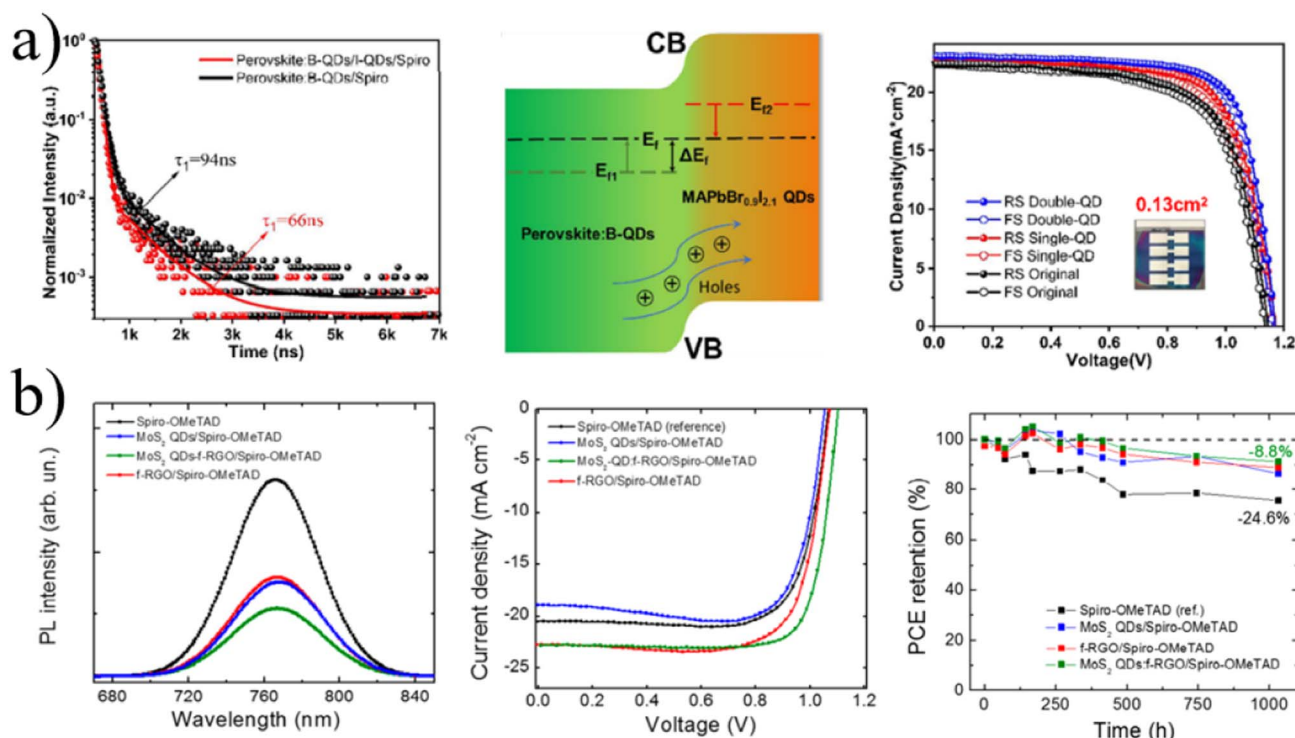
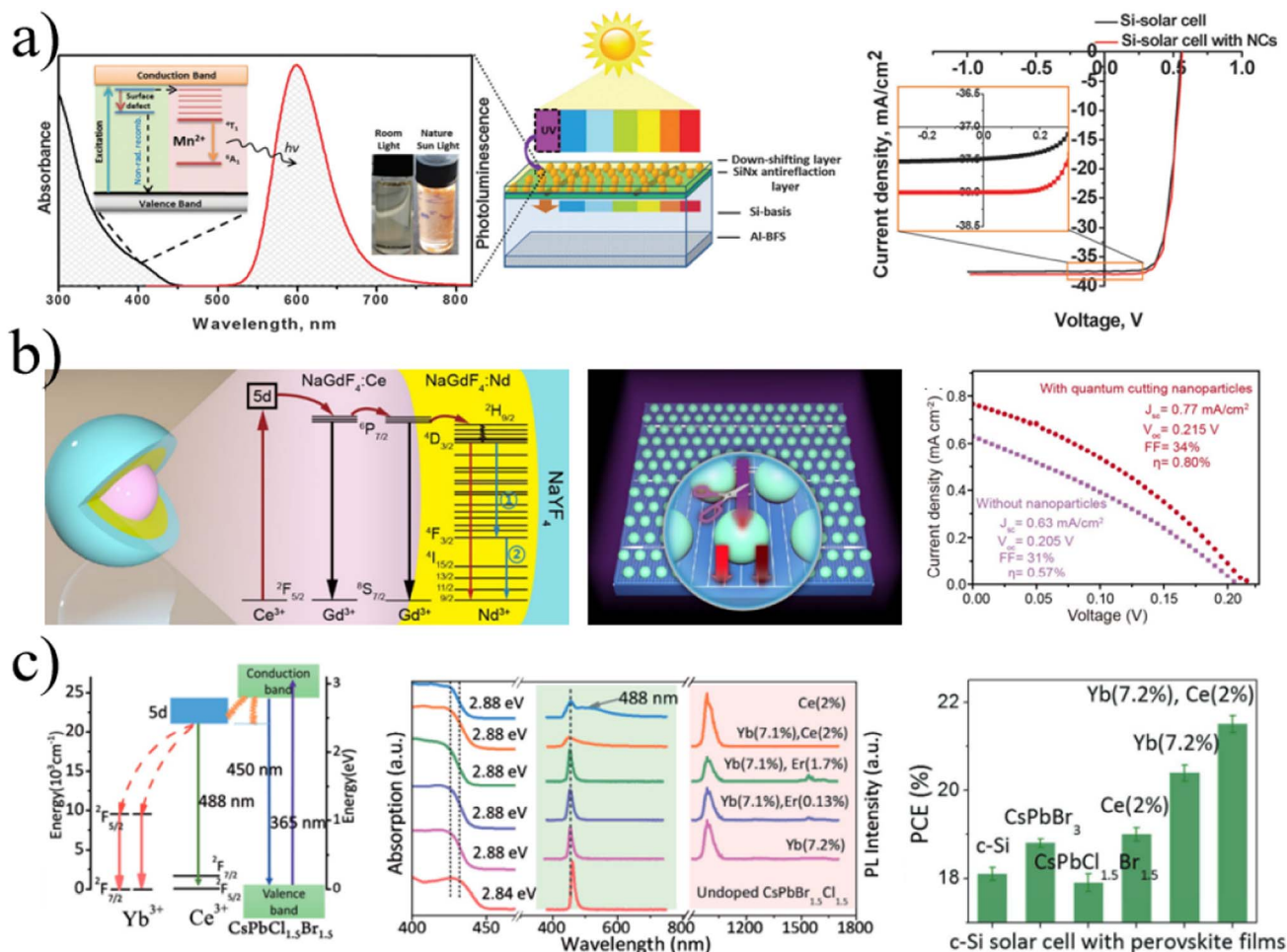


Fig. 9 (a) TRPL spectra of the perovskite film with and without  $\text{MAPbBr}_{0.9}\text{I}_{2.1}$  NCs, schematic diagram of band bending in the heterojunction structure formed by the perovskite and  $\text{MAPbBr}_{0.9}\text{I}_{2.1}$  NCs. (b) Steady-state PL measurements of  $\text{MAPbBr}_{0.9}\text{I}_{2.1}$  after the deposition of spiro-OMeTAD and different IFL/spiro-OMeTAD,  $I$ - $V$  characteristics of tested PSCs using different IFLs, normalized PCE trends vs. time extracted by  $I$ - $V$  characteristics under 1 sun illumination, periodically acquired during the shelf life test for the PSCs. (a) Adapted with permission.<sup>206</sup> Copyright 2020, American Chemical Society. (b) Adapted with permission.<sup>208</sup> Copyright 2018, American Chemical Society.





**Fig. 10** (a) Scheme of the down-shifting mechanism of the Zn<sub>0.5</sub>Cd<sub>0.5</sub>S:Mn (5%)/ZnS NC converter material and the design of proof-of-concept solar cell;  $J$ - $V$  curves of the corresponding solar cells. (b) Schematic and proposed energy transfer for Ce<sup>3+</sup>-sensitized quantum cutting in Nd<sup>3+</sup> ions; schematic design for boosting the energy-harvesting efficiency of c-Si solar cells with quantum cutting nanocrystals; comparison of current density-voltage characteristic for c-Si solar cells with and without a nanocrystal coating layer (the solar cells were illuminated with a 254 nm UV lamp at a power density of 7 mW cm<sup>-2</sup>). (c) Schematic diagram of energy transfer mechanism in the Yb<sup>3+</sup>, Ce<sup>3+</sup> codoped CsPbCl<sub>1.5</sub>Br<sub>1.5</sub>NCs, absorption; visible and near-infrared emission spectra of CsPbCl<sub>1.5</sub>Br<sub>1.5</sub> perovskite NCs codoping with different rare earth ions; PCE of Si solar cells with different perovskite NCs. (a) Adapted with permission.<sup>217</sup> Copyright 2016, the Royal Society of Chemistry. (b) Adapted with permission.<sup>219</sup> Copyright 2017, American Chemical Society. (c) Adapted with permission.<sup>220</sup> Copyright 2017, Wiley-VCH.

enhancement.<sup>216</sup> In Fig. 10a, we can see that Mn-doped NCs expand the spectral range response of solar cells by absorbing short-wave lights and emitting the characteristic light around 580 nm, suggesting a larger range of light harvesting by active layer and PCE improvement. Zn<sub>x</sub>Cd<sub>1-x</sub>S/ZnS:Mn<sup>2+</sup> NCs were also used to broaden the light response range of Si solar cells.<sup>217</sup> Furthermore, Mn-doped semiconductor NCs have a large Stokes shift, avoiding self-absorption and thus reducing energy loss. Sr<sub>2</sub>CeO<sub>4</sub> NCs with down-shifting properties could improve the stability of organic P3HT:PCBM solar cells without significant loss of short-circuit current.<sup>185</sup> Certainly, by using NCs with a Stokes shift for expanded light harvesting, the photoluminescence yield and other photoelectronic properties should keep the rules of high-performance solar cells.

Besides the above NCs, rare elements are good at light conversion due to their special energy levels. Undoped and doped NCs based on rare elements were massively applied to

broaden the light response in solar cells and efficiently boost the device performance. As seen in Fig. 10b and c, Yb<sup>3+</sup>, Ce<sup>3+</sup>, and Nd<sup>3+</sup> based NC layers efficiently convert light and enhance the device performance. Additionally, Eu<sup>3+</sup>, Er<sup>3+</sup>, and Pr<sup>3+</sup> were also used for efficient solar cells.

### 3.4 Energy level optimization

To ensure propitious charge transfer among the functional layers in solar cells, un-matched energy levels are a tricky issue that we need to address. One origin of the open-circuit voltage ( $V_{oc}$ ) loss of NC-LHSC, Si solar cells, PSCs, and OSCs is mainly analyzed quantitatively *via* the energy difference between bandgap and the Schokley-Queisser limit voltage.<sup>15</sup> For n-i-p solar cells, band alignment between the active layer and ETL directly limits the splitting of the quasi-Fermi level. For p-i-n solar cells, the band alignment between HTL and active layer has a great impact on the  $V_{oc}$ . The conduct band of recent HTL



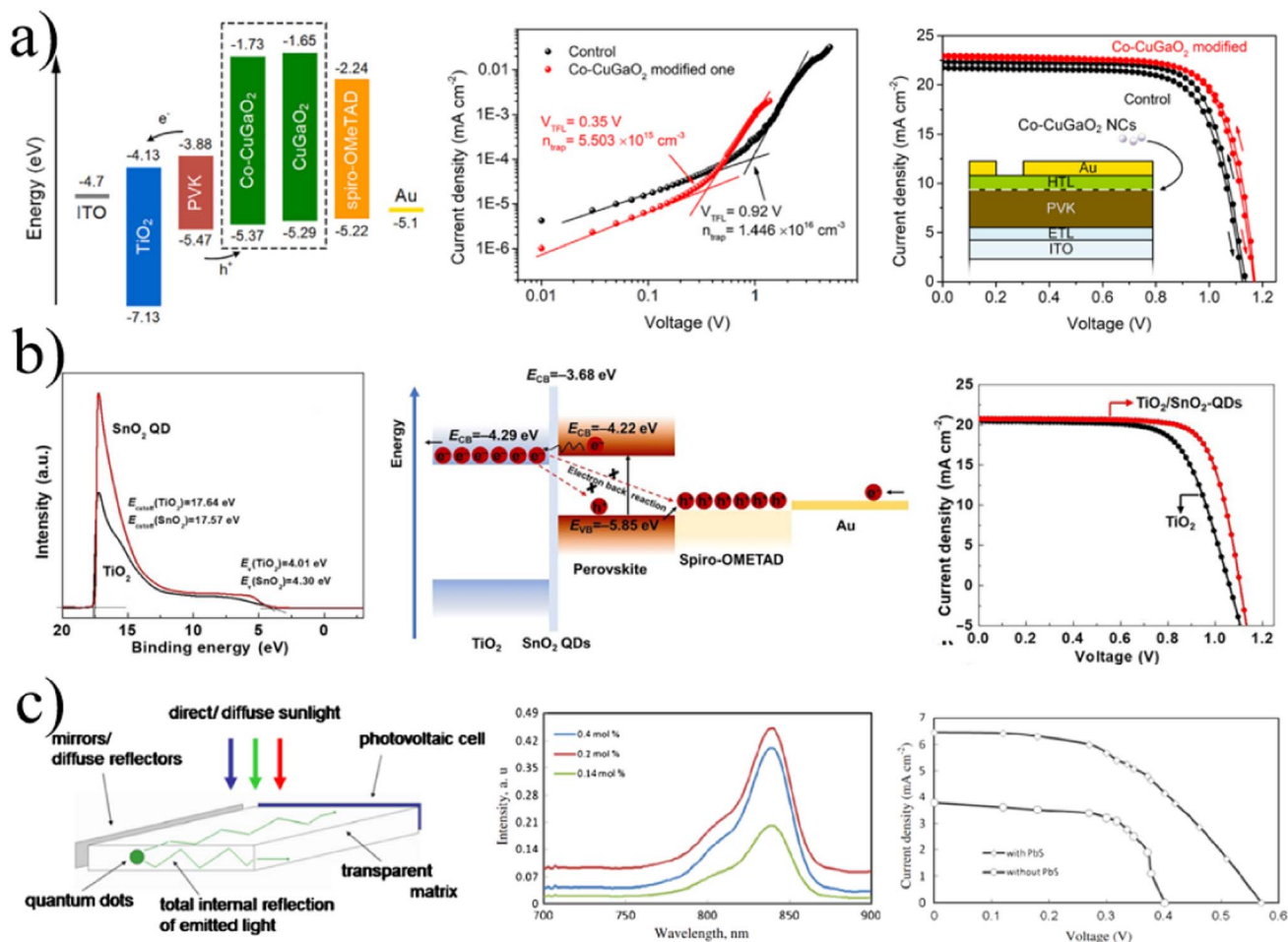


Fig. 11 (a) Energy level diagram of PSCs with the ITO/TiO<sub>2</sub>/PVK/Co-CuGaO<sub>2</sub>/Spiro-OMeTAD/Au structure, dark  $I-V$  curves of devices based on Spiro-OMeTAD and Co-CuGaO<sub>2</sub>/Spiro-OMeTAD, forward and reverse scan  $J-V$  curves based on Spiro-OMeTAD and Co-CuGaO<sub>2</sub>/Spiro-OMeTAD. (b) Band edge alignment and photocarrier dynamics in the resultant device. (c) Schematic illustration of an NC-luminescent solar concentrator, PL spectra of PbS NC-luminescent solar concentrator with different concentrations of PbS, and  $J-V$  curves for solar cells with and without PbS NC-luminescent solar concentrator. (a) Adapted with permission.<sup>207</sup> Copyright 2022, Elsevier. (b) Adapted with permission.<sup>202</sup> Copyright 2019, Elsevier. (c) Adapted with permission.<sup>215</sup> Copyright 2015, Springer.

is relatively deep, and the barrier for electron transport is not sufficient, resulting in electron leakage and reducing the device performance. Therefore, energy level is of great importance to improve the performance of solar cells. Shown in Fig. 11a and b, Co-doped CuGaO<sub>2</sub> and SnO<sub>2</sub>NCs film were used for energy level optimization for high-performance solar cells, illuminating the large potential of NCs as ITL for reducing  $V_{oc}$  loss of solar cells.

### 3.5 Concentrating luminescent solar radiation

Solar radiation is geographically extensive, but the energy density is not high. So, concentrating solar light for higher density is a feasible strategy to improve solar cell performance. PbS NC luminescent solar concentrator (LSC) was found to show potential advantages over silicon solar cell panels (Fig. 11c). They can reduce the size of solar cells and offer great flexibility in design, which results in cost reduction with any desired shape. One of the attractive LSCs is based on NCS.

### 3.6 Prevention

The main reason for unstable solar cells is the invasion of oxygen and water. IFL between the active layer and HTL, ETL, or electrode can arrest this invasion to a great degree and increase the stability of solar cells. The above-mentioned IFL of Co-CuGaO<sub>2</sub> NCs in Fig. 11a not only acts as a hole transport accelerator but also prevents the direct contact of perovskite with oxygen and moisture, boosting the stability of the PSCs.<sup>207</sup>

## 4. Nanocrystals as efficient additives

Besides an independent layer to improve the performance of solar cells, NCs have also been used as additives for boosting active layer quality, carrier transfer acceleration, spectral response broadening due to plasmonic effect, light conversion, light scattering/reflection, heat sinking, and some other functions. Table 4 lists the recent progress of NCs as efficient additives for high-performance solar cells.



Table 4 Recent advances in NC additives for high-performance solar cells

| NC   | Added layer  | NC additives and the mixture  | PCE (%)      | Functions  | Ref. |
|--|--------------|---|--------------|--|------|
| SnO <sub>2</sub> -Sb <sub>2</sub> O <sub>3</sub>   | Bottom ETL   | SnO <sub>2</sub> -Sb <sub>2</sub> O <sub>3</sub> + TiO <sub>2</sub>   | 7.7          | ①Improve the electron mobility and light harvesting; ②avoid the recombination  | 222  |
| PbS  |              | PbS + m-TiO <sub>2</sub>  | 5.04         | ①Enlarge the grain size of CsPbBr <sub>3</sub> perovskite film;  | 223  |
|  |              | PbS + TiO <sub>2</sub>  | 14.95        | ②suppress the activation of intrinsic trap sites of m-TiO <sub>2</sub><br>Downshift the conduction band of TiO <sub>2</sub> , promote the driving force of an electron injection | 227  |
| Cu-Zn-In-S-Se (CZISSe)   |              | CZISSe + mp-TiO <sub>2</sub> + CsPbBr <sub>3</sub>  | 5.37         | ①Enhance charge extraction;  | 225  |
| Ho <sup>3+</sup> -Yb <sup>3+</sup> -F <sup>-</sup> tri-doped TiO <sub>2</sub>                |              | Ho <sup>3+</sup> -Yb <sup>3+</sup> -F <sup>-</sup> tri-doped TiO <sub>2</sub> + TiO <sub>2</sub>                | 9.91 ± 0.3   | ②reduce charge recombination<br>Convert NIR light to green light   | 232  |
| Gd <sub>1.54</sub> Er <sub>0.46</sub> (MoO <sub>4</sub> ) <sub>3</sub> (GMO:Er)              |              | GMO:Er + TiO <sub>2</sub>   | 3.41         | Convert NIR light to the visible region (near 550 nm)  | 233  |
| β-NaYF <sub>4</sub> :Yb <sup>3+</sup> /Er <sup>3+</sup> /Sc <sup>3+</sup> @NaYF <sub>4</sub> |              | β-NaYF <sub>4</sub> :Yb <sup>3+</sup> /Er <sup>3+</sup> /Sc <sup>3+</sup> @NaYF <sub>4</sub> + TiO <sub>2</sub> | 20.19        | Convert NIR to red and green light   | 243  |
| SrAl <sub>2</sub> O <sub>4</sub> :Eu <sup>3+</sup>   |              | SrAl <sub>2</sub> O <sub>4</sub> :Eu <sup>3+</sup> + TiO <sub>2</sub>   | 4.64         | Elevation of the Fermi energy level of TiO <sub>2</sub> , improves light harvesting  | 245  |
| ZnS/Te   | Bottom HTL   | ZnS/Te + PEDOT:PSS  | 2.31         | Reduce series resistance, increase shunt resistance, improve mobility  | 230  |
| NaCsWO <sub>3</sub> @NaYF <sub>4</sub> @NaYF <sub>4</sub> :Yb,Er                             | Top HTL      | NaCsWO <sub>3</sub> @NaYF <sub>4</sub> @NaYF <sub>4</sub> :Yb,Er + spiro  | 18.28 ± 0.34 | ①Widen the perovskite spectral response range; ②increase the light reflection; ③ prolong the light path, and light absorption  | 231  |
| NaLuF <sub>4</sub> :Yb,Er@NaLuF <sub>4</sub>   |              | NaLuF <sub>4</sub> :Yb,Er@NaLuF <sub>4</sub> + PTAA   | 15.86        | Convert NIR light to visible light, scatter light  | 237  |
| Li(Gd,Y)F <sub>4</sub> :Yb,Er  | Active layer | Li(Gd,Y)F <sub>4</sub> :Yb,Er + spiro-MeOTAD  | 18.34        | Convert NIR to visible light   | 242  |
| SnO <sub>2</sub>   |              | SnO <sub>2</sub> + P3HT-PCBM  | 3.39         | Reduce the recombination   | 224  |
| Fe-doped SnO <sub>2</sub>  |              | Fe-doped SnO <sub>2</sub> + P3HT  | 3.04         | Extension of photogenerated exciton lifetime, overcome the burn-in regime faster   | 247  |
| NaYF <sub>4</sub> :Yb,Er/NaYF <sub>4</sub>   |              | NaYF <sub>4</sub> :Yb,Er/NaYF <sub>4</sub> + N719   | 9.15         | Convert NIR light to visible light (450–700 nm)  | 235  |
| TiO <sub>2</sub> :Sm <sup>3+</sup>   |              | TiO <sub>2</sub> :Sm <sup>3+</sup> + P25 + N719   | 5.31         | Convert UV to visible light  | 244  |
| SnS  |              | SnS + MAPbI <sub>3</sub>  | 14.26        | ①Provide more nucleation sites for the growth of perovskite grains; ② accelerate carrier transfer and reduce the recombination   | 226  |
| NaYF <sub>4</sub> :Yb/Er   |              | NaYF <sub>4</sub> :Yb,Er + MAPbI <sub>3</sub>   | 17.8         | Broaden the solar spectral use to NIR light, minimize the non-absorption energy loss   | 236  |
| IR-806-β-NaYF <sub>4</sub> :Yb,Er  |              | IR-806-β-NaYF <sub>4</sub> :Yb,Er + MAPbI <sub>3</sub> Er <sup>3+</sup> -Yb <sup>3+</sup> doped Zn              | 17.49        | Convert NIR light (800–1000 nm) to visible emissions   | 238  |
| Ho <sup>3+</sup> -Yb <sup>3+</sup> -Li <sup>+</sup> -doped TiO <sub>2</sub>                  |              | Ho <sup>3+</sup> -Yb <sup>3+</sup> -Li <sup>+</sup> -doped TiO <sub>2</sub> + FAMAPbBrI <sub>3</sub>            | 16.88 ± 0.5  | Convert NIR to visible light, improve electron injection efficiency, and decrease recombination  | 240  |
| β-NaYF <sub>4</sub> :Yb <sup>3+</sup> ,Tm <sup>3+</sup> @TiO <sub>2</sub>                    |              | β-NaYF <sub>4</sub> :Yb <sup>3+</sup> ,Tm <sup>3+</sup> @TiO <sub>2</sub> + MAPbI <sub>3</sub>                  | 16.27        | Convert NIR to visible light, serve as the light scatter centers   | 241  |

#### 4.1 Active layer quality improvement and carrier transfer accelerator

The performance of solar cells largely depends on the quality of the active layer, such as the purity of Si for Si solar cells and the composition of perovskite for PSCs. For example, defects unavoidably exist at the surface of perovskite thin film during

the low-temperature fabrication process, and reducing defects is a very useful way to improve the performance of PSC.<sup>254</sup> This subsection discusses NCs as outstanding additives in the active layer for boosting its quality and carrier transfer acceleration.

SnO<sub>2</sub>-Sb<sub>2</sub>O<sub>3</sub> NCs were used to modify TiO<sub>2</sub> nanorod arrays for electron mobility improvement and electron transport



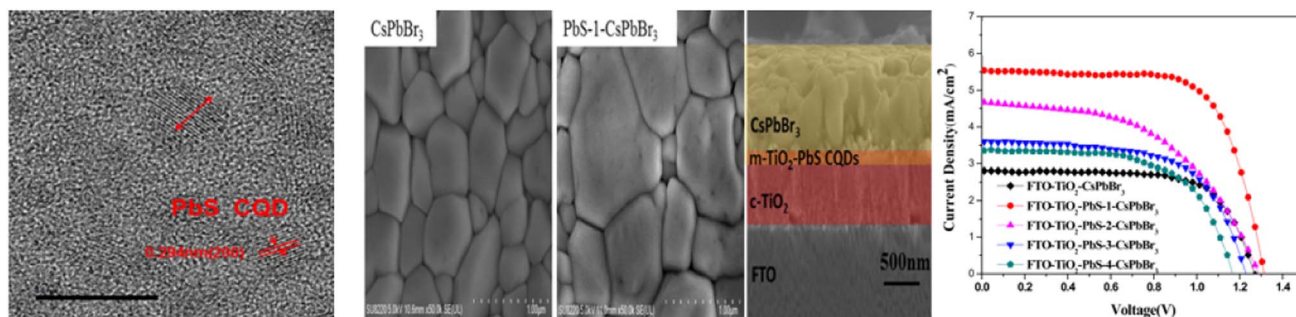


Fig. 12 Top-view and cross-section images of CsPbBr<sub>3</sub> film decorated with PbS NCs, and J–V curves of all-inorganic PSCs based on different TiO<sub>2</sub>/PbS photoanodes. Adapted with permission.<sup>243</sup> Copyright 2019, American Chemical Society.

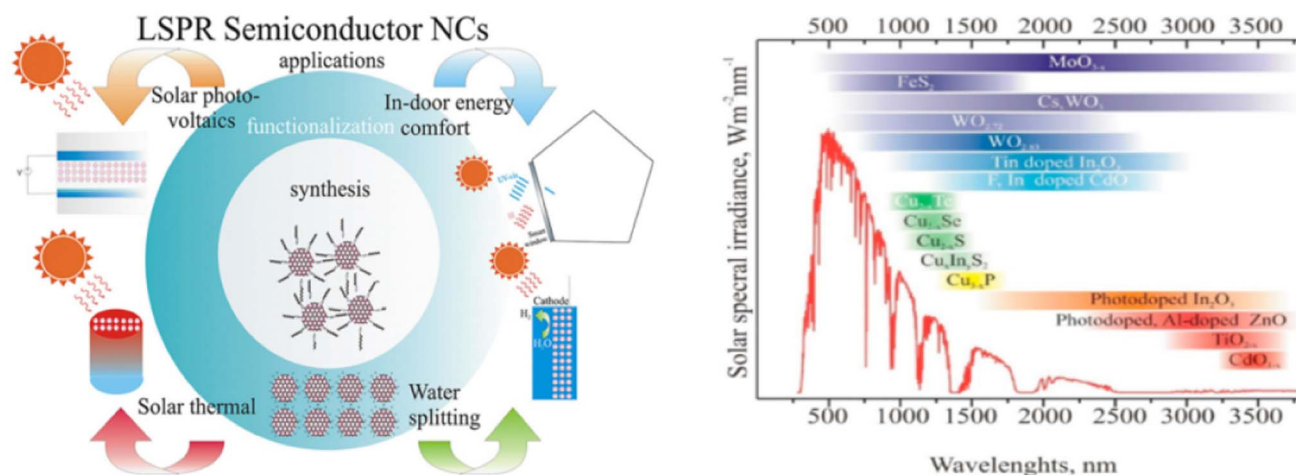


Fig. 13 Schematic of the applications of LSPR semiconductor NCs; the solar spectrum and its relevancy for energy-targeted applications of LSPR semiconductor NCs via their tunable plasmon absorbance. Adapted with permission.<sup>255</sup> Copyright 2021, Elsevier.

resistance reduction. This NCs modified ETL enhanced the PCE of CH<sub>3</sub>NH<sub>3</sub>PbI<sub>3-x</sub>Cl<sub>x</sub> PSC from 6.5% to 7.7%.<sup>222</sup> PbS NCs suppress the activation of the intrinsic trap sites, provide nucleation sites to enlarge the grain size, and suppress the charge combination in CsPbBr<sub>3</sub> PSCs (Fig. 12).<sup>223</sup> Adding SnO<sub>2</sub> NCs of size around 5 nm into the active layer of P3HT:PC<sub>61</sub>BM made electrons more easily pass through the active layer and accelerate the electron transfer, improving the PCE of OSC from 2.67% to 3.39%.<sup>224</sup> S<sub>2</sub>O<sub>3</sub><sup>2-</sup>-capped Cu–Zn–In–S–Se NCs with ~5 nm size was introduced in the perovskite precursor of PbBr<sub>2</sub> solution to boost 22.6% enhancement of the PCE of inorganic Cs-based PSCs, which was due to promoted crystallization of CsPbBr<sub>3</sub> and hole extraction.<sup>225</sup> SnS NCs with an average size of 6.9 nm were implanted into the active layer of carbon-based HTL-free mesoporous PSCs, and the device gained a high PCE of 14.26% with a 12.42% improvement. This improvement was demonstrated by more nucleation sites for the growth of perovskite grains and the accelerated carrier transfer.<sup>226</sup> PbS NCs doped TiO<sub>2</sub> nanotubes (TNTs) modified the electronic and optical properties by downshifting the conduction band of TiO<sub>2</sub> ETL from –4.22 to –4.58 eV and promoting the driving force of an electron injection to the conductive electrode.<sup>227</sup>

#### 4.2 Plasmonic Effect

Semiconductor NCs have exhibited localized surface plasmon resonances (LSPR), and this plasmonic effect has been used in many fields, such as solar photovoltaics, in-door energy comfort, water splitting, and so on (Fig. 13). Compared with traditional LSPR materials (noble metals), the semiconductor LSPR NCs allow a wide range of wavelength tunability from visible towards near-infrared (NIR) and further to mid-IR, leading to larger absorption of solar light. Higher absorption of the active layer in solar cells increases the current intensity and thus, the device performance. DSSCs based on plasmonic effect by ZnO or SnO<sub>2</sub> and TiO<sub>2</sub>/SnO<sub>2</sub> have been investigated.<sup>254</sup> From Fig. 13, it can be seen that different oxides, sulfides, and selenides such as MoO<sub>3-x</sub>, Cs<sub>x</sub>WO<sub>3</sub>, TiO<sub>2-x</sub>, CdO<sub>1-x</sub>, doped In<sub>2</sub>O<sub>3</sub>, doped ZnO, Cu<sub>2-x</sub>S, Cu<sub>x</sub>In<sub>y</sub>S<sub>2</sub>, Cu<sub>2-x</sub>Se, *etc.* broaden the response spectra from 500 nm to nearly 3800 nm. Effective light harvesting due to the plasmonic effect shows great potential in solar cell application. Given the limited self-absorption bands of solar cells, the above oxide and sulfide NCs can be applied as additives to widen the light harvesting range. Clearly, this will reduce energy loss and raise the device performance in a considerable way.



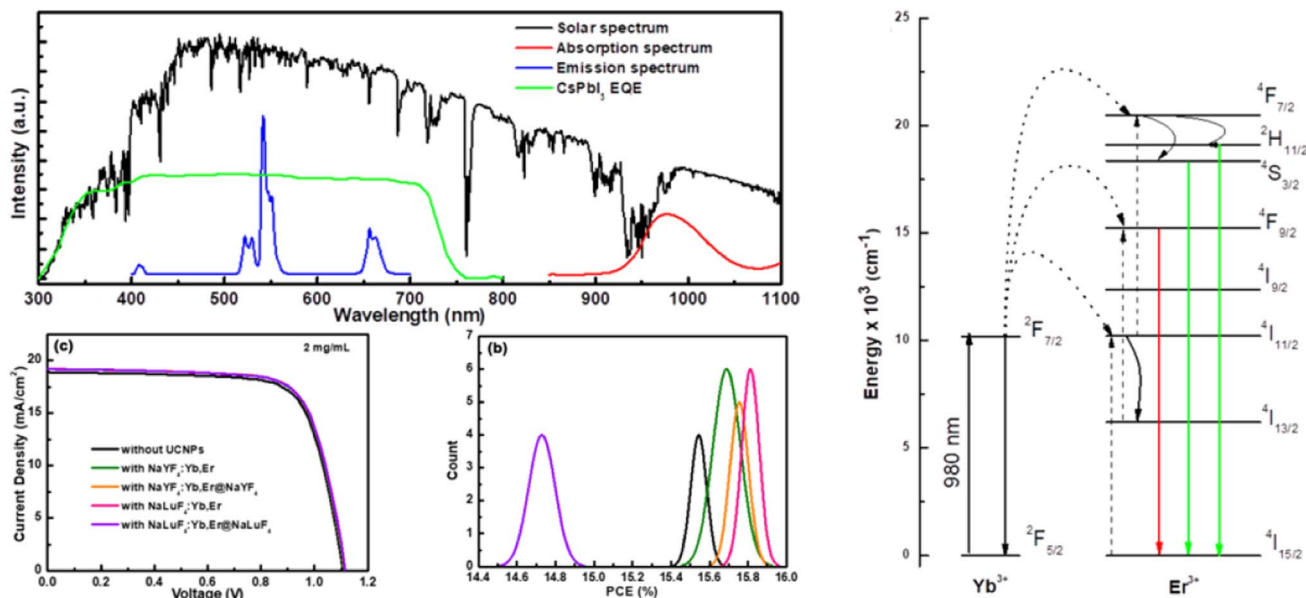


Fig. 14 Solar spectrum, absorption and emission spectrum of up-conversion nanocrystals and EQE curve of  $\gamma$ -CsPbI<sub>3</sub> PSC,  $J$ - $V$  curves of PSCs based on different nanocrystals, and statistical PCE distribution histograms of 30 devices, schematic energy diagram for Yb<sup>3+</sup> and Er<sup>3+</sup>. Adapted with permission.<sup>237</sup> Copyright 2019, American Chemical Society.

### 4.3 Light conversion

As discussed in Section 3, light conversion is an efficient way to boost the PCE and stability of solar cells. Based on this point, NC light-converting layers were investigated in the previous part. It is also true that light conversion can be realized by NC additives, which will be summarized in this part.

**4.3.1 Up-conversion.** Rare-earth (RE) elements are famous for light up-conversion and further application in solar cells. RE element-doped semiconductor NCs have been added as additives in active layers and charge transport layers for high-performance DSSCs and PSCs. NIR lights were up-converted to visible lights and thus elevated the device PCE due to wider solar radiation absorption (Fig. 14). The RE element-based NCs, which can be used in up-converting materials as additives in solar cells, mainly contain Yb, Er, Ho, and Sc doped materials like Ho–Yb–F doped TiO<sub>2</sub>, Er–Yb doped ZnO<sub>2</sub>, Ho–Yb doped Gd<sub>2</sub>O<sub>3</sub>, Yb–Er doped NaYF<sub>4</sub> and Yb–Er doped Li(Gd,Y)F<sub>4</sub>. As shown in Fig. 14, the schematic energy diagram for Yb<sup>3+</sup> and Er<sup>3+</sup> are suitable for up-conversion and the related solar cells gain high efficiency. The up-conversion NCs can be added in the active layer, ETL, and HTL in different solar cells like OSC, DSSC, and PSC. The original active layers cannot absorb the whole range of sunlight and thus result in energy loss. After assembling NCs with up-conversion ability, the non-responsive long-wavelength range of sunlight will be converted to shorter wavelengths and absorbed by active layers to re-generate hole-electron pairs. This strategy can enhance the utilization of the infrared range of sunlight and the performance of solar cells.

**4.3.2 Down-conversion and down-shifting.** Down-conversion and down-shifting NCs are advantageous for high-performance solar cells due to the efficient utilization of UV lights. Typical Sm<sup>3+</sup>-based TiO<sub>2</sub>NCs were used in DSSCs and obvious improvement of PCE was gained (Fig. 15) through

converting ultraviolet to visible light. Better performance of solar cells was obtained by means of down-converting NCs such as ZnS:Er in Si-based devices and CeO<sub>2</sub>:Gd in OSC.<sup>249,250</sup> The shortest wavelength response by perovskite is about 400 nm.<sup>256</sup> The energy of sunlight with wavelengths shorter than 400 nm will be wasted. Furthermore, the UV lights can damage the perovskite or organic active layer and reduce the device stability. So, the PCE and light stability of solar cells can be increased by using down-conversion or down-shifting NCs.

### 4.4 Light scattering and reflection

Light scattering and reflection are well-known for boosting the optical absorption of different solar cells. TiO<sub>2</sub>:Zn NCs can scatter light and promote the performance of conventional DSSCs.<sup>257</sup> Due to the ultralow (<1%) photoluminescence quantum yield, NaLuF<sub>4</sub>:Yb,Er@NaLuF<sub>4</sub>NCs acted as scattering centers and extended the sunlight optical path by combining scattering and reflecting sunlight.<sup>237</sup> NaYF<sub>4</sub>:Yb<sup>3+</sup>,Tm<sup>3+</sup> NCs serve as scatter centers to enhance light harvesting for PSCs.<sup>241</sup> We can conclude that NCs are good at light absorption enhancement due to light scattering and reflecting, and this is an available approach for improving the device performance.

### 4.5 Heat sinks

Except for optical management, heat control is also important for solar cell operation because elevated temperatures may increase energy loss and destroy the devices. In the traditional photovoltaic/thermal (PV/T) system, the temperature of thermal energy is always limited by the operation temperature of PV cells. The oleylamine solution of Cu<sub>9</sub>S<sub>5</sub>NCs was adopted in the spectral splitting filter to harvest the moderate-temperature heat. After successful thermal energy collection, the maximum



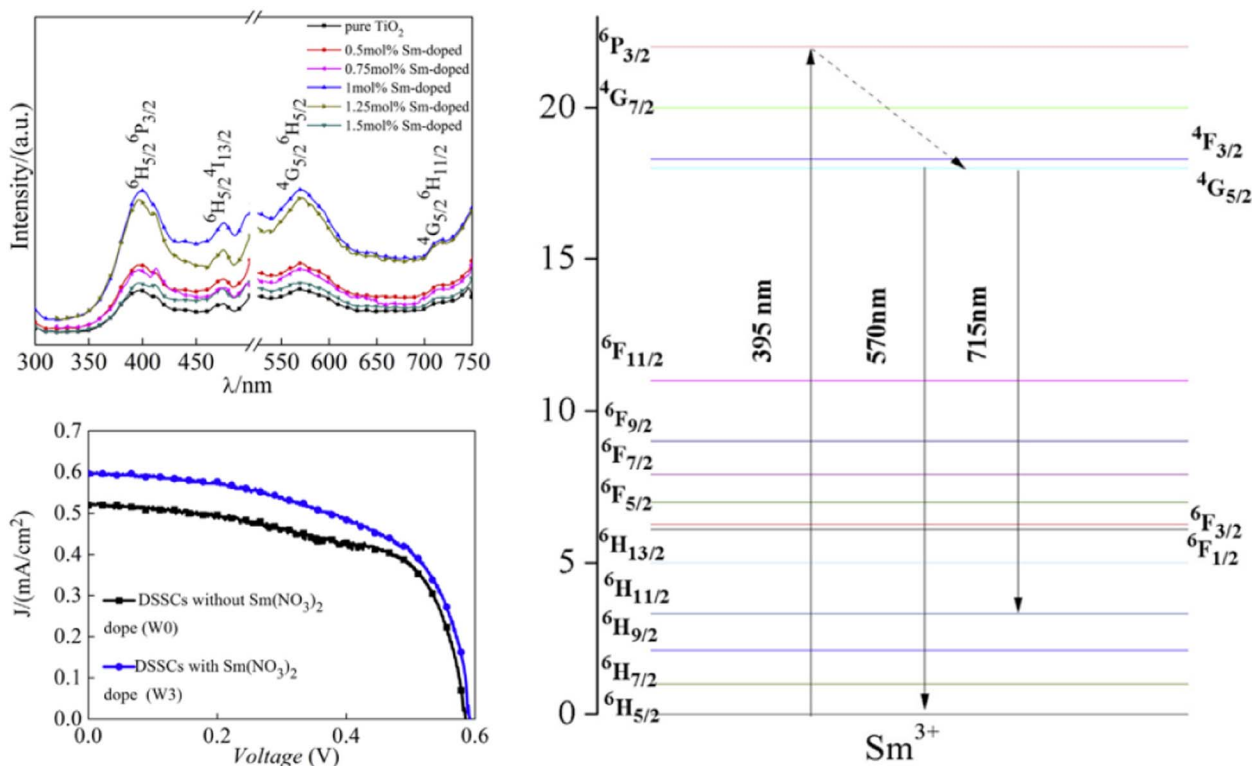


Fig. 15 Excitation spectrum ( $\lambda_{em} = 567$  nm) and emission spectrum ( $\lambda_{ex} = 395$  nm) of  $\text{TiO}_2:\text{Sm}^{3+}$  NCs with different  $\text{Sm}^{3+}$  doping concentrations, and schematic energy-level diagrams to show the details of down-conversion mechanisms *via* excitation using 395 nm radiation for  $\text{TiO}_2:\text{Sm}^{3+}$  NCs. Adapted with permission.<sup>244</sup> Copyright 2016, Elsevier.

overall efficiency of the present PV/T collector is 34.2%, with a 17.9% improvement.<sup>258</sup> In a concentrator photovoltaic nanocrystal-phase change material (PCM) hybrid system,  $\text{Al}_2\text{O}_3$ ,  $\text{CuO}$ , and  $\text{SiO}_2$  were used to save energy and offer safe operating conditions. Compared with pure PCM (0 wt%),  $\text{Al}_2\text{O}_3$ -PCM at 5 wt% increased the thermal conductivity, and the melting rate reduced the solar cell temperature. The electrical efficiency was improved from 6.36% to 8% and gained temperature uniformity from 20 °C to 12 °C. This strategy would be recommended for residential and industrial applications in solar cells.<sup>259</sup>

#### 4.6 Other functions

ZnTe NCs with an average of 2.96 nm in the active layer demonstrated increased photo-generation and improved efficiency by reduced series resistance and improved mobility.<sup>230</sup> Fe-doped  $\text{SnO}_2$  NCs incorporated into the active layer of P3HT:PCBM improved the  $J_{sc}$  of OSC due to the extension of photogenerated exciton lifetime as a result of the magnetic field. Meanwhile, these NC-reinforced devices showed the tendency to overcome the burn-in regime faster and indicated the diluted magnetic semiconductor NCs had the potential to increase the stability of the devices.<sup>247</sup>

## 5. Summary and outlook

In recent years, NCs as functional layers and additives have been widely used in solar cells, significantly enhancing their

performance. Here, we summarize NCs-based HTL, ETL, IFL, and additives for solar cells. NCs can boost the device performance in many ways, such as increasing the charge transport ability, suppressing charge recombination, broadening light harvest, and so on.

Based on previous investigations, we propose some promising strategies to enhance the performance of solar cells by using NCs.

(I) Optical management. Full spectrum absorption under low-cost conditions: both up-converting and down-shifting materials. For down-shifting, doped NCs with large Stokes shift, such as Mn or Cu doped NCs, have great potential due to no self-absorption, facile synthesis, and low cost.  $\text{Cu}^+$ ,  $\text{Ag}^+$  doped n-type metal oxide NCs,<sup>260</sup>  $\text{Fe}_{1-x}\text{S}_2$  NCs,<sup>261</sup> and In doped  $\text{Cu}_x\text{S}$  NCs,<sup>262</sup> with great potential for spectra broadening are also suggested for high-performance solar cells.  $\text{CaMoO}_4:\text{Er}^{3+}, \text{Yb}^{3+}$  NCs would offer great potential for conserving energy in Si solar cells.<sup>263</sup> Certainly, the photoluminescence efficiency of NCs is very important when they are used to convert light in solar cells. Excellent optical management of solar cells can utilize more sunlight and improve the device performance.

(II) Electronic optimization. The charge transfer ability is mainly determined by the electronic properties of charge transport materials. The performance of solar cells can be improved by electronic optimization. One approach is a component change of materials such as n doping for n-type NCs and p doping for p-type NCs. Finding more suitable dopants for NCs will further boost the PCE and stability of solar



cells. Meanwhile, the size and ligand control of NCs are also considered to optimize their electronic properties and fabricate better-performance solar cells.

(III) Interface engineering. Interfacial layers between different functional layers show different functions in solar cells. In further developments, more NCs IFL will be used to improve device performance by preventing direct contact between the active layer and charge transport layer, impeding the entry of water and oxygen, and protecting and destroying the active layer with UV lights.<sup>264</sup> So, NC IFL, with good photo-electronic properties, can adjust energy alignment, accelerate charge transport, enhance light harvest, and protect the active layer.

(IV) Cross utilization. The metal-organic framework (MOF) materials can improve the efficiency and stability of solar cells due to their unique properties.<sup>265</sup> NCs with small sizes can be considered to mix with MOF and enhance the performance of devices. In addition, NCs can be utilized as light harvesters, HTL, ETL, and IFL, so we suggest their application in all-NC solar cells.

## Conflicts of interest

The authors declare no conflict of interest.

## Acknowledgements

This work was supported by the Natural Science Foundation of the Guizhou Province (No. 2071). The authors thank Prof. Ma Wanli, Liu Zeke, and Dr Lu Huiyuan at Soochow University for their helpful discussion and suggestions for improving the manuscript.

## References

- 1 I. J. Kramer and E. H. Sargent, The architecture of colloidal quantum dot solar cells: Materials to devices, *Chem. Rev.*, 2014, **114**, 863.
- 2 G. H. Carey, A. L. Abdelhady, Z. Ning, S. M. Thon, O. M. Bakr and E. H. Sargent, Colloidal quantum dot solar cells, *Chem. Rev.*, 2015, **115**, 12732.
- 3 K. R. Ryan, M. P. Down, N. J. Hurst, E. M. Keefe and C. E. Banks, Additive manufacturing (3D printing) of electrically conductive polymers and polymer nanocomposites and their applications, *eScience*, 2022, **2**, 365–381.
- 4 M. J. Yuan, M. X. Liu and E. H. Sargent, Colloidal quantum dot solids for solution-processed solar cells, *Nat. Energy*, 2016, **1**, 16016.
- 5 J. H. Jing, Y. J. Dou, S. H. Chen, K. Zhang and F. Huang, Solution sequential deposited organic photovoltaics: From morphology control to large-area modules, *eScience*, 2023, **3**, 100142.
- 6 Z. K. Liu, J. Y. Yuan, S. A. Hawks, G. Z. Shi, S.-T. Lee and W. L. Ma, Photovoltaic devices based on colloidal PbX quantum dots: Progress and prospects, *Sol. RRL*, 2017, **1**, 1600021.
- 7 Z. X. Pan, H. S. Rao, I. Mora-Seró, J. Bisquert and X. H. Zhong, Quantum dot-sensitized solar cells, *Chem. Soc. Rev.*, 2018, **47**, 7659–7702.
- 8 S. Aftab, M. Z. Iqbal, S. Hussain, F. Kabir, A. A. Al-Kahtani and H. H. Hegazy, Quantum junction solar cells: Development and prospects, *Adv. Funct. Mater.*, 2023, **33**, 2303449.
- 9 A. Shrestha, M. Batmukh, A. Tricoli, S. Qiao and S. Dai, Near-infrared active lead chalcogenide quantum dots: Preparation, post-synthesis ligand exchange, and applications in solar cells, *Angew. Chem., Int. Ed.*, 2019, **58**, 5202–5224.
- 10 A. O. El-Ballouli, O. M. Bakr and O. F. Mohammed, Compositional, processing, and interfacial engineering of nanocrystal-and quantum-dot-based perovskite solar cells, *Chem. Mater.*, 2019, **31**, 6387–6411.
- 11 G. S. Selopal, H. Zhao, Z. M. Wang and F. Rosei, Core/shell quantum dots solar cells, *Adv. Funct. Mater.*, 2020, **30**, 1908762.
- 12 J. Y. Yuan, A. Hazarika, Q. Zhao, X. F. Ling, T. Moot, W. L. Ma and J. M. Luther, Metal halide perovskite in quantum dot solar cells: Progress and prospect, *Joule*, 2020, **4**, 1160–1185.
- 13 F. G. Zhou, Z. Z. Li, H. Y. Chen, Q. Wang, L. M. Ding and Z. W. Jin, Application of perovskite nanocrystals (NCs)/ quantum dots (QDs) in solar cells, *Nano Energy*, 2020, **73**, 104757.
- 14 M. Albaladejo-Siguan, E. C. Baird, D. Becker-Koch, Y. X. Li, A. L. Rogach and Y. Vaynzof, Stability of quantum dots solar cells: A matter of (life) time, *Adv. Energy Mater.*, 2021, **11**, 2003457.
- 15 J. W. Liu, K. H. Xian, L. Ye and Z. H. Zhou, Open-circuit voltage loss in lead chalcogenide quantum dot solar cell, *Adv. Mater.*, 2021, **33**, 2008115.
- 16 S. Liang, M. Y. Zhang, M. Biesold, W. Choi, Y. J. He, Z. L. Li, D. F. Shen and Z. Q. Lin, Recent advances in synthesis, properties, and applications of metal halide perovskite nanocrystals/polymer nanocomposites, *Adv. Mater.*, 2021, **33**, 2005888.
- 17 T. Kim, S. Lim, S. Yun, S. Jeong, T. Park and J. Choi, Design strategy of quantum dot thin-film solar cells, *Small*, 2020, **16**, 2002460.
- 18 T. Blachowicz and A. Ehrmann, Recent development of solar cells from PbS colloidal quantum dots, *Appl. Sci.*, 2020, **10**, 1743.
- 19 Y. Liu, G. Z. Shi, Z. K. Liu and W. L. Ma, Toward printable solar cells based on PbX colloidal quantum dot inks, *Nanoscale Horiz.*, 2021, **6**, 8–23.
- 20 Y. Liu, F. Li, G. Z. Shi, Z. K. Liu, X. F. Lin, Y. Shi, Y. F. Chen, X. Meng, Y. Lv, W. Deng, X. Q. Pan and W. L. Ma, PbSe quantum dot solar cells based on directly synthesized semiconductive inks, *ACS Energy Lett.*, 2020, **5**, 3797–3803.
- 21 Y. Li, F. Yang, Y. J. Wang, G. Z. Shi, Y. M. Maung, J. Y. Yuan, S. J. Huang and W. L. Ma, Magnetron sputtered SnO<sub>2</sub> constituting double electron transport layers for efficient PbS quantum dot solar cells, *Sol. RRL*, 2020, **4**, 2000218.



- 22 Y. N. Zhang, Y. Y. Kan, K. Gao, M. F. Gu, Y. Shi, X. L. Zhang, Y. Xue, X. N. Zhang, Z. K. Liu, Y. Zhang, J. Y. Yuan, W. L. Ma and A. K.-Y. Jen, Hybrid quantum dot/organic heterojunction: A route to improve open-circuit voltage in PbS colloidal quantum dot solar cells, *ACS Energy Lett.*, 2020, 5, 2335–2342.
- 23 J. Khan, X. L. Zhang, J. Y. Yuan, Y. Wang, G. Z. Shi, R. Patterson, J. W. Shi, X. F. Ling, L. Hu, T. Wu, S. Y. Dai and W. L. Ma, Tuning the surface-passivating ligand anchoring position enables phase robustness in CsPbI<sub>3</sub> perovskite quantum dot solar cells, *ACS Energy Lett.*, 2020, 5, 3322–3329.
- 24 X. F. Ling, J. Y. Yuan, X. L. Zhang, Y. L. Qian, S. M. Zakeeruddin, B. W. Larson, Q. Zhao, J. W. Shi, J. C. Yang, K. Ji, Y. N. Zhang, Y. J. Wang, C. Y. Zhang, S. Duhm, J. M. Luther, M. Grätzel and W. L. Ma, Guanidinium-assisted surface matrix engineering for highly efficient perovskite quantum dot photovoltaics, *Adv. Mater.*, 2020, 32, 2001906.
- 25 K. Ji, J. B. Yuan, F. C. Li, Y. Shi, X. F. Ling, X. L. Zhang, Y. N. Zhang, H. Y. Lu, J. Y. Yuan and W. L. Ma, High-efficiency perovskite quantum dot solar cells benefiting from a conjugated polymer-quantum dot bulk heterojunction connecting layer, *J. Mater. Chem. A*, 2020, 8, 8104–8112.
- 26 X. L. Zhang, Y. L. Qian, X. F. Ling, Y. Wang, Y. N. Zhang, J. W. Shi, Y. Shi, J. Y. Yuan and W. L. Ma,  $\alpha$ -CsPbBr<sub>3</sub> perovskite quantum dots for application in semitransparent photovoltaics, *ACS Appl. Mater. Interfaces*, 2020, 12, 27307–27315.
- 27 S. Lim, J. Kim, J. Y. Park, J. Min, S. Yun, T. Park, Y. Kim and J. Choi, Suppressed degradation and enhanced performance of CsPbI<sub>3</sub> perovskite quantum dot solar cells via engineering of electron transport layers, *ACS Appl. Mater. Interfaces*, 2021, 13, 6119–6129.
- 28 S. Manzhos, C. C. Chueh, G. Giorgi, T. Kubo, G. Saianand, J. Lüder and M. Ihara, Materials design and optimization for next-generation solar cell and light-emitting technologies, *J. Phys. Chem. Lett.*, 2021, 12, 4638–4657.
- 29 Y. Li, J. Zhu, Y. Huang, J. F. Wei, F. Liu, Z. P. Shao, L. H. Hu, S. H. Chen, S. F. Yang, J. W. Tang, J. X. Yao and S. Y. Dai, Efficient inorganic solid solar cells composed of perovskite and PbS quantum dots, *Nanoscale*, 2015, 7, 9902–9907.
- 30 J. Choi, Y. Kim, J. W. Jo, J. Kim, B. Sun, G. Walters, F. P. García de Arquer, R. Quintero-Bermudez, Y. Li, C. S. Tan, L. N. Quan, A. P. T. Kam, S. Hoogland, Z. H. Lu, O. Voznyy and E. H. Sargent, Chloride passivation of ZnO electrodes improves charge extraction in colloidal quantum dot photovoltaics, *Adv. Mater.*, 2017, 29, 1702350.
- 31 J. C. An, X. C. Yang, W. H. Wang, J. J. Li, H. X. Wang, Z. Yu, C. H. Gong, X. N. Wang and L. C. Sun, Stable and efficient PbS colloidal quantum dot solar cells incorporating low-temperature processed carbon paste counter electrodes, *Sol. Energy*, 2017, 158, 28–33.
- 32 X. L. Zhang, P. K. Santra, L. Tian, M. B. Johansson, H. Rensmo and E. M. J. Johansson, Highly efficient flexible quantum dot solar cells with improved electron extraction using MgZnO nanocrystals, *ACS Nano*, 2017, 11, 8478–8487.
- 33 J. Yang, J. Lee, J. Lee and W. Yi, Oxygen annealing of the ZnO nanoparticle layer for the high-performance PbS colloidal quantum-dot photovoltaics, *J. Power Sources*, 2019, 421, 124–131.
- 34 C. Mahajan, A. Sharma and A. K. Rath, Solution-phase hybrid passivation for efficient infrared-band gap quantum dot solar cells, *ACS Appl. Mater. Interfaces*, 2020, 12, 49840–49848.
- 35 Y. Y. Wei, M. B. Xing, D. D. Wang and R. X. Wang, Current density improvement of colloidal PbS quantum dot solar cells by adding NaCl in ZnO electron transport layer, *Energy Rep.*, 2020, 6, 2370–2375.
- 36 M. B. Xing, Y. Y. Wei, D. D. Wang, Q. Shen and R. X. Wang, Mg-doped ZnO layer to enhance electron transporting for PbS quantum dot solar cells, *Curr. Appl. Phys.*, 2021, 21, 14–19.
- 37 M. Biondi, M.-J. Choi, S. Lee, K. Bertens, M. Y. Wei, A. R. Kirmani, G. Lee, H. T. Kung, L. J. Richter, S. Hoogland, Z.-H. Lu, F. P. García de Arquer and E. H. Sargent, Control over ligand exchange reactivity in hole transport layer enables high-efficiency colloidal quantum dot solar cells, *ACS Energy Lett.*, 2021, 6, 468–476.
- 38 S. Q. Liu, L. Hu, S. J. Huang, W. Q. Zhang, J. J. Ma, J. C. Wang, X. W. Guan, C.-H. Lin, J. Kim, T. Wan, Q. Lei, D. W. Chu and T. Wu, Enhancing the efficiency and stability of PbS quantum dot solar cells through engineering an ultrathin NiO nanocrystalline interlayer, *ACS Appl. Mater. Interfaces*, 2020, 12, 46239–46246.
- 39 M.-J. Choi, F. P. García de Arquer, A. H. Proppe, A. Seifitokaldani, J. Choi, J. Kim, S.-W. Baek, M. X. Liu, B. Sun, M. Biondi, B. Scheffel, G. Walters, D.-H. Nam, J. W. Jo, O. Ouellette, O. Voznyy, S. Hoogland, S. O. Kelley, Y. S. Jung and E. H. Sargent, Cascade surface modification of colloidal quantum dot inks enables efficient bulk homojunction photovoltaics, *Nat. Commun.*, 2020, 11, 103.
- 40 A. Sharma, N. V. Dambhare, J. Bera, S. Sahu and A. K. Rath, Crack-free conjugated PbS quantum dot-hole transport layers for solar cells, *ACS Appl. Nano Mater.*, 2021, 4, 4016–4025.
- 41 M. Biondi, M.-J. Choi, O. Ouellette, S.-W. Baek, P. Todorović, B. Sun, S. Lee, M. Y. Wei, P. C. Li, A. R. Kirmani, L. K. Sagar, L. J. Richter, S. Hoogland, Z.-H. Lu, F. P. García de Arquer and E. H. Sargent, A chemically orthogonal hole transport layer for efficient colloidal quantum dot solar cells, *Adv. Mater.*, 2020, 32, 1906199.
- 42 Z. L. Teh, L. Hu, Z. L. Zhang, A. R. Gentle, Z. H. Chen, Y. J. Gao, L. Yuan, Y. C. Hu, T. Wu, R. J. Patterson and S. J. Huang, Enhanced power conversion efficiency via hybrid ligand exchange treatment of p-type PbS quantum dots, *ACS Appl. Mater. Interfaces*, 2020, 12, 22751–22759.



- 43 H. B. Wang, M. Desbordes, Y. Xiao, T. Kubo, T. Bessho, J. Nakazaki and H. Segawa, Highly stable interdigitated PbS quantum dot and ZnO nanowire solar cells with an automatically embedded electron-blocking layer, *ACS Appl. Energy Mater.*, 2021, **4**, 5918–5926.
- 44 G. Z. Shi, H. B. Wang, Y. H. Zhang, C. Cheng, T. S. Zhai, B. T. Chen, X. Y. Liu, R. Jono, X. N. Mao, Y. Liu, X. L. Zhang, X. F. Ling, Y. N. Zhang, X. Meng, Y. F. Chen, S. Duhm, L. Zhang, T. Li, L. Wang, S. Y. Xiong, T. Sagawa, T. Kubo, H. Segawa, Q. Shen, Z. K. Liu and W. L. Ma, The effect of water on colloidal quantum solar cells, *Nat. Commun.*, 2021, **12**, 4381.
- 45 X. K. Yang, J. Yang, M. I. Ullah, Y. Xia, G. J. Liang, S. Wang, J. B. Zhang, H.-Y. Su, H. S. Song and J. Tang, Enhanced passivation and carrier collection in ink-processed PbS quantum dot solar cells via a supplementary ligand strategy, *ACS Appl. Mater. Interfaces*, 2020, **12**, 42217–42225.
- 46 K. Bertens, J. Z. Fan, M. Biondi, A. S. Rasouli, S. Lee, P. C. Li, B. Sun, S. Hoogland, F. P. García de Arquer, Z.-H. Lu and E. H. Sargent, Colloidal quantum dot solar cell band alignment using two-step ionic doping, *ACS Mater. Lett.*, 2020, **2**, 1583–1589.
- 47 D. Becker-Koch, M. Albaladejo-Siguan, Y. J. Hofstetter, O. Solomeshch, D. Pohl, B. Rellinghaus, N. Tessler and Y. Vaynzof, Doped organic hole extraction layers in efficient PbS and AgBiS<sub>2</sub> quantum dot solar cells, *ACS Appl. Mater. Interfaces*, 2021, **12**, 18750–18757.
- 48 A. Chiu, E. Rong, C. Bambini, Y. D. Lin, C. C. F. Lu and S. M. Thon, Sulfur-infused hole transport materials to overcome performance-limiting transport in colloidal quantum dot solar cells, *ACS Energy Lett.*, 2020, **5**, 2897–2904.
- 49 O. Ouellette, A. Lesage-Landry, B. Scheffel, S. Hoogland, F. P. García de Arquer and E. H. Sargent, Spatial collection in colloidal quantum dot solar cell, *Adv. Funct. Mater.*, 2020, **30**, 1908200.
- 50 L. Hu, Q. Lei, X. W. Guan, R. Patterson, J. Y. Yuan, C.-H. Lin, J. Kim, X. Geng, A. Younis, X. X. Wu, X. F. Liu, T. Wan, D. W. Chu, T. Wu and S. J. Huang, Optimizing surface chemistry of PbS colloidal quantum dot for highly efficient and stable solar cells via chemical binding, *Adv. Sci.*, 2021, **8**, 2003138.
- 51 L. Hu, X. Geng, S. Singh, J. J. Shi, Y. C. Hu, S. Y. Li, X. W. Guan, T. Y. He, X. N. Li, Z. X. Cheng, R. Patterson, S. J. Huang and T. Wu, Synergistic effect of electron transport layer and colloidal quantum dot solid enable PbSe quantum dot solar cell achieving over 10% efficiency, *Nano Energy*, 2019, **64**, 103922.
- 52 M. H. Zhu, X. X. Liu, S. S. Liu, C. Chen, J. G. He, W. W. Liu, J. Yang, L. Gao, G. D. Niu, J. Tang and J. B. Zhang, Efficient PbSe colloidal quantum dot solar cells using SnO<sub>2</sub> as a buffer layer, *ACS Appl. Mater. Interfaces*, 2019, **12**, 2566–2571.
- 53 M. Albaladejo-Siguan, D. Becker-Koch, A. D. Taylor, Q. Sun, V. Lami, P. G. Oppenheimer, F. Paulus and Y. Vaynzof, Efficient and stable PbS quantum dot solar cells by triplecation perovskite passivation, *ACS Nano*, 2020, **14**, 384–393.
- 54 A. R. Kirmani, F. García de Arquer, J. Z. Fan, J. I. Khan, G. Walters, S. Hoogland, N. Wehbe, M. M. Said, S. Barlow, F. Laquai, S. R. Marder, E. H. Sargent and A. Amassian, Molecular doping of the hole-transporting layer for efficient, single-step-deposited colloidal quantum dot photovoltaics, *ACS Energy Lett.*, 2017, **2**, 1952–1959.
- 55 C. Chen, L. Wang, L. Gao, D. Nam, D. B. Li, K. H. Li, Y. Zhao, C. Ge, H. Cheong, H. Liu, H. S. Song and J. Tang, 6.5% certified efficiency Sb<sub>2</sub>Se<sub>3</sub> solar cells using PbS colloidal quantum dot film as hole-transporting layer, *ACS Energy Lett.*, 2017, **2**, 2125–2132.
- 56 J. Choi, M.-J. Choi, J. Kim, F. Dinic, P. Todorovic, B. Sun, M. Y. Wei, S. Hoogland, F. P. García de Arquer, O. Voznyy and E. H. Sargent, Stabilizing surface passivation enables stable operation of colloidal quantum dot photovoltaic devices at maximum power point in an air ambient, *Adv. Mater.*, 2020, **32**, 1906497.
- 57 M. Lv, J. Zhu, Y. Huang, Y. Li, Z. P. Shao, Y. F. Xu and S. Y. Dai, Colloidal CuInS<sub>2</sub> quantum dot as inorganic hole-transporting material in perovskite solar cells, *ACS Appl. Mater. Interfaces*, 2015, **7**, 17482–17488.
- 58 Q. H. Li, J. K. Bai, T. T. Zhang, C. Nie, J. L. Duan and Q. W. Tang, CdZnSe@ZnSe colloidal alloy quantum dots for high-efficiency all-inorganic perovskite solar cells, *Chem. Commun.*, 2018, **54**, 9575–9578.
- 59 M. Yuan, X. M. Zhang, J. Kong, W. H. Zhou, Z. J. Zhou, Q. W. Tian, Y. N. Meng, S. X. Wu and D. X. Kou, Controlling the band gap to improve open-circuit voltage in metal chalcogenide based perovskite solar cells, *Electrochim. Acta*, 2016, **215**, 374–379.
- 60 Y. Li, Z. W. Wang, D. Ren, Y. H. Liu, A. B. Zheng, S. M. Zakeeruddin, X. D. Dong, A. Hagfeldt, M. Grätzel and P. Wang, SnS quantum dots as hole transporter of perovskite solar cells, *ACS Appl. Energy Mater.*, 2019, **2**, 3822–3829.
- 61 Y. Zhang, Z. L. Zhang, Y. Y. Liu, Y. F. Liu, H. P. Gao and Y. L. Mao, An inorganic hole-transport material of CuInSe<sub>2</sub> for stable and efficient perovskite solar cells, *Org. Electron.*, 2019, **67**, 168–174.
- 62 F. Li, J. H. Wei, G. Q. Liao, C. Y. Guo, Y. Huang, Q. Zhang, X. Jin, S. Q. Jiang, Q. W. Tang and Q. H. Li, Quaternary quantum dots with gradient valence band for all-inorganic perovskite solar cells, *J. Colloid Interface Sci.*, 2019, **549**, 33–41.
- 63 Y. L. Liu, X. Z. Zhao, Z. F. Yang, Q. T. Li, W. Wei, B. Hu and W. Chen, Cu<sub>12</sub>Sb<sub>4</sub>S<sub>13</sub> quantum dots with ligand exchanges as hole transport materials in all-inorganic perovskite CsPbI<sub>3</sub> quantum dot solar cells, *ACS Appl. Energy Mater.*, 2020, **3**, 3521–3529.
- 64 M. Hedariramsheh, M. Mirhosseini, K. Abdizadeh, S. M. Mahdavi and N. Taghavinia, Evaluating Cu<sub>2</sub>SnS<sub>3</sub> nanoparticle layers as hole-transporting materials in perovskite solar cells, *ACS Appl. Energy Mater.*, 2021, **4**, 5560–5573.
- 65 W. B. Ma, Z. L. Zhang, M. G. Ma, Y. F. Liu, G. C. Pan, H. P. Gao and Y. L. Mao, CuGaS<sub>2</sub> quantum dots with controlled surface defects as an hole-transport material



- for high-efficient and stable perovskite solar cells, *Sol. Energy*, 2020, **211**, 55–61.
- 66 Y. Y. Liu, Z. L. Zhang, H. P. Gao, H. F. Zhang and Y. L. Mao, A novel inorganic hole-transporting material of CuInS<sub>2</sub> for perovskite solar cells with high efficiency and improved stability, *Org. Electron.*, 2019, **75**, 105430.
- 67 A. Kotta and H. K. Seo, Nickel oxide monodispersed quantum dots as hole transport layer in n-i-p hybrid perovskite solar cells, *J. Nanoelectron. Optoelectron.*, 2019, **14**, 895–899.
- 68 K. C. Icli and M. Ozenbas, Fully metal oxide charge selective layers for n-i-p perovskite solar cells employing nickel oxide nanoparticles, *Electrochim. Acta*, 2018, **263**, 338–345.
- 69 S. Chakrabarti, D. Carolan, B. Alessi, P. Maguire, V. Svrcek and D. Mariotti, Microplasma-synthesized ultra-small NiO nanocrystals, a ubiquitous hole transport material, *Nanoscale Adv.*, 2019, **1**, 4915–4925.
- 70 K. Im, J. H. Heo, S. H. Im and J. Kim, Scalable synthesis of Ti-doped MoO<sub>2</sub> nanoparticle-hole-transporting-material with high moisture stability for CH<sub>3</sub>NH<sub>3</sub>PbI<sub>3</sub> perovskite solar cells, *Chem. Eng. J.*, 2017, **330**, 698–705.
- 71 A. Bashir, S. Shukla, J. H. Lew, S. Shukl, A. Bruno, D. Gupta, T. Baikie, R. Patidar, Z. Akhter, A. Priyadarshi, N. Mathews and S. G. Mhaisalkar, Spinel Co<sub>3</sub>O<sub>4</sub> nanomaterials for efficient and stable large area carbon-based printed perovskite solar cells, *Nanoscale*, 2018, **10**, 2341–2350.
- 72 C. Liu, X. Y. Zhou, S. M. Chen, X. Z. Zhao, S. Y. Dai and B. M. Xu, Hydrophobic Cu<sub>2</sub>O quantum dots enabled by surfactant modification as top hole-transport materials for efficient perovskite solar cells, *Adv. Sci.*, 2019, **6**, 1801169.
- 73 S. Akin, Y. Liu, M. I. Dar, S. M. Zakeeruddin, M. Grätzel, S. Turan and S. Sonmezoglu, Hydrothermally processed CuCrO<sub>2</sub> nanoparticles as an inorganic hole transporting material for low-cost perovskite solar cells with superior stability, *J. Mater. Chem. A*, 2018, **6**, 20327–20337.
- 74 H. Zhang, H. Wang, W. Chen and A. K.-Y. Jen, CuGaO<sub>2</sub>: A promising inorganic hole-transporting material for highly efficient and stable perovskite solar cells, *Adv. Mater.*, 2017, **29**, 1604984.
- 75 T.-C. Liang, H.-Y. Su, S.-A. Chen, Y.-J. Chen, C.-Y. Chiang, C.-H. Chiang, T.-T. Kao, L.-C. Chen and C.-C. Lin, Planar perovskite solar cells using perovskite CsPbI<sub>3</sub> quantum dots as efficient hole transporting layers, *Materials*, 2022, **24**, 8902.
- 76 L. Hu, W. W. Wang, H. Liu, J. Peng, H. F. Cao, G. Shao, Z. Xia, W. L. Ma and J. Tang, PbS colloidal quantum dots as an effective hole transporter for planar heterojunction perovskite solar cells, *J. Mater. Chem. A*, 2015, **3**, 515–518.
- 77 L. S. Khanzada, I. Levchuk, Y. Hou, H. Azimi, A. Osvet, R. Ahmad, M. Brandl, P. Herre, M. Distaso, R. Hock, W. Peukert, M. Batentschuk and C. J. Brabec, Effective ligand engineering of the Cu<sub>2</sub>ZnSnS<sub>4</sub> nanocrystal surface for increasing hole transport efficiency in perovskite solar cells, *Adv. Funct. Mater.*, 2016, **26**, 8300–8306.
- 78 G. Y. Ashebir, C. Dong, Z. Y. Wan, J. J. Qi, J. W. Chen, Q. Y. Zhao, W. W. Chen and M. T. Wang, Solution-processed Cu<sub>2</sub>ZnSnS<sub>4</sub> nanoparticle film as efficient hole transporting layer for stable perovskite solar cells, *J. Phys. Chem. Solids*, 2019, **129**, 204–208.
- 79 W. Lee, I. Kim, H. Choi and K. Kim, Synthesis of Ni/NiO core-shell nanoparticles for wet-coated hole transport layer of the organic solar cell, *Surf. Coat. Technol.*, 2013, **231**, 93–97.
- 80 S. S. Chen, S. W. Yang, H. Sun, L. Zhang, J. J. Peng, Z. Q. Liang and Z.-S. Wang, Enhanced interfacial electron transfer of inverted perovskite solar cells by introduction of CoSe into the electron-transporting-layer, *J. Power Sources*, 2017, **353**, 123–130.
- 81 S. Weber, T. Rath, J. Mangalam, B. Kunert, A. M. Coclite, M. Bauch, T. Dimopoulos and G. Trimmel, Investigation of NiO<sub>x</sub>-hole transport layers in triple cation perovskite solar cells, *J. Mater. Sci.*, 2018, **29**, 1847–1855.
- 82 D. Saranin, T. Komaricheva, L. Luchnikov, D. S. Muratov, T. S. Le, Y. Karpov, P. Gostishchev, S. Yurchuk, D. Kuznetsov, S. Didenko and A. D. Carlo, Hysteresis-free perovskite solar cells with compact and nanoparticle NiO for indoor application, *Sol. Energy Mater. Sol. Cells*, 2021, **227**, 111095.
- 83 G. Luo, Y. X. Zhang, Q. L. Zhu, Z. Q. An, P. Lv, J. H. Chen, Y. Q. Zhu, M. Hu, W. N. Li, K. Cao, Z. L. Ku, W. C. Huang, Y.-B. Cheng and J. F. Lu, Ruthenium complex optimized contact interfaces of NiO<sub>x</sub> nanocrystals for efficient and stable perovskite solar cells, *Sol. RRL*, 2023, 2300890.
- 84 J. B. You, L. Meng, T.-B. Song, T.-F. Guo, Y. Yang, W.-H. Chang, Z. R. Hong, H. J. Chen, H. P. Zhou, Q. Chen, Y. S. Liu, N. D. Marco and Y. Yang, Improved air stability of perovskite solar cells via solution-processed metal oxide transport layers, *Nat. Nanotechnol.*, 2016, **11**, 75–81.
- 85 M. Najafi, F. D. Giacomo, D. Zhang, S. Shanmugam, A. Senes, W. Verhees, A. Hadipour, Y. Galagan, T. Aernouts, S. Veenstra and R. Andriessen, Highly efficient and stable flexible perovskite solar cells with metal oxides nanoparticle charge extraction layers, *Small*, 2018, **14**, 1702775.
- 86 H. Zhang, J. Q. Cheng, F. Lin, H. X. He, J. Mao, K. S. Wong, A. K.-Y. Jen and W. C. H. Choy, Pinhole-free and surface-nanostructured NiO<sub>x</sub> film by room-temperature solution process for high-performance flexible perovskite solar cells with good stability and reproducibility, *ACS Nano*, 2016, **10**, 1503–1511.
- 87 J. J. He, E. B. Bi, W. T. Tang, Y. B. Wang, Z. M. Zhou, X. D. Yang, H. Chen and L. Y. Han, Ligand-free, highly dispersed NiO<sub>x</sub> nanocrystal for efficient, stable, low-temperature processable perovskite solar cells, *Sol. RRL*, 2018, **2**, 1800004.
- 88 Q. Q. He, K. Yao, X. F. Wang, X. F. Xia, S. F. Leng and F. Li, Room-temperature and solution-processable Cu-doped nickel oxide nanoparticles for efficient hole-transport layers of flexible large-area perovskite solar cells, *ACS Appl. Mater. Interfaces*, 2017, **9**, 41887–41897.



- 89 J. J. He, Y. R. Xiang, F. Zhang, J. R. Lian, R. Hu, P. J. Zeng, J. Song and J. L. Qu, Improvement of red light harvesting ability and open circuit voltage of Cu:NiO<sub>x</sub> based p-i-n planar perovskite solar cells boosted by cysteine enhanced interface contact, *Nano Energy*, 2018, **45**, 471.
- 90 D. Ouyang, J. W. Zheng, Z. F. Huang, L. Zhu and W. C. H. Choy, An efficacious multifunction codoping strategy on a room-temperature solution-processed hole transport layer for realizing high-performance perovskite solar cells, *J. Mater. Chem. A*, 2021, **9**, 371–379.
- 91 J. Wang, J. Zhang, Y. Z. Zhou, H. B. Liu, Q. F. Xue, X. S. Li, C.-C. Chueh, H.-L. Yip, Z. L. Zhu and A. K.-Y. Jen, Highly efficient all-inorganic perovskite solar cells with suppressed non-radiative recombination by a Lewis base, *Nat. Commun.*, 2020, **11**, 177.
- 92 A. Savva, I. T. Papadas, D. Tsikritzis, G. S. Armatas, S. Kennou and S. A. Choulis, Room temperature nanoparticulate interfacial layers for perovskite solar cells via solvothermal synthesis, *J. Mater. Chem. A*, 2017, **5**, 2038120389.
- 93 W. A. Dunlap-Shohl, T. B. Daunis, X. M. Wang, J. Wang, B. Y. Zhang, D. Barrera, Y. F. Yan, J. W. P. Hsu and D. B. Mitzi, Room-temperature fabrication of a delafossite CuCrO<sub>2</sub> hole transport layer for perovskite solar cells, *J. Mater. Chem. A*, 2018, **6**, 469–477.
- 94 H. Zhang, H. Wang, H. M. Zhu, C.-C. Chueh, W. Chen, S. H. Yang and A. K.-Y. Jen, Low-temperature solution-processed CuCrO<sub>2</sub> hole-transporting layer for efficient and photostable perovskite solar cells, *Adv. Energy Mater.*, 2018, **8**, 1702762.
- 95 I. T. Papadas, A. Savva, A. Loakeimidis, P. Eleftheriou, G. S. Armatas and S. A. Choulis, Employing surfactant-assisted hydrothermal synthesis to control CuGaO<sub>2</sub> nanoparticle formation and improved carrier selectivity of perovskite solar cells, *Mater. Today Energy*, 2018, **8**, 57–64.
- 96 D. Ouyang, J. Y. Xiao, F. Ye, Z. F. Huang, H. Zhang, L. Zhu, J. Q. Cheng and W. C. H. Choy, Strategic synthesis of ultrasmall NiCo<sub>2</sub>O<sub>4</sub> NPs as hole transport layer for highly efficient perovskite solar cells, *Adv. Energy Mater.*, 2018, **16**, 1702722.
- 97 I. T. Papadas, A. Ioakeimidis, G. S. Armatas and S. A. Choulis, Low-temperature combustion synthesis of a spinel NiCo<sub>2</sub>O<sub>4</sub> hole transport layer for perovskite photovoltaics, *Adv. Sci.*, 2018, **5**, 1701029.
- 98 Z. F. Huang, D. Ouyang, R. M. Ma, W. Wu, V. A. L. Roy and W. C. H. Choy, A general method: Designing a hypocrySTALLINE hydroxide intermediate to achieve ultrasmall and well-dispersed ternary metal oxide for efficient photovoltaic devices, *Adv. Funct. Mater.*, 2019, **29**, 1904684.
- 99 B. P. Yang, D. Ouyang, Z. F. Huang, X. G. Ren, H. Zhang and W. C. H. Choy, Multifunctional synthesis approach of In:CuCrO<sub>2</sub> nanoparticles for hole transport layer in high-performance perovskite solar cells, *Adv. Funct. Mater.*, 2019, **29**, 1902600.
- 100 A. Kumar, D. K. Jarwal, A. K. Mishra, S. Ratan, C. Kumar, R. K. Upadhyay, B. Mukherjee and S. Jit, Effects of HTL and ETL thicknesses on the performance of PQT-12/PCDTBT:PC<sub>61</sub>BM/ZnO QDs solar cells, *IEEE Photonics Technol. Lett.*, 2020, **32**, 677–680.
- 101 B. P. Yang, S. M. Peng and W. C. H. Choy, Inorganic top electron transport layer for high performance inverted perovskite solar cells, *EcoMat*, 2021, **3**, e12127.
- 102 A. Wibowo, M. A. Marsudi, M. I. Amal, M. B. Ananda, R. Stephanie, H. Ardy and L. J. Diguna, ZnO nanostructured materials for emerging solar cell applications, *RSC Adv.*, 2020, **10**, 42838–42859.
- 103 S. B. Shivarudraiah, M. Ng, C.-H. A. Li and J. E. Halpert, All-inorganic, solution-processed, inverted CsPbI<sub>3</sub> quantum dot solar cells with a PCE of 13.1% achieved via a layer-by-layer FAI treatment, *ACS Appl. Energy Mater.*, 2020, **3**, 5620–5627.
- 104 L. J. Meng, Q. W. Xu, U. K. Thakur, L. Gong, H. B. Zeng, K. Shankar and X. H. Wang, Unusual surface ligand doping-induced p-type quantum dot slides and their application in solar cells, *ACS Appl. Mater. Interfaces*, 2020, **12**, 53942–53949.
- 105 T. T. Jiang and W. F. Fu, Improved performance and stability of perovskite solar cells with bilayer electron-transporting layers, *RSC Adv.*, 2018, **8**, 5897–5901.
- 106 C.-J. Chen, A. Chandel, D. Thakur, J.-R. Wu, S.-E. Chiang, G.-S. Zeng, J.-L. Shen, S.-H. Chen and S. H. Chang, Ag modified bathocuproine:ZnO nanoparticles electron buffer layer based bifacial inverted-type perovskite solar cells, *Org. Electron.*, 2021, **92**, 106110.
- 107 Y.-H. Chiang, C.-K. Shih, A.-S. Sie, M.-H. Li, C.-C. Peng, P.-S. Shen, Y.-P. Wang, T.-F. Guo and P. Chen, Highly stable perovskite solar cells with all-inorganic selective contacts from microwave-synthesized oxide nanoparticles, *J. Mater. Chem. A*, 2017, **5**, 25485–25493.
- 108 P.-H. Lee, T.-T. Wu, K.-Y. Tian, C.-F. Li, C.-H. Hou, J.-J. Shyue, C.-F. Lu, Y.-C. Huang and W.-F. Su, Work-function-tunable electron transport layer of molecule-capped metal oxide for a high-efficiency and stable p-i-n perovskite solar cells, *ACS Appl. Mater. Interfaces*, 2020, **12**, 45936–45949.
- 109 Y. Zhao, H. Zhang, X. G. Ren, H. L. Zhu, Z. F. Huang, F. Ye, D. Ouyang, K. W. Cheah, A. K.-Y. Jen and W. C. H. Choy, Thick TiO<sub>2</sub>-based top electron transport layer on perovskite for highly efficient and stable solar cells, *ACS Energy Lett.*, 2018, **3**, 2891–2898.
- 110 S. S. Zhang, W. T. Chen, S. H. Wu, R. Chen, Z. H. Liu, Y. Q. Huang, Z. C. Yang, H. M. Zhu, J. Y. Li, L. Y. Han and W. Chen, Hybrid inorganic electron-transporting layer coupled with a halogen-resistant electrode in CsPbI<sub>2</sub>Br-based perovskite solar cells to achieve robust long-term stability, *ACS Appl. Mater. Interfaces*, 2019, **11**, 43303–43311.
- 111 J. Lim, W. Jang, M. S. Kim, M. Ji, Y.-I. Lee and D. H. Wang, Hydrogenerated black titanium dioxide-embedded conducting polymer for boosting electron flow in perovskite devices, *J. Alloys Compd.*, 2020, **846**, 156329.
- 112 R. Fang, S. H. Wu, W. T. Chen, Z. H. Liu, S. S. Zhang, R. Chen, Y. F. Yue, L. L. Deng, Y.-B. Cheng, L. Y. Han and



- W. Chen, [6,6]-Phenyl-C<sub>61</sub>-butyric acid methyl ester/cerium oxide bilayer structure as efficient and stable electron transport layer for inverted perovskite solar cells, *ACS Nano*, 2018, **12**, 2403–2414.
- 113 B. P. Yang, R. M. Ma, Z. S. Wang, D. Ouyang, Z. F. Huang, J. L. Lu, X. H. Duan, L. Yue, N. Xu and W. C. H. Choy, Efficient gradient potential top electron transport structures achieved by combining an oxide family for inverted perovskite solar cells with high efficiency and stability, *ACS Appl. Mater. Interfaces*, 2021, **13**, 27179–27187.
- 114 F. R. Tan, W. Z. Xu, X. D. Hu, P. Yu and W. F. Zhang, Highly efficient inverted perovskite solar cells with CdSe QDs/LiF electron transporting layer, *Nanoscale Res. Lett.*, 2017, **12**, 614.
- 115 R. T. Ako, P. Ekanayake, D. J. Young, J. Hobley, V. Chellappan, A. Tan, S. Gorelik, G. S. Subramanian and C. M. Lim, Evaluation of surface energy state distribution and bulk defect concentration in DSSC photoanodes based on Sn, Fe, and Cu doped TiO<sub>2</sub>, *Appl. Surf. Sci.*, 2015, **351**, 950–961.
- 116 M. Neetu, I. C. Maurya, A. K. Gupta, P. Srivastava and L. Bahadur, Extensive enhancement in power conversion efficiency of dye-sensitized solar cell by using Al-doped TiO<sub>2</sub> photoanode, *J. Solid State Electrochem.*, 2017, **21**, 1229–1241.
- 117 B. Ünlü, S. Çakar and M. Özacar, The effects of metal doped TiO<sub>2</sub> and dithizone-metal complexes on DSSCs performance, *Sol. Energy*, 2018, **166**, 441–449.
- 118 J. Manju and S. J. Jawhar, Facile synthesis and characterization of Ti<sub>(1-x)</sub>Cu<sub>x</sub>O<sub>2</sub> nanoparticles for high efficiency dye sensitized solar cell applications, *Opt. Mater.*, 2017, **69**, 119–127.
- 119 M.-J. Lee, J.-Y. Park, C.-S. Kim, K. Okuyama, S.-E. Lee and T.-O. Kim, Improvement of light scattering capacity in dye-sensitized solar cells by doping with SiO<sub>2</sub> nanoparticles, *J. Power Sources*, 2016, **327**, 96–103.
- 120 S. Kundu, P. Sarojinijeeva, R. Karthick, G. Anantharaj, G. Saritha, R. Bera, S. Anandan, A. Patra, P. Ragupathy, M. Selvaraj, D. Jeyakumar and K. Pillai, Enhancing the efficiency of DSSCs by the modification of TiO<sub>2</sub> photoanodes using N, F, and S, co-doped graphene quantum dots, *Electrochim. Acta*, 2017, **242**, 337–343.
- 121 X. Z. Zhang, T. Y. Wu, X. X. Xu, L. Zhang, J. Tang, X. He, J. H. Wu and Z. Lan, Ligand-exchange TiO<sub>2</sub> nanocrystals induced formation of high-quality electron transporting layers at low temperature for efficient planar perovskite solar cells, *Sol. Energy Mater. Sol. Cells*, 2018, **178**, 65–73.
- 122 K. Sanglee, S. Chuangcote, T. Krajangsang, J. Sritharathikhun, K. Sriprapha and T. Sagawa, Quantum dot-modified titanium dioxide nanoparticles as an energy-band tunable electron-transporting layer for open air-fabricated planar perovskite solar cells, *Nanomater. Nanotechnol.*, 2020, **10**, 1847980420961638.
- 123 R. Singh, I. Ryu, H. Yadav, J. Park, J. W. Jo, S. Yim and J.-J. Lee, Non-hydrolytic sol-gel route to synthesize TiO<sub>2</sub> nanoparticles under ambient condition for highly efficient and stable perovskite solar cells, *Sol. Energy*, 2019, **185**, 307–314.
- 124 A. Badawi, N. Al-Hosiny and S. Abdallah, The photovoltaic performance of CdS quantum dots sensitized solar cell using graphene/TiO<sub>2</sub> working electrode, *Superlattices Microstruct.*, 2015, **81**, 88–96.
- 125 P. N. Kumar, R. Narayanan, S. Laha, M. Deepa and A. K. Srivastava, Phoro-electrochromic cell with a CdS quantum dots/graphitic-nanoparticles sensitized anode and a molybdenum oxide cathode, *Sol. Energy Mater. Sol. Cells*, 2016, **153**, 138–147.
- 126 Z. Zolfaghari-Isavandi and Z. Shariatnia, Enhanced efficiency of quantum dot sensitized solar cells using Cu<sub>2</sub>O/TiO<sub>2</sub> nanocomposite photoanodes, *J. Alloys Compd.*, 2018, **737**, 99–112.
- 127 S. Zhang, Z. Lan, J. H. Wu, X. Chen and C. Y. Zhang, Preparation of novel TiO@ quantum dot blocking layers at conductive glass/TiO<sub>2</sub> interfaces for efficient CdS quantum dot sensitized solar cells, *J. Alloys Compd.*, 2016, **656**, 253–258.
- 128 M. Marandi, P. Talebi and S. Bayat, Optimization of the doping process and light scattering in CdS:Mn quantum dots sensitized solar cells for the efficiency enhancement, *J. Mater. Sci.: Mater. Electron.*, 2019, **30**, 3820–3832.
- 129 Y. B. Lu, L. Li, S. C. Su, Y. J. Chen, Y. L. Song and S. J. Jiao, A novel TiO<sub>2</sub> nanostructure as photoanode for highly efficient CdSe quantum dot-sensitized solar cells, *RSC Adv.*, 2017, **7**, 9795–9802.
- 130 J. P. Deng, M. Q. Wang, J. F. Fang, X. H. Song, Z. Yang and Z. L. Yuan, Synthesis of Zn-doped TiO<sub>2</sub> nano-particles using metal Ti and Zn as raw materials and application in quantum dot sensitized solar cells, *J. Alloys Compd.*, 2019, **791**, 371–379.
- 131 S. M. Thon, A. H. Ip, O. Voznyy, L. Levina, K. W. Kemp, G. H. Carey, S. Masala and E. H. Sargent, Role of bond adaptability in the passivation of colloidal quantum dot solids, *ACS Nano*, 2013, **7**, 7680–7688.
- 132 A. E. Tom, A. Thomas and V. V. Ison, Novel post-synthesis purification strategies and the ligand exchange processes in simplifying the fabrication of PbS quantum dot solar cells, *RSC Adv.*, 2020, **10**, 30707–30715.
- 133 N. L. Zhang, D. C. J. Neo, Y. Tazawa, X. T. Li, H. E. Assender, R. G. Compton and A. A. R. Watt, Narrow band gap lead sulfide hole transport layers for quantum dot photovoltaics, *ACS Appl. Mater. Interfaces*, 2016, **8**, 21417–21422.
- 134 D. C. J. Neo, N. L. Zhang, Y. Tazawa, H. B. Jiang, G. M. Hughes, C. R. M. Grovenor, H. E. Assender and A. A. R. Watt, Poly(3-hexylthiophene-2,5-diyl) as a hole transport layer for colloidal quantum dot solar cells, *ACS Appl. Mater. Interfaces*, 2016, **8**, 12101.
- 135 A. Mnoyan, K. Kim, J. Y. Kim and D. Y. Jeon, Colloidal nanocomposite of reduced graphene oxide and quantum dots for enhanced surface passivation in optoelectronic applications, *Sol. Energy Mater. Sol. Cells*, 2016, **144**, 181–186.



- 136 S. P. Zang, Y. L. Wang, M. Y. Li, W. Su, H. C. Zhu, X. T. Zhang and Y. C. Liu, Fabrication of efficient PbS colloidal quantum dot solar cell with low temperature sputter-deposited ZnO electron transport layer, *Sol. Energy Mater. Sol. Cells*, 2017, **169**, 264–269.
- 137 J. Choi, J. W. Jo, F. P. García de Arquer, Y.-B. Zhao, B. Sun, J. Kim, M.-J. Choi, S.-W. Baek, A. H. Proppe, A. Seifitokaldani, D.-H. Nam, P. Li, O. Ouellette, Y. Kim, O. Voznyy, S. Hoogland, S. O. Kelley, Z.-H. Lu and E. H. Sargent, Activated electron-transport layers for infrared quantum dot optoelectronics, *Adv. Mater.*, 2018, **30**, 1801720.
- 138 Y. Xue, F. Yang, J. Y. Yuan, Y. N. Zhang, M. F. Gu, Y. L. Xu, X. F. Ling, Y. Wang, F. C. Li, T. S. Zhai, J. N. Li, C. H. Cui, Y. W. Chen and W. L. Ma, Toward scalable PbS quantum dot solar cells using a tailored polymeric hole conductor, *ACS Energy Lett.*, 2019, **4**, 2850–2858.
- 139 E. G. Durmusoglu, G. S. Selopal, M. Mohammadnezhad, H. Zhang, P. Dagtepe, D. Barba, S. H. Sun, H. G. Zhao, H. Y. Acar, Z. M. Wang and F. Rosei, Low-cost, air-processed quantum dot solar cells via diffusion-controlled synthesis, *ACS Appl. Mater. Interfaces*, 2020, **12**, 36301–36310.
- 140 C. Ding, F. Liu, Y. H. Zhang, S. Hayase, T. Masuda, R. X. Wang, Y. Zhou, Y. F. Yao, Z. G. Zou and Q. Shen, Passivation strategy of reducing both electron and hole states for achieving high-efficiency PbS quantum-dot solar cells with power conversion efficiency over 12%, *ACS Energy Lett.*, 2020, **5**, 3224–3236.
- 141 T. S. Zhao, E. D. Goodwin, J. C. Guo, H. Wang, B. T. Diroll, C. B. Murray and C. R. Kagan, Advanced architecture for colloidal PbS quantum dot solar cells exploiting a CdSe quantum dot buffer layer, *ACS Nano*, 2016, **10**, 9267–9273.
- 142 S. Kumar, R. Upadhyay and B. Pradhan, Performance enhancement of heterojunction ZnO/PbS quantum dot solar cells by interface engineering, *Sol. Energy*, 2020, **211**, 283–290.
- 143 J. P. Deng, M. Q. Wang, W. Ye, J. F. Fang, P. C. Zhang, Y. P. Yang and Z. Yang, CdS/CdSe-sensitized solar cell based on Al-doped ZnO nanoparticles prepared by the decomposition of zinc acetate solid solution, *Solid-State Electron.*, 2017, **127**, 38–44.
- 144 F. Yang, Y. L. Xu, M. F. Gu, S. J. Zhou, Y. J. Wang, K. Y. Lu, Z. K. Liu, X. F. Ling, Z. J. Zhu, J. M. Chen, Z. Y. Wu, Y. N. Zhang, Y. Xue, F. C. Li, J. Y. Yuan and W. L. Ma, Synthesis of cesium-doped ZnO nanoparticles as an electron extraction layer for efficient PbS colloidal quantum dot solar cells, *J. Mater. Chem. A*, 2018, **6**, 17688–17697.
- 145 N. Sukharevska, D. Bederak, V. M. Goossens, J. Momand, H. Duim, D. N. Dirin, M. V. Kovalenko, B. J. Kooi and M. A. Loi, Scalable PbS quantum dot solar cell production by blade coating from stable inks, *ACS Appl. Mater. Interfaces*, 2021, **13**, 5195–5207.
- 146 X. S. Zhang, Z. W. Jin, J. R. Zhang, D. L. Bai, H. Bian, K. Wang, J. Sun, Q. Wang and S. Z. F. Liu, All-inorganic processed binary CsPbBr<sub>3</sub>-CsPb<sub>2</sub>Br<sub>5</sub> perovskites with synergistic enhancement for high-efficiency Cs-Pb-Br-based solar cells, *ACS Appl. Mater. Interfaces*, 2018, **10**, 7145–7154.
- 147 Y. N. Zhang, Y. Y. Kan, K. Gao, M. F. Gu, Y. Shi, X. L. Zhang, Y. Xue, X. N. Zhang, Z. K. Liu, Y. Zhang, J. Y. Yuan, W. L. Ma and A. K.-Y. Jen, Hybrid quantum dot/organic heterojunction: A route to improve open-circuit voltage in PbS colloidal quantum dot solar cells, *ACS Energy Lett.*, 2020, **5**, 2335–2342.
- 148 P. D. Li, T. G. Jiu, G. Tang, G. J. Wang, J. Li, X. F. Li and J. F. Fang, Solvents induced ZnO nanoparticles aggregation associated with their interfacial effect on organic solar cells, *ACS Appl. Mater. Interfaces*, 2014, **6**, 18172–18179.
- 149 S. Bishnoi, V. Gupta, C. Sharma, D. Haranath, M. Kumar and S. Chand, Luminescent cathode buffer layer for enhanced power conversion efficiency and stability of bulk-heterojunction solar cells, *Org. Electron.*, 2016, **38**, 193–199.
- 150 M. Abrari, M. Ghanaatshoar, H. R. Moazami and S. S. H. Davarani, Synthesis of SnO<sub>2</sub> nanoparticles by electrooxidation method and their application in dye-sensitized solar cells: The influence of the counterion, *J. Electron. Mater.*, 2019, **48**, 445–453.
- 151 A. E. Shalan, M. Rasly, I. Osama, M. M. Rashad and I. A. Ibrahim, Photocurrent enhancement by Ni<sup>2+</sup> and Zn<sup>2+</sup> ion doped in SnO<sub>2</sub> nanoparticles in highly porous dye-sensitized solar cells, *Ceram. Int.*, 2014, **40**, 11619–11626.
- 152 Y. Wang, M. L. Feng, H. R. Chen, M. Ren, H. F. Wang, Y. F. Miao, Y. T. Chen and Y. X. Zhao, Highly crystallized Cl-doped SnO<sub>2</sub> nanocrystals for stable aqueous dispersion toward high-performance perovskite photovoltaics, *Adv. Mater.*, 2023, 23058498.
- 153 M. Saeidi, M. Abrari and M. Ahmadi, Fabrication of dye-sensitized solar cell based on mixed tin and zinc oxide nanoparticles, *Appl. Phys. A*, 2019, **125**, 409.
- 154 M. Asemi and M. Ghanaatshoar, Studying the effect of the controlled off-stoichiometry on the properties of Zn<sub>2</sub>SnO<sub>4</sub> nanoparticles for DSSC applications, *J. Mater. Sci.*, 2018, **29**, 6730–6740.
- 155 A. P. S. Souza, F. G. S. Oliveira, V. F. Nunes, F. M. Lima, A. F. L. Almeida, I. M. M. de Carvalho and M. P. F. Graca, High performance SnO<sub>2</sub> pure photoelectrode in dye-sensitized solar cells achieved via electrophoretic technique, *Sol. Energy*, 2020, **211**, 312–323.
- 156 K. Balasubramanian and G. Venkatachari, Synthesis and characterization of Sb doped SnO<sub>2</sub> for the photovoltaic applications: different route, *Mater. Res. Express*, 2019, **6**, 1250k6.
- 157 S. J. In, M. Park and J. W. Jung, Reduced interface energy loss in non-fullerene organic solar cells using room temperature-synthesis SnO<sub>2</sub> quantum dots, *J. Mater. Sci. Technol.*, 2020, **52**, 12–19.
- 158 T. Y. Kong, R. Wang, D. Zheng and J. S. Yu, Modification of the SnO<sub>2</sub> electron transporting layer by using perylene



- diimide derivative for efficient organic solar cells, *Front. Chem.*, 2021, **9**, 703561.
- 159 S. Guang, J. Yu, H. Wang, X. Liu, S. Qu, R. Zhu and W. Tang, *J. Energy Chem.*, 2021, **56**, 496.
- 160 S. N. Vijayaraghavan, J. Wall, L. Li, G. Xing, Q. Zhang and F. Yan, Low-temperature processed highly efficient hole transport layer free carbon-based planar perovskite solar cells with SnO<sub>2</sub> quantum dot electron transport layer, *Mater. Today Phys.*, 2020, **13**, 100204.
- 161 Z. Ma, W. Y. Zhou, Z. Xiao, H. Zhang, Z. Y. Li, J. Zhuang, C. T. Peng and Y. L. Huang, Negligible hysteresis planar perovskite solar cells using Ga-doped SnO<sub>2</sub> nanocrystal as electron transport layers, *Org. Electron.*, 2019, **71**, 98–105.
- 162 S. Y. Park and H. C. Shim, Highly efficient and air-stable heterostructured perovskite quantum dot solar cells sing a solid-state cation-exchange reaction, *ACS Appl. Mater. Interfaces*, 2020, **12**, 57124–57133.
- 163 M. Singh, A. Ng, Z. Ren, H. L. Hu, H.-C. Lin, C.-W. Chu and G. Li, Facile synthesis of composite tin oxide nanostructures for high-performance planar perovskite solar cells, *Nano Energy*, 2019, **60**, 275–284.
- 164 H. X. Xie, X. T. Yin, P. Chen, J. Liu, C. H. Yang, W. X. Que and G. F. Wang, Solvothermal synthesis of highly crystalline SnO<sub>2</sub> nanoparticles for flexible perovskite solar cells application, *Mater. Lett.*, 2019, **234**, 311–314.
- 165 Z. C. Wang, T. Wu, L. Xiao, P. L. Qin, X. L. Yu, L. Ma, L. Xiong, H. X. Li, X. B. Chen, Z. Wang, T. Wu, L. Xiao, P. Qin, X. Yu, L. Ma, L. Xiong, H. Li and X. Chen, Multifunctional potassium hexafluorophosphate passivates interface defects for high efficiency perovskite solar cells, *J. Power Sources*, 2021, **488**, 229451.
- 166 H. R. Liu, Z. L. Chen, H. B. Wang, F. H. Ye, J. J. Ma, X. L. Zheng, P. B. Gui, L. B. Xiong, J. Wen and G. J. Fang, A facial room temperature solution synthesis of SnO<sub>2</sub> quantum dots for perovskite solar cells, *J. Mater. Chem. A*, 2019, **7**, 10636–10643.
- 167 G. Yang, C. Chen, F. Yao, Z. L. Chen, Q. Zhang, X. L. Zheng, J. J. Ma, H. W. Lei, P. L. Qin, L. B. Xiong, W. J. Ke, G. Li, Y. F. Yan and G. J. Fang, Effective carrier-concentration tuning of SnO<sub>2</sub> quantum dot electron-selective layers for high-performance planar perovskite solar cells, *Adv. Mater.*, 2018, **30**, 1706023.
- 168 M. Kim, J. Jeong, H. Lu, T. K. Lee, F. T. Eickemeyer, Y. Liu, I. W. Choi, S. J. Choi, Y. Jo, H.-B. Kim, S.-I. Mo, Y.-K. Kim, H. Lee, N. G. An, S. Cho, W. R. Tress, S. M. Zakeeruddin, A. Hagfeldt, J. Y. Kim, M. Grätzel and D. S. Kim, Conformal quantum dot-SnO<sub>2</sub> layers as electron transporters for efficient perovskite solar cells, *Science*, 2022, **375**, 302–306.
- 169 Y. Wang, C. H. Duan, X. L. Zhang, N. Rujisamphan, Y. Liu, Y. Y. Li, J. Y. Yuan and W. L. Ma, Dual interfacial engineering enables efficient and reproducible CsPbI<sub>2</sub>Br all-inorganic perovskite solar cells, *ACS Appl. Mater. Interfaces*, 2020, **12**, 31659–31666.
- 170 R. X. Peng, T. T. Yan, J. W. Chen, S. F. Yang, Z. Y. Ge and M. T. Wang, Passivating surface defects of n-SnO<sub>2</sub> electron transporting layer by InP/ZnS quantum dots: Toward efficient and stable organic solar cells, *Adv. Electron. Mater.*, 2020, **6**, 1901245.
- 171 N. Huang, G. W. Li, H. Huang, P. P. Sun, T. L. Xiong, Z. F. Xia, F. Zheng, J. Xu and X. H. Sun, One-step solvothermal tailoring the compositions and phases of nickel cobalt sulfides on conducting oxide substrates as counter electrodes for efficient dye-sensitized solar cells, *Appl. Surf. Sci.*, 2016, **390**, 847–855.
- 172 K. Al-Attafi, F. H. Jawdat, H. Qutaish, P. Hayes, A. Al-Keisy, K. Shim, Y. Yamauchi, S. X. Dou, A. Nattestad and J. H. Kim, Cubic aggregates of Zn<sub>2</sub>SnO<sub>4</sub> nanoparticles and their application in dye-sensitized solar cells, *Nano Energy*, 2019, **57**, 202–213.
- 173 Q. Jiang, L. Zhang, H. Wang, X. Yang, J. Meng, H. Liu, Z. Yin, J. Wu, X. Zhang and J. You, *Nat. Energy*, 2017, **2**, 16177.
- 174 H.-J. Kim, G.-C. Xu, C. V. V. M. Gopi, H. Seo, M. Venkata-Haritha and M. Shiratani, Enhanced light harvesting and charge recombination control with TiO<sub>2</sub>/PbCdS/CdS based quantum dot-sensitized solar cells, *J. Electroanal. Chem.*, 2017, **788**, 131–136.
- 175 E. Jalali-Moghadam and Z. Shariatnia, Al<sup>3+</sup> doping into TiO<sub>2</sub> photoanodes improved the performance of amine anchored CdS quantum dot sensitized solar cells, *Mater. Res. Bull.*, 2018, **98**, 121–132.
- 176 S. Muthu, G. Zaiats, M. B. Sridharan and P. V. Kamat, influence of plasmonic Cu<sub>x</sub>S interfacing layer on photovoltaic performance of CIZS quantum dot sensitized solar cells, *J. Electrochem. Soc.*, 2019, **166**, H3133–H3137.
- 177 H. T. Dastjerdi, P. F. Qi, Z. Y. Fan and M. M. Tavakoli, Cost-effective and semi-transparent PbS quantum dot solar cells using copper electrodes, *ACS Appl. Mater. Interfaces*, 2020, **12**, 818–825.
- 178 Z. L. Zhang, Z. H. Chen, J. B. Zhang, W. J. Chen, J. F. Yang, X. M. Wen, B. Wang, N. Kobamoto, L. Yuan, J. A. Stride, G. J. Conibeer, R. J. Patterson and S. J. Huang, Significant improvement in the performance of PbSe quantum dot solar cell by introducing CsPbBr<sub>3</sub> perovskite colloidal nanocrystal back layer, *Adv. Energy Mater.*, 2017, **7**, 1601773.
- 179 H. Ren, A. Xu, Y. Y. Pan, D. H. Qin, L. T. Hou and D. Wang, Efficient PbS quantum dot solar cells with both Mg-doped ZnO window layer and ZnO nanocrystal interface passivation layer, *Nanomaterials*, 2021, **11**, 219.
- 180 K. M. Kim, J. H. Jeon, Y. Y. Kim, H. K. Lee, O. O. Park and D. H. Wang, Effects of ligand exchange CdSe quantum dot interlayer for inverted organic solar cells, *Org. Electron.*, 2015, **25**, 44–49.
- 181 Z. Q. Li, S. J. Li, Z. H. Zhang, X. Y. Zhang, J. F. Li, C. Y. Liu, L. Shen, W. B. Guo and S. P. Ruan, Enhanced electron extraction capability of polymer solar cells via modifying the cathode buffer layer with inorganic quantum dots, *Phys. Chem. Chem. Phys.*, 2016, **18**, 11435–11442.
- 182 J. H. Jeon, D. H. Wang, H. Park, J. H. Park and O. O. Park, Stamping transfer of a quantum dot interlayer for organic photovoltaic cells, *Langmuir*, 2012, **28**, 9893–9898.
- 183 C. H. Duan, W. N. Luo, T. G. Jiu, J. S. Li, Y. Wang and F. S. Lu, Facile preparation and characterization of ZnCdS



- nanocrystals for interfacial applications in photovoltaic devices, *J. Colloid Interface Sci.*, 2018, **512**, 353–360.
- 184 S. Huang, Y. T. Tang, A. C. Yu, Y. H. Wang, S. Shen, B. N. Kang, S. R. P. Silva and G. Y. Lu, Solution-processed SnO<sub>2</sub> nanoparticle interfacial layers for efficient electron transport in ZnO-based polymer solar cells, *Org. Electron.*, 2018, **62**, 373–381.
- 185 M. Dusza, M. Stefanski, M. Wozniak, D. Hreniak, Y. Gerasymchuk, L. Marciniak, F. Granek and W. Strek, Luminescent Sr<sub>2</sub>CeO<sub>4</sub> nanocrystals for applications in organic solar cells with conjugated polymers, *J. Lumin.*, 2016, **169**, 857–861.
- 186 Z. Zhang, Y. Yang, J. Gao, S. Xiao, C. H. Zhou, D. Q. Pan, G. Liu and X. Y. Guo, Highly efficient Ag<sub>2</sub>Se quantum dots blocking layer for solid-state dye-sensitized solar cells: Size effects on device performance, *Mater. Mater. Today Energy*, 2018, **7**, 27–36.
- 187 S. S. Hosseini, M. Ebadi and K. Motevalli, Facial microwave approach for synthesis of CdS quantum dots as barrier layer for increasing dye-sensitized solar cells efficiency, *J. Mater. Sci.: Mater. Electron.*, 2016, **27**, 12240–12246.
- 188 W. Zhang, D. Wang, Q. M. Wang and H. Q. Sun, The high performance of quantum dot sensitized solar cells co-sensitized with mixed-joint CdS and SnS quantum dots, *ECS J. Solid State Sci. Technol.*, 2019, **8**, Q96–Q100.
- 189 M. Zahedifar, Z. Chamanzadeh and S. M. M. Hosseinpoor, Synthesis of LaVO<sub>4</sub>:Dy<sup>3+</sup> luminescent nanostructured and optimization of its performance as down-converter in dye-sensitized solar cells, *J. Lumin.*, 2013, **135**, 66–73.
- 190 J. Roh, S. H. Hwang and J. Jang, Dual-functional CeO<sub>2</sub>:Eu<sup>3+</sup> nanocrystals for performance-enhanced dye-sensitized solar cells, *ACS Appl. Mater. Interfaces*, 2014, **22**, 19825–19832.
- 191 J. Shen, Z. Q. Li, R. Cheng, Q. Luo, Y. D. Luo, Y. W. Chen, X. H. Chen, Z. Sun and S. M. Huang, Eu<sup>3+</sup>-doped NaGdF<sub>4</sub> nanocrystal down-converting layer for efficient dye-sensitized solar cells, *ACS Appl. Mater. Interfaces*, 2014, **6**, 17454–17462.
- 192 M. S. Morassaei, A. Salehabadi, A. Akbari, S. H. Tavassoli and M. Salavati-Niasari, Enhanced dye sensitized solar cells efficiency by utilization of an external layer of CaCe<sub>2</sub>(MoO<sub>4</sub>)<sub>4</sub>:Er<sup>3+</sup>/Yb<sup>3+</sup> nanoparticles, *J. Alloys Compd.*, 2018, **769**, 732–739.
- 193 T. Chen, Y. F. Shang, S. W. Hao, L. Tian, Y. D. Hou and C. H. Yang, Enhancement of dye sensitized solar cell efficiency through introducing concurrent upconversion/downconversion core/shell nanoparticles as spectral converters, *Electrochim. Acta*, 2018, **282**, 743–749.
- 194 A. K. Kaliampurthy, H. C. Kang, F. K. Asiam, K. Yoo and J.-J. Lee, Trap-assisted transition energy levels of SrF<sub>2</sub>:Pr<sup>3+</sup>-Yb<sup>3+</sup> nanophosphor in TiO<sub>2</sub> photoanode for luminescence tuning in dye-sensitized photovoltaic cells, *Sol. RRL*, 2021, **10**, 2100411.
- 195 R. Kamal and H. Hafez, Novel down-converting single-phased white light Pr<sup>3+</sup> doped BaWO<sub>4</sub> nanophosphors material for DSSC applications, *Opt. Mater.*, 2021, **121**, 111646.
- 196 M. Y. Cha, P. M. Da, J. Wang, W. Y. Wang, Z. H. Chen, F. X. Xiu, G. F. Zheng and Z.-S. Wang, Enhancing perovskite solar cell performance by interface engineering using CH<sub>3</sub>NH<sub>3</sub>PbBr<sub>0.9</sub>I<sub>2.1</sub> quantum dots, *J. Am. Chem. Soc.*, 2016, **138**, 8581–8587.
- 197 P. Liu, Y. Sun, S. F. Wang, H. J. Zhang, Y. N. Gong, F. J. Li, Y. F. Shi, Y. X. Du, X. F. Li, S.-S. Guo, Q. D. Tai, C. L. Wang and X.-Z. Zhao, Two dimensional graphitic carbon quantum dots modified perovskite solar cells and photodetectors with high performances, *J. Power Sources*, 2020, **451**, 227825.
- 198 Y. Z. Ma, P. Vashishtha, S. B. Shivarudraiah, K. Chen, Y. Liu, J. M. Hodgkiss and J. E. Halpert, A hybrid perovskite solar cell modified with copper indium sulfide nanocrystals to enhance hole transport and moisture stability, *Sol. RRL*, 2017, **1**, 1700078.
- 199 J. J. Ma, G. Yang, M. C. Qin, X. L. Zheng, H. W. Lei, C. Chen, Z. L. Chen, Y. X. Guo, H. W. Han, X. Z. Zhao and G. J. Fang, MgO nanoparticles modified anode for highly efficient SnO<sub>2</sub>-based planar perovskite solar cells, *Adv. Sci.*, 2017, **4**, 1700031.
- 200 S. M. Ali, S. M. Ramay, M. H. Aziz, N. Ur-Rehman, M. S. AlGarawi, S. S. AlGhamd, A. Mahmood, T. S. Alkhuraiji and S. Atiq, Efficiency enhancement of perovskite solar cells by incorporation of CdS quantum dot through fast electron injection, *Org. Electron.*, 2018, **62**, 21–25.
- 201 Y. Wang, C. H. Duan, J. S. Li, W. Han, M. Zhao, L. L. Yao, Y. Y. Wang, C. Yan and T. G. Jiu, Performance enhancement of inverted perovskite solar cells based on smooth and compact PC<sub>61</sub>BM:SnO<sub>2</sub> electron transport layers, *ACS Appl. Mater. Interfaces*, 2018, **10**, 20128–20135.
- 202 T. T. Wu, C. Zhen, J. B. Wu, C. X. Jia, M. Haider, L. Z. Wang, G. Liu and H.-M. Cheng, Chlorine capped SnO<sub>2</sub> quantum-dots modified TiO<sub>2</sub> electron selective layer to enhance the performance of planar perovskite solar cells, *Sci. Bull.*, 2019, **64**, 547–552.
- 203 L.-C. Chen, C.-H. Tien, Z.-L. Tseng and J.-H. Ruan, Enhanced efficiency of MAPbI<sub>3</sub> perovskite solar cells with FAPbX<sub>3</sub> perovskite quantum dots, *NanoMaterials*, 2019, **9**, 121.
- 204 X. Y. Zhu, B. Cheng, X. H. Li, J. J. Zhang and L. Y. Zhang, Enhanced efficiency of perovskite solar cells by PbS quantum dot modification, *Appl. Surf. Sci.*, 2019, **487**, 32–40.
- 205 Y. H. Ma, Y. W. Zhang, H. Y. Zhang, H. Lv, R. Y. Hu, W. Liu, S. L. Wang, M. Jiang, L. Chug, J. Zhang, X. A. Li, R. D. Xia and W. Huang, Effective carrier transport tuning of CuO<sub>x</sub> quantum dots hole interfacial layer for high-performance inverted perovskite solar cell, *Appl. Surf. Sci.*, 2021, **547**, 149117.
- 206 J. Y. Yin, Y. J. Yuan, J. Ni, J. Y. Guan, X. J. Zhou, Y. Liu, Y. Ding, H. K. Cai and J. J. Zhang, CH<sub>3</sub>NH<sub>3</sub>PbBr<sub>3-x</sub>I<sub>x</sub> quantum dots enhance bulk crystallization and interface charge transfer for efficient and stable perovskite solar cells, *ACS Appl. Mater. Interfaces*, 2020, **12**, 48861–48873.



- 207 R. S. Li, Y. F. Dou, Y. S. Liao, D. Wang, G. D. Li, J. H. Wu and Z. Lan, Enhancing efficiency of perovskite solar cells from surface passivation of Co<sup>2+</sup> doped CuGaO<sub>2</sub> nanocrystals, *J. Colloid Interface Sci.*, 2022, **607**, 1280–1286.
- 208 L. Najafi, B. Taheri, B. Martín-García, S. Bellani, D. D. Girolamo, A. Agresti, R. Oropesa-Nuñez, S. Pescetelli, L. Vesce, E. Calabrò, M. Prato, A. E. D. R. Castillo, A. D. Carlo and F. Bonaccorso, MoS<sub>2</sub> quantum dot/graphene hybrids for advanced interface engineering of a CH<sub>3</sub>NH<sub>3</sub>PbI<sub>3</sub> perovskite solar cell with an efficiency of over 20%, *ACS Nano*, 2018, **12**, 10736–10754.
- 209 C. Yang, Z. J. Wang, Y. H. Lv, R. H. Yuan, Y. H. Wu and W.-H. Zhang, Colloidal CsCu<sub>5</sub>S<sub>3</sub> nanocrystals as an interlayer in high-performance perovskite solar cells with an efficiency of 22.29, *Chem. Eng. J.*, 2021, **406**, 126855.
- 210 D. L. Zhou, D. L. Liu, J. J. Jin, X. Chen, W. Xu, Z. Yin, G. C. Pan, D. Y. Li and H. W. Song, Semiconductor plasmon-sensitized broadband upconversion and its enhancement effect on the power conversion efficiency of perovskite solar cells, *J. Mater. Chem. A*, 2017, **5**, 16559–16567.
- 211 J. B. Jia, J. M. Dong, J. M. Lin, Z. Lan, L. Q. Fan and J. H. Wu, Improved photovoltaic performance of perovskite solar cells by utilizing down-conversion NaYF<sub>4</sub>:Eu<sup>3+</sup> nanophosphors, *J. Mater. Chem. C*, 2019, **7**, 937–942.
- 212 W. B. Bi, Y. J. Wu, C. Chen, D. L. Zhou, Z. L. Song, D. Y. Li, G. Y. Chen, Q. L. Dai, Y. S. Zhu and H. W. Song, Dye sensitization and local surface plasmon resonance-enhanced upconversion luminescence for efficient perovskite solar cells, *ACS Appl. Mater. Interfaces*, 2020, **12**, 24737–24746.
- 213 J. Ma, Y. J. Yuan and P. Sun, Approaching 23% silicon heterojunction solar cells with dual-functional SiO<sub>x</sub>/MoS<sub>2</sub> quantum dots interface layers, *Sol. Energy Mater. Sol. Cells*, 2021, **227**, 111110.
- 214 A. Thomas, R. Vinayakan and V. V. Ison, An inverted ZnO/P3HT:PbS bulk-heterojunction hybrid solar cell with a CdSe quantum dot interface buffer layer, *RSC Adv.*, 2020, **10**, 16693–16699.
- 215 S. M. Reda, Enhanced efficiency of solar cell using luminescence PbS quantum dots concentrators, *J. Fluoresc.*, 2015, **3**, 631–639.
- 216 W. L. Feng, Y. W. Wang, J. Liu and X. B. Yu, Polycrystalline Si nanocrystals/CdS quantum dots composited solar cell with efficient light harvesting and surface passivation, *Chem. Phys. Lett.*, 2014, **608**, 314–318.
- 217 I. Levchuk, C. Wuerth, F. Krause, A. Osvet, M. Batentschuk, U. Resch-Genger, C. Kolbeck, P. Herre, H. P. Steinruck, W. Peukert and C. J. Brabec, Industrially scalable and cost-effective Mn<sup>2+</sup> doped Zn<sub>x</sub>Cd<sub>1-x</sub>S/ZnS nanocrystals with 70% photoluminescence quantum yield, as efficient down-shifting materials in photovoltaics, *Energy Environ. Sci.*, 2016, **9**, 1083–1094.
- 218 M. Jalalah, Y.-H. Ko, F. A. Harraz, M. S. Al-Assiri and J.-G. Park, Enhanced efficiency and current density of solar cells via energy-down-shift having energy-tuning-effect of highly UV-light-harvesting Mn<sup>2+</sup>-doped quantum dots, *Nano Energy*, 2017, **33**, 257–265.
- 219 T. Y. Sun, X. Chen, L. M. Jin, H.-W. Li, B. Chen, B. Fan, B. Moine, X. S. Qiao, X. P. Fan, S.-W. Tsang, S. F. Yu and F. Wang, Broadband Ce(III)-sensitized quantum cutting in core-shell nanoparticles: Mechanistic investigation and photovoltaic application, *J. Phys. Chem. Lett.*, 2017, **20**, 5099–5104.
- 220 D. L. Zhou, D. L. Liu, G. C. Pan, X. Chen, D. Y. Li, W. Xu, X. Bai and H. W. Song, Cerium and ytterbium codoped halide perovskite quantum dots: A novel and efficient downconverter for improving the performance of silicon solar cells, *Adv. Mater.*, 2017, **42**, 1704149.
- 221 M. Rwaimi, C. G. Bailey, P. J. Shwa, T. M. Mercier, C. Krishnan, T. Rahman, P. G. Lagoudakis, R.-H. Horng, S. A. Boden and M. D. B. Charlton, FAPbBr<sub>3</sub> perovskite quantum dots as a multifunctional luminescent-downshifting passivation layer for GaAs solar cells, *Sol. Energy Mater. Sol. Cells*, 2022, **234**, 111406.
- 222 Y. M. Li, Q. S. Zhang, L. Y. Niu, J. Liu and X. F. Zhou, TiO<sub>2</sub> nanorod arrays modified with SnO<sub>2</sub>-Sb<sub>2</sub>O<sub>3</sub> nanoparticles and application in perovskite solar cell, *Thin Solid Films*, 2017, **621**, 6–11.
- 223 M. X. Huang, Z. Z. Lu, L. L. Wen, X. S. Zhang, T. J. Huang, Y. B. Meng, J. J. Tang and L. Y. Zhou, Core/shell-structured TiO<sub>2</sub>/PbS photoanodes for high-performance CsPbBr<sub>3</sub> perovskite solar cells, *Mater. Lett.*, 2019, **256**, 126619.
- 224 Z. H. Wu, Y. Z. Wang, Y. H. Zhang, W. J. Zhang, Q. R. Liu, Q. M. Liu, Q. Chen, Y. L. Li, J. S. Li and D. Y. He, Enhanced performance of polymer solar cells by adding SnO<sub>2</sub> nanoparticles in the photoactive layer, *Org. Electron.*, 2019, **73**, 7–12.
- 225 E. J. Lee, D.-H. Kim and D.-K. Hwang, Effect of embedded chalcogenide quantum dots in PbBr<sub>2</sub> film on CsPbBr<sub>3</sub> inorganic perovskite solar cells, *J. Ind. Eng. Chem.*, 2020, **90**, 281–286.
- 226 X. H. Luo, Z. Y. He, R. W. Meng, C. Zhang, M. W. Chen, H. F. Lu and Y. P. Yang, SnS quantum dots with different sizes in active layer for enhancing the performance of perovskite solar cells, *Appl. Phys. A*, 2021, **127**, 317.
- 227 P. Kumnorkaew, N. Rattanawichai, C. Ratanatawanate, S. Yoriya, K. Lohawet, Y. X. Zhao and P. Vas-Umuay, Influence of PbS quantum dots-doped TiO<sub>2</sub> nanotubes in TiO<sub>2</sub> film as an electron transport layer for enhanced perovskite solar cell, *IEEE J. Photovoltaics*, 2020, **10**, 287–295.
- 228 A. Kirkeminde, R. Scott and S. Q. Ren, All inorganic iron pyrite nano-heterojunction solar cells, *Nanoscale*, 2012, **4**, 7649–7654.
- 229 J. S. Niezgodna, E. Yap, J. D. Keene, J. R. McBride and S. J. Rosenthal, Plasmonic Cu<sub>x</sub>In<sub>y</sub>S<sub>2</sub> quantum dots make better photovoltaics than their nonplasmonic counterparts, *Nano Lett.*, 2014, **14**, 3262–3269.
- 230 M. A. Najeeb, S. M. Abdullah, F. Aziz, Z. Ahmad, R. A. Shakoor, A. M. A. Mohamed, U. Khalil, W. Swelm, A. A. Al-Ghamdi and K. Sulaiman, A comparative study on the performance of hybrid solar cells containing ZnSTe



- QDs in hole transporting layer and photoactive layer, *J. Nanopart. Res.*, 2016, **18**, 384.
- 231 F. Xu, Y. Sun, H. P. Gao, S. Y. Jin, Z. L. Zhang, H. F. Zhang, G. C. Pan, M. Kang, X. Q. Ma and Y. L. Mao, High-performance perovskite solar cells based on NaCsWO<sub>3</sub>@NaYF<sub>4</sub>@NaYF<sub>4</sub>:Yb,Er upconversion nanoparticles, *ACS Appl. Mater. Interfaces*, 2021, **13**, 2674–2684.
- 232 J. Yu, Y. L. Yang, R. Q. Fan, D. Q. Liu, L. G. Wei, S. Chen, L. Li, B. Yang and W. W. Cao, Enhanced near-infrared to visible upconversion nanoparticles of Ho<sup>3+</sup>-Yb<sup>3+</sup>-F<sup>-</sup> tri-doped TiO<sub>2</sub> and its application in dye-sensitized solar cells with 37% improvement in power conversion efficiency, *Inorg. Chem.*, 2014, **53**, 8045–8053.
- 233 D. Y. Li, W. F. Sun, L. X. Shao, S. Y. Wu, Z. Huang, X. Jin, Q. Zhang and Q. H. Li, Tailoring solar energy spectrum for efficient organic/inorganic hybrid solar cells by up-conversion luminescence nanophosphors, *Electrochim. Acta*, 2015, **182**, 416–423.
- 234 N. N. Yao, J. Z. Huang, K. Fu, X. L. Deng, M. Ding, M. H. Shao and X. J. Xu, Enhanced light harvesting of dye-sensitized solar cells with up/down conversion materials, *Electrochim. Acta*, 2015, **154**, 273–277.
- 235 N. Chander, A. F. Khan, V. K. Komarala, S. Chawla and V. Dutta, Enhancement of dye sensitized solar cell efficiency via incorporation of upconverting phosphor nanoparticles as a spectral converters, *Prog. Photovoltaics*, 2016, **24**, 692–703.
- 236 M. He, X. C. Pang, X. Q. Liu, B. B. Jiang, Y. J. He, H. Snaith and Z. Q. Lin, Monodisperse dual-functional upconversion nanoparticles enabled near-infrared organolead halide perovskite solar cells, *Angew. Chem., Int. Ed.*, 2016, **55**, 4280–4284.
- 237 L. Liang, M. Liu, Z. W. Jin, Q. Wang, H. R. Wang, H. Bian, F. Shi and S. Z. Liu, Optical management with nanoparticles for a light conversion efficiency enhancement in inorganic  $\gamma$ -CsPbI<sub>3</sub> solar cells, *Nano Lett.*, 2019, **19**, 1796–1804.
- 238 X. S. Lai, X. T. Li, X. D. Lv, Y.-Z. Zheng, F. L. Meng and X. Tao, Broadband dye-sensitized upconversion nanocrystals enable near-infrared planar perovskite solar cells, *J. Power Sources*, 2017, **372**, 125–133.
- 239 V. Kumar, A. Pandey, S. K. Swami, O. M. Ntwaeaborwa, H. C. Swart and V. Dutta, Synthesis and characterization of Er<sup>3+</sup>-Yb<sup>3+</sup> doped ZnO upconversion nanoparticles for solar cell application, *J. Alloys Compd.*, 2018, **766**, 429–435.
- 240 W. J. Shi, Z. L. Zhang, J. Q. Qin, Y. Zhang, Y. Y. Liu, Y. F. Liu, H. P. Gao and Y. L. Mao, Interface modification by up-conversion material of Ho<sup>3+</sup>-Yb<sup>3+</sup>-Li<sup>+</sup> tri-doped TiO<sub>2</sub> to improve the performance of perovskite solar cells, *J. Alloys Compd.*, 2018, **754**, 124–130.
- 241 J. W. Liang, H. P. Gao, M. J. Yi, W. J. Shi, Y. F. Liu, Z. L. Zhang and Y. L. Mao,  $\beta$ -NaYF<sub>4</sub>:Yb<sup>3+</sup>,Tm<sup>3+</sup>@TiO<sub>2</sub> core/shell nanoparticles incorporated into the mesoporous layer for high efficiency perovskite solar cells, *Electrochim. Acta*, 2018, **261**, 14–22.
- 242 X. S. Deng, C. X. Zhang, J. F. Zheng, X. Zhou, M. D. Yu, X. H. Chen and S. M. Huang, Highly bright Li(Gd,Y)F<sub>4</sub>:Yb,Er upconverting nanocrystals incorporated hole transport layer for efficient perovskite solar cells, *Appl. Surf. Sci.*, 2019, **485**, 332–341.
- 243 Q. Y. Guo, J. H. Wu, Y. Q. Yang, X. P. Liu, J. B. Jia, J. Dong, Z. Lan, J. M. Lin, M. L. Huang, Y. L. Wei and Y. F. Huang, High performance perovskite solar cells based on  $\beta$ -NaYF<sub>4</sub>:Yb<sup>3+</sup>/Er<sup>3+</sup>/Sc<sup>3+</sup>@NaYF<sub>4</sub> core/shell upconversion nanoparticles, *J. Power Sources*, 2019, **426**, 178–187.
- 244 Y. Y. Qin, Z. Q. Hu, B. H. Lim, W. S. Chang, K. K. Chong, P. T. Zhang and H. T. Zhang, So-hydrothermal synthesis of TiO<sub>2</sub>:Sm<sup>3+</sup> nanoparticles and their enhanced photovoltaic properties, *J. Alloy. Comp.*, 2016, **686**, 803–809.
- 245 L. J. Wang, W. H. Guo, H. S. Hao, Q. Su, S. S. Jin, H. Li, X. F. Hu, L. Qin, W. Y. Gao and G. S. Liu, Enhancing photovoltaic performance of dye-sensitized solar cells by rare-earth doped oxide of SrAl<sub>2</sub>O<sub>4</sub>:Eu<sup>3+</sup>, *Mater. Res. Bull.*, 2016, **76**, 459–465.
- 246 A. Pattnaik, S. Jha, M. Tomar, V. Gupta, B. Prasad and S. Mondal, Improving the quantum efficiency of the monocrystalline silicon solar cell using erbium-doped zinc sulphide nanophosphor in downshift layer, *Mater. Res. Express*, 2018, **5**, 095014.
- 247 M. S. Pereira, F. A. S. Lima, T. S. Ribeiro, M. R. da Silva, R. Q. Almeida, E. B. Barros and I. F. Vasconcelos, Application of Fe-doped SnO<sub>2</sub> nanoparticles in organic solar cells with enhanced stability, *Opt. Mater.*, 2017, **64**, 548–556.
- 248 J. M. Luther, M. Law, Q. Song, C. L. Perkins, M. C. Beard and A. J. Nozik, Structural, optical, and electrical properties of self-assembled films of PbSe nanocrystals treated with 1,2-ethanedithiol, *ACS Nano*, 2008, **2**, 271–280.
- 249 P. R. Brown, D. Kim, R. R. Lunt, N. Zhao, M. G. Bawendi, J. C. Grossman and V. Bulović, Energy level modification in lead sulfide quantum dot thin films through ligand exchange, *ACS Nano*, 2014, **8**, 5863–5872.
- 250 X. S. Lin, D. Y. Cui, X. H. Luo, C. Y. Zhang, Q. F. Han, Y. B. Wang and L. Y. Han, Efficiency progress of inverted perovskite solar cells, *Energy Environ. Sci.*, 2020, **13**, 3823–3847.
- 251 W. Chen, Y. Z. Wu, J. Liu, C. J. Qin, X. D. Yang, A. Islam, Y.-B. Cheng and L. Y. Han, Hybrid interfacial layer leads to solid performance improvement of inverted perovskite solar cells, *Energy Environ. Sci.*, 2015, **8**, 629–640.
- 252 M. A. Haque, A. D. Sheikh, X. W. Guan and T. Wu, Metal oxides as efficient charge transporters in perovskite solar cells, *Adv. Energy Mater.*, 2017, **7**, 1602803.
- 253 B. B. Liu, H. Bi, D. M. He, L. Bai, W. Q. Wang, H. K. Yuan, Q. L. Song, P. Y. Su, Z. G. Zang, T. W. Zhou and J. Z. Chen, Interfacial defect passivation and stress release via multi-active-site ligand anchoring enables efficient and stable methylammonium-free perovskite solar cells, *ACS Energy Lett.*, 2021, **6**, 2526–2538.
- 254 H. M. A. Javed, M. Sarfaraz, Z. Nisar, A. A. Qureshi, M. Fakhar e Alam, W. X. Que, X. T. Yin, H. S. M. Abd-Rabbob, A. Shahid, M. I. Ahmad and S. Ullah, Plasmonic



- dye-sensitized solar cells: Fundamentals, recent developments, and future perspectives, *ChemistrySelect*, 2021, **62021**, 9337–9350.
- 255 O. A. Balitskii, Recent Energy Targeted Application of Localized Surface Plasmon Resonance Semiconductor Nanocrystals: A Mini-Review, *Mater. Today Energy*, 2021, **20**, 100629.
- 256 B. S. Richards, Enhancing the performance of silicon solar cells via the application of passive luminescence conversion layers, *Sol. Energy Mater. Sol. Cells*, 2006, **90**, 2329–2337.
- 257 A. H. G. Niaki, A. M. Bakhshayesh and M. R. Mohammadi, Double-layer dye-sensitized solar cells based on Zn-doped TiO<sub>2</sub> transparent and light scattering layers: Improving electron injection and light scattering effect, *Sol. Energy*, 2014, **103**, 210–222.
- 258 W. An, J. R. Wu, T. Zhu and Q. Z. Zhu, Experimental investigation of a concentrating PV/T collector with Cu<sub>9</sub>S<sub>5</sub> nanofluid spectral splitting filter, *Appl. Energy*, 2016, **184**, 197–206.
- 259 I. Zarma, M. Ahmed and S. Ookawara, Enhancing the performance of concentrator photovoltaic systems using nanoparticle-phase change material heat sinks, *Energy Convers. Manage.*, 2019, **179**, 229–242.
- 260 Z. K. Liu, Y. X. Zhong, I. Shafei, R. Borman, S. Jeong, J. Chen, Y. Losovyj, X. F. Gao, N. Li, Y. P. Du, E. Sarnello, T. Li, W. L. Ma and X. C. Ye, Tuning infrared plasmon resonances in doped metal-oxide nanocrystals through cation-exchange reactions, *Nat. Commun.*, 2019, **10**, 1394.
- 261 M. G. Gong, D. Ewing, M. Casper, A. Stramel, A. Elliot and J. Z. Wu, Controllable synthesis of monodispersed Fe<sub>1-x</sub>S<sub>2</sub> nanocrystals for high-performance optoelectronic devices, *ACS Appl. Mater. Interfaces*, 2019, **11**, 19286–19293.
- 262 C. Beynis, Indium insertions in non-stoichiometric copper sulfides, Cu<sub>x</sub>S, and their effect on the localized surface plasmon resonance of the nanocrystals, *Appl. Phys. A*, 2019, **125**, 310.
- 263 A. Verma and S. K. Sharma, Down-conversion from Er<sup>3+</sup>-Yb<sup>3+</sup> codoped CaMoO<sub>4</sub> phosphor: A spectral conversion to improve solar cell efficiency, *Ceram. Int.*, 2017, **43**, 8879–8885.
- 264 Y. Q. Yin, M. Q. Wang, V. Malgras and Y. Yamauchi, Stable and efficient Tin-based perovskite solar cell via semiconducting-insulating structure, *ACS Appl. Energy Mater.*, 2020, **3**, 10447–10452.
- 265 Y. X. Ye, Y. Q. Yin, Y. Chen, S. Li, L. Li and Y. Yamauchi, Metal-organic framework materials in perovskite solar cells: Recent advancements and perspectives, *Small*, 2023, **19**, 2208119.

